Characterizing Dominant Processes in Landfills to Quantify the Emission Potential

van Turnhout, Andre

DOI
10.4233/uuid:67b99fa5-cb8d-4230-b683-5a045323e772

Publication date
2017

Document Version
Final published version

Citation (APA)
van Turnhout, A. (2017). *Characterizing Dominant Processes in Landfills to Quantify the Emission Potential*. [Dissertation (TU Delft), Delft University of Technology]. https://doi.org/10.4233/uuid:67b99fa5-cb8d-4230-b683-5a045323e772

Characterizing Dominant Processes in Landfills to Quantify the Emission Potential

Characterizing Dominant Processes in Landfills to Quantify the Emission Potential

Proefschrift

ter verkrijging van de graad van doctor
aan de Technische Universiteit Delft,
op gezag van de Rector Magnificus prof. ir. K.C.A.M. Luyben,
voorzitter van het College voor Promoties,
in het openbaar te verdedigen op vrijdag 16 juni 2017 om 10:00 uur

door

André Gerard van Turnhout

Master of Life Science & Technology,
Universiteit Leiden & Technische Universiteit Delft,
geboren te ’s-Gravenhage, Nederland.

Dit proefschrift is goedgekeurd door de

promotor: prof. dr. ir. T.J. Heimovaara
copromotor: dr. ir. R. Kleerebezem

Samenstelling promotiecommissie:

Rector Magnificus,	voorzitter
Prof. dr. ir. T.J. Heimovaara,	Technische Universiteit Delft
Dr. ir. R. Kleerebezem,	Technische Universiteit Delft
Onafhankelijke leden:	
Prof. dr. ir. M.C.M. van Loosdrecht,	Technische Universiteit Delft
Prof. dr. C. Jommi,	Technische Universiteit Delft
Prof. dr. R.N.J. Comans,	Wageningen University & Research
Ass. prof. dipl.-ing. dr. techn. J. Fellner,	Technical University Wien, Austria
Overige leden:	
Dr. R. Beaven,	University of Southampton, UK

Keywords: Municipal Solid Waste, quantification, emission potential, biogeochemical modeling toolbox, aeration, recirculation, stochastic, hydrology

Printed by: Ipskamp Printing, Enschede

Front & Back: Harold Wiegel, graphic designer, haroldwiegel@gmail.com.

ISBN 978-94-028-0680-9

An electronic version of this dissertation is available at
http://repository.tudelft.nl/.

Dedicated to my grandpa Gerard van Turnhout

Summary

Our ever-growing amount of solid waste puts a burden on future generations and the environment due to emissions of contaminants such as CO_2, CH_4, Cl^- and heavy-metals for hundreds of years. It is therefore essential that landfill after-care methods are developed that reduce the emission potential of landfills to acceptable levels within the time-span of one generation. Several treatment methods such as aeration and leachate recirculation have shown promising results in reducing concentrations of problematic compounds in leachate and landfill gas emissions. However for application as full-scale technologies, long term evidence of sustainable reduction in emission potential has yet to be provided in practice. It is not possible to measure emission potential directly. Predictions of future emissions from landfills require emission modeling where emission potential is a crucial parameter. The aim of the research presented in this thesis is to present a conceptual modeling approach which increases the confidence in such long term predictions by reducing the parameter and model uncertainty in a systematic way. As such the approach allows us to quantify the emission potential.

Chapter 2 and 3 of this thesis present an approach to develop and select biochemical and physical process networks in a generic conceptual model that allows us to optimally describe measured emissions from lysimeter experiments under anaerobic and aerobic conditions. These networks give a detailed description of the mass balances of contaminants and bacteria in the solid, liquid and gas phase. As a consequence, main emission pathways and rate-limiting processes are identified. Our results give strong indications that only a relatively small amount of the solid waste material present contributes to the measured emissions. The toolbox developed for this thesis, integrates information from different databases with approaches to obtain and couple thermodynamic/kinetic parameters and processes in order to efficiently evaluate a wide variety of networks via Bayesian inference using quantitative criteria.

In chapter 4, the optimal biochemical and physical process networks calibrated at the lysimeter and column scale, are applied to predict the emissions at landfill scale. This is achieved by coupling the process networks to a water balance model that calculates the leachate production using a stochastic residence time distribution of water within the waste-body. The parameters of the stochastic residence time model are obtained by optimization using daily leachate production, rainfall and evaporation measurements. After calibration, the decrease in mass of different contaminants present in the waste body, gives a quantitative estimate of the full scale emission potential as a function of time. Results are shown for measured time series of leachate quantity and leachate quality (e.g. Cl^-, Na^+ and NH_4^+), but can easily be extended to other parameters.

In chapter 5, the effectiveness of different aeration strategies is investigated

based on modeled distributions of oxygen throughout a waste-body. The model is based on Darcy's law for two-phase flow with parameters measured in laboratory experiments. Modeled gas extraction rates are in reasonable agreement with extraction rates measured at landfills. The results present optimal well configurations and aeration strategies for effective treatment.

The thesis concludes with a list of the most important research steps for reducing the uncertainty in the approaches for quantification of full scale emission potential in the near future.

Samenvatting

De alsmaar groeiende hoeveelheid afval legt een zware last op toekomstige generaties en het milieu, door de lange termijn emissies van verontreinigingen zoals CO_2, CH_4, Cl^- en zware metalen. Daarom is het van belang dat er nazorg methoden voor stortplaatsen ontwikkeld worden die het emissie potentieel binnen de periode van één generatie verlagen naar acceptable niveaus. Behandelmethoden zoals beluchting en percolaat recirculatie hebben veelbelovende resultaten laten zien waarbij concentraties van verontreinigende stoffen in percolaat en gas emissies zijn verlaagd. Voordat deze technieken in de praktijk grootschalig kunnen worden toegepast, moet wel worden aangetoond dat de verlaging van het emissiepotentieel duurzaam is. Het is echter niet mogelijk om emissiepotentieel direct te meten. Wel is het mogelijk om lange termijn emissies te voorspellen met modellen waarvoor het emissiepotentieel een parameter is. Dit proefschrift beschrijft een conceptuele rekenmethode waarbij het vertrouwen in lange termijn emissiepotentieel voorspellingen wordt vergroot door parameter en model onzekerheid op een systematische manier te reduceren.

Hoofdstuk 2 en 3, presenteren een methode voor het ontwikkelen en selecteren van biochemische en fysische procesnetwerken in een generiek conceptueel model waarmee metingen uit aërobe en anaërobe lysimeter en kolomexperimenten op een optimale manier worden beschreven. Deze benadering geeft gedetailleerd inzicht in de massa balansen van verontreinigingen en micro-organismen in het afvalpakket en daardoor ook inzicht in de belangrijkste emissie routes en snelheids bepalende processen. Onze resultaten geven een sterke indicatie dat een relatief klein deel van het afvalmateriaal in een stortlichaam bijdraagt aan het emissiepotentieel. De toolbox die is ontwikkeld integreert informatie van meerdere databases met methoden voor het schatten en koppelen van thermodynamische en kinetische parameters met processen. Hiermee kan een grote verscheidenheid aan netwerken via Bayesiaanse inferentie en kwantitatieve criteria worden geevalueerd.

In hoofdstuk 4 worden de optimale reactie en procesmodellen gecalibreerd op kolom en lysimeter schaal, toegepast om emissies op stortplaats schaal te voorspellen. Dit wordt bereikt door de netwerken van processen te koppelen aan een waterbalans model dat percolaat productie berekent op basis van de stochastische verblijftijden van water in het stortlichaam. De parameters in dit stochastische verblijftijden model worden bepaald door optimalisatie op basis van metingen aan percolaatproductie, neerslag en verdamping. Eenmaal gecalibreerd, kan het emissie potentieel worden gekwantificeerd op basis van de afname in berekende massa van verontreinigingen in het model als functie van tijd. Resultaten worden gepresenteerd voor tijdseries van percolaat productie en percolaat kwaliteit zoals Cl^-, Na^+ and NH_4^+. Deze kunnen eenvoudig worden uitgebreid naar andere parameters.

In hoofdstuk 5 is de effectiviteit van beluchtingsstrategieën onderzocht op basis

van de gemodelleerde distributie van zuurstof door het stortlichaam. Het gebruikte model is gebaseerd op de wet van Darcy voor twee-fase stroming waarbij de parameters zijn bepaald in laboratorium experimenten. Gemodelleerde gasextractie snelheden komen overeen met gasextractie stromingen gemeten op stortplaatsen. De resultaten presenteren optimale bronconfiguratie en beluchtingsstrategieën om een effectieve behandeling te krijgen.

Dit proefschrift wordt afgerond met een opsomming van de belangrijkste onderzoeksstappen om de onzekerheid in het kwantificeren van emissiepotentieel op stortplaats schaal op korte termijn te verminderen.

Contents

1

Introduction

1

1.1. Landfill After-care & Emission Potential

For centuries, we got rid of our municipal solid wastes (MSW) at waste dump sites. Rather ignorantly, we cared little about the impact that our ever-growing pile of solid waste has on the environment. It is only in the last decades that we have moved towards sanitary landfilling where waste is stored in engineered facilities where we prevent long term emissions in order to protect human health and the environment (HHE). In addition large efforts have been undertaken to recycle and burn most of our solid waste, so that only a small percentage is left to be landfilled. Worldwide, however, most solid waste is still landfilled and even in Europe it will remain to be an essential part of our waste management approach because it is the only viable final solution for some waste streams. Modern landfills and the legacy of old landfills and dump-sites require after-care in order to protect HHE from the adverse effects occurring due to emissions (Hoornweg and Bhada-Tata, 2012).

Landfills lead to environmental threats via two main emission pathways: 1) water in the form of precipitation infiltrates through the waste-body and gets polluted forming leachate. This leachate, subsequently flows in to the soil and eventually reaches groundwater and possibly surface water and 2) gasses, produced during biochemical mineralization of the organic waste migrate to the surface of the landfill and enter the atmosphere. These emissions may contribute to severe environmental problems such as contamination of groundwater and drinking water, global warming and eutrophication of surface waters. In addition landfill gas emissions can lead to nasty odours which is a nuisance to communities surrounding landfills (Belevi and Baccini, 1989, Kjeldsen et al., 2002, Macklin et al., 2011).

Landfill after-care is a long-term effort and minimal required time periods mentioned in regulations in different countries vary from 30 years to eternity. However all regulations state that after-care is required for as long as a threat to HHE remains and in general a decision to release a landfill from after-care has to be made by the competent authority (Laner et al., 2012). Releasing a landfill from after-care implies that we are sure that in the future no adverse effects will occur. This requires prediction of future emission behavior either by extrapolation of data series or using models based on landfill processes. Such predictions, however, are hampered because many of the mechanisms behind landfill processes and emissions are not well known. Most modeling approaches view the waste-body as a black box producing emissions.

The last decades, treatment methods were applied on landfills in order to reduce methane emissions to the atmosphere by enhancing the degradation of organic matter (Kumar et al., 2011). Initially, this led to increased storage capacity due to settlements and increased commercial use of methane (Berge et al., 2009). However, it also became evident that accelerated degradation has a significant impact on the long-term behavior of emissions. Two treatment methods have become popular. One is re-infiltration of leachate into the waste-body. It minimizes the amount of leachate to be discharged to the water treatment plant and increases the water content in the waste body. It is hypothesized that biodegradation is enhanced by the increased water content (Khalid et al., 2011, McDougall, 2007, Meima et al., 2008), but also by the induced water flow which improves mixing of bacteria and

substrates through-out the waste-body (White et al., 2011). The other treatment is aerating the landfill with air or pure oxygen. The aerobic conditions significantly reduce methane emissions, decreasing the impact on global warming. In addition aerobic biodegradation is in general faster than anaerobic degradation (Heijnen and Kleerebezem, 1999). Aeration also decreases the levels of dissolved organic matter in the leachate (Hrad et al., 2013, Ritzkowski et al., 2006) which leads to reduced emissions of heavy metals (Dijkstra et al., 2006). Both treatment methods are successful in reducing short-term emissions, however, it still needs to be confirmed if they are effective in reducing long-term emissions.

1.2. Sustainable After-care

The Netherlands is the only country in the world where the landfill regulations explicitly state that after-care is eternal. After the operational period, landfills are fitted with a water tight cover which has to be maintained for ever. Funds for the after-care have to be accrued during the active period of landfilling and eventually pass from the landfill operator to the competent authority (Scharff, 2014). Given the high cost of the after-care and the fact that eternal after-care is not sustainable, Dutch landfill operators have started a program aiming to introduce so called sustainable after-care approaches which no longer require the installation of an impermeable cover. The idea of these approaches is to try to actively reduce the emission potential of waste bodies by recirculation of leachate and aeration in order to achieve a condition where long-term emissions no longer pose a threat to HHE. In 2006 this led to an agreement with the national and local authorities which allows the Dutch landfill operators to carry out three pilot projects to test the sustainable after-care approaches in full scale landfills.

In order to demonstrate the impact of the sustainable approaches on the long term emission potential, the mechanisms underlying emissions need to be understood and modeled; the black box must be opened. A major challenge is to develop approaches which allow to estimate emissions from full scale waste-bodies. Waste-bodies which can have volumes of several 100 thousands cubic meters and contain thousands of compounds which are part of a huge number of different materials. Realizing this makes it obvious that no models can be created which include all processes and heterogeneity required in full detail. It is also clear that simple prediction models or sampling procedures will have high uncertainty due to significant errors and reducing these errors by increasing the measurement effort is economically not realistic. This all leads then to the main question for this thesis: **How to quantify the emission potential of a landfill?**

The research done for this PhD-thesis shows that the rates of processes in an environment are generally controlled by a set of dominant processes which can be characterized via modeling using relatively simple measurements and comparison of results with known data from the literature. The insight obtained can then be used to optimize treatment approaches for reducing long-term emissions and to develop approaches to quantify the emission potential of a MSW landfill.

1.3. Structure of this Thesis

In chapters 2 and 3, a numerical toolbox is presented which was developed to quantitatively characterize those processes which control the measured gas and leachate emissions. The toolbox allows us to identify and quantify the set of dominant reaction processes in MSW at the lysimeter scale under both anaerobic and aerobic conditions. The numerical toolbox has been applied to data sets published in the literature and implications for the efficiency of leachate recirculation and aeration methods are discussed based on the obtained results. In chapter 4, the quantitative description of reaction processes in MSW is used to describe the leachate development of a full-scale landfill waste body.

Chapter 5 reports the findings of optimizing the aeration strategy in a full-scale waste body with a 3D-model. Different aeration scenarios and well spacing dimensions have been tested and the implications of distribution of water and gas on the dominant biodegradation reactions and leaching processes are described. Chapter 6, gives a summary of the main consequences of the findings from this thesis in the context of quantification of emission potential and the implementation of full-scale treatment methods to reduce the impact of long-term emissions to HHE. Some remaining knowledge gaps to quantify emission potential and suggestions how to investigate them are indicated.

2

A toolbox to find the best mechanistic model to predict the behavior of environmental systems

Reliable prediction of the long-term behavior of environmental systems such as Municipal Solid Waste (MSW) landfills is challenging. While many driving forces influence this behavior, characterization of them is limited by measurement techniques. Therefore, a model structure for reliable prediction needs to optimally combine all measured information with suitable mechanistic information from literature. How to get such an optimal model structure? This study presents a toolbox to find and build the model structure that describes an environmental system as close as possible. The toolbox combines environmental frameworks to include all suitable mechanistic information; it fully couples kinetic and equilibrium reactions and contains multiple resources to obtain biogeochemical parameters. Several possible optimal model structures are quickly built and evaluated with objective statistical performance criteria obtained via Bayesian inference. By applying the novel methodology, we select the best model structure for anaerobic digestion of MSW in full scale landfills.

This chapter has been published in Environmental Modelling & Software **344-355**, 83 (2016) (van Turnhout et al., 2016).

2.1. Introduction

It is challenging to make reliable predictions of the long-term behavior of environmental systems such as Municipal Solid Waste (MSW) landfills. In such systems, there are many driving forces influencing behavior, while current measurement techniques are not sufficient to characterize them. Therefore, for reliable predictions we require a mechanistic description with minimal uncertainty for extrapolation of measured data.

Reliable prediction of long-term emissions is needed for landfill management. Decisions about ending of landfill after care strongly depend on these predictions because after care can only be stopped when emissions are below certain threshold values. Furthermore, reliable predictions also improve estimations of energy recovery from emissions such as methane. This energy is directly utilized in the facilities at the landfill.

So far, prediction of emissions by any modeling strategy is highly uncertain. In general, models have been developed according to two strategies. One strategy extrapolates measured emissions using empirical relations. Some of these models fit exponential equations to measured gas and leachate data (Fellner et al., 2009, Gönüllü, 1994, Kamalan et al., 2011, Scharff et al., 2011). Others apply neural networks on emission data (Karaca and Özkaya, 2006, Ozkaya et al., 2007). Although the fit of these empirical models with measured data is very good, their extrapolations are poor because these models are not constrained by mechanistic principles. These models do not consider the impact of changes in environmental conditions on the emissions while multiple studies have shown that e.g. pH and mass transport limitation significantly influence the performance of waste water and solid waste treatment(Angelidaki et al., 1999, Batstone et al., 2002, Siegrist et al., 2002, Vavilin et al., 2003, Veeken and Hamelers, 2000).

The other modeling strategy to predict emissions is mechanistic (Garcia de Cortazar and Monzon, 2007, Gawande et al., 2010, Kouzeli-Katsiri et al., 1999, McDougall, 2007, Reichel et al., 2007, White et al., 2004). These models vary a lot in complexity and the type of mechanistic information they include. Model concepts range from single point to three dimensional implementation and from a single type of framework such as biochemistry to frameworks coupling biochemistry, hydrology and settlement. Although these models do restrict their predictions with mechanistic principles and have given interesting insights, their prediction accuracy is often also very poor. Prediction with these models is poor because the uncertainty in mechanistic assumptions is very large, especially for very complex models. In addition it is difficult to reduce this uncertainty by model calibration because measured data is limited. The large uncertainty in mechanistic correctness is reflected by the wide spread of parameter values published in literature (Meima et al., 2008).

To improve prediction accuracy, the challenge is to select a model structure that is constrained by mechanistic principles and has minimum uncertainty in assumptions. In order to find such a model, a more objective integrated assessment of environmental systems is needed (Kelly et al., 2013, Vrugt, 2016) in which model performance evaluation is generalized (Bennett et al., 2013). This type of assessment requires several prerequisites for developing models. First, mechanisms from

different environmental fields should be available to be combined in order to include all suitable mechanistic information. Second, well established mechanistic parameters with relative low uncertainty should be readily obtainable from databases or derivation methods. Third, model performance should be able to be analyzed qualitatively and quantitatively. Statistical analysis of the remaining uncertainty in parameters in light of the measured data should allow us to quantify the uncertainty in model structure, calibrated parameter values and mechanistic correctness of the model. Finally, multiple reaction networks should be able to be quickly built and the results quickly assessed in order to find the optimal model. Current modeling approaches do not fulfill all these prerequisites and therefore limit the possibility to find optimal models for prediction purposes.

The aim of this study is to develop a methodology that includes all the prerequisites previously mentioned in order to enable us to find an optimal mechanistic model for anaerobic degradation of MSW. The toolbox allows us to quickly build mechanistic biogeochemical reaction networks that may include kinetic reactions, equilibrium reactions and environmental inhibitions in a multi-phase system. Parameter values are obtained from an extensive geochemical database (Meeussen, 2003), a derivation method based on thermodynamic principles (Kleerebezem and van Loosdrecht, 2010) and calibration based on measured data. Performances of these reaction networks are evaluated quantitatively with statistical criteria obtained by applying Bayesian inference with the DREAM algorithm (Laloy and Vrugt, 2012, Vrugt et al., 2003). We illustrate our generic approach by finding an optimal mechanistic model for describing a data set measured on a series of landfill lysimeters, previously published by Valencia et al. (Valencia et al., 2009a,b,c, 2011, Valencia Vazquez, 2008), by evaluating four possible reaction networks. Our aim is to find a description which we can apply to full-scale anaerobic landfills.

2.2. Theory

2.2.1. The cycle of finding an optimal model structure

The toolbox we present here is a novel combination of several approaches enabling us to find an optimal mechanistic model for describing measured data. This method follows the scheme depicted in figure 2.1 and allows a generic evaluation of model performance such as proposed by Bennett et al. (2013). We start by defining a first possible mechanistic reaction network which should provide a good fit to the measured data.

Subsequently, this reaction network is evaluated qualitatively by plotting the modeled data against the measured data and quantitatively by using a range of performance criteria which we obtain by applying Bayesian inference on the most uncertain parameters. These criteria allow us to judge aspects such as mechanistic correctness, parameter identifiability, model uncertainty, model sensitivity and model complexity. Based on the results and the purpose of the model, we decide if the model describes the measured data with sufficient (mechanistic) accuracy. If the accuracy is not sufficient, a next iteration is started where an update to the reaction network is evaluated until an optimal model is found. All prerequisites

combined in the toolbox are discussed in detail below.

Figure 2.1: Scheme for finding an optimal mechanistic description for measured data with the toolbox

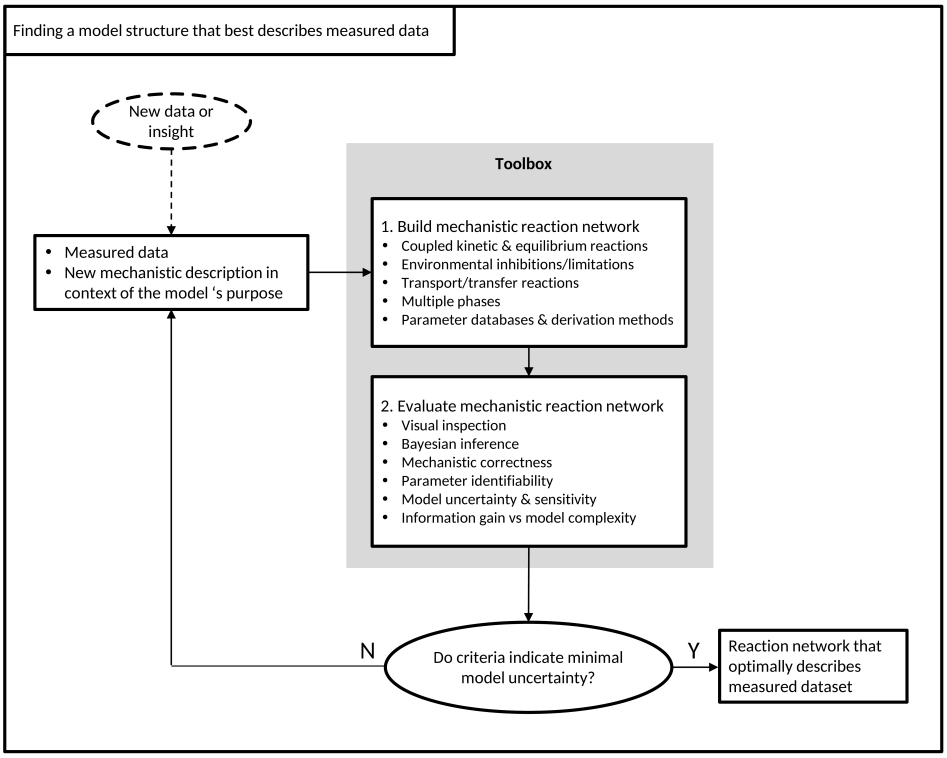

2.2.2. Defining the model structure with mechanistic information from different environmental frameworks

Multiphase, multicomponent and multiprocess environment

Model structures can be built that contain biogeochemical reaction networks within a multiphase environment with mass transport across the model domain and mass transfer between the phases. A schematic example of such a structure is given in figure 2.2. The model describes the fate of chemical compounds present in the solid, gas and liquid phase. In each phase we track the change of the total concentrations ($C_{\mathrm{ref}}^{\mathrm{T}}$) and derived concentrations (C^{D}) as a function of time. Total concentrations are calculated with the mass balances of building blocks of species e.g. H^{+} and $\mathrm{CO_3}^{-2}$ which are expressed in terms of one reference species. Using chemical equilibrium approaches, we can calculate the derived concentrations from the set of total concentrations (i.e. mass balances). Changes in total concentrations with time are caused by kinetic processes which can be either biochemical redox reactions, transfer of compounds between phases and transport in or out of the model domain. Biochemical reactions are influenced by environmental inhibitions

and limitations.

To support quick implementation of a model structure, it is completely defined within a single spreadsheet and solved with a generic matrix calculation method.

Figure 2.2: Schematic example of a model structure that can be build with the toolbox

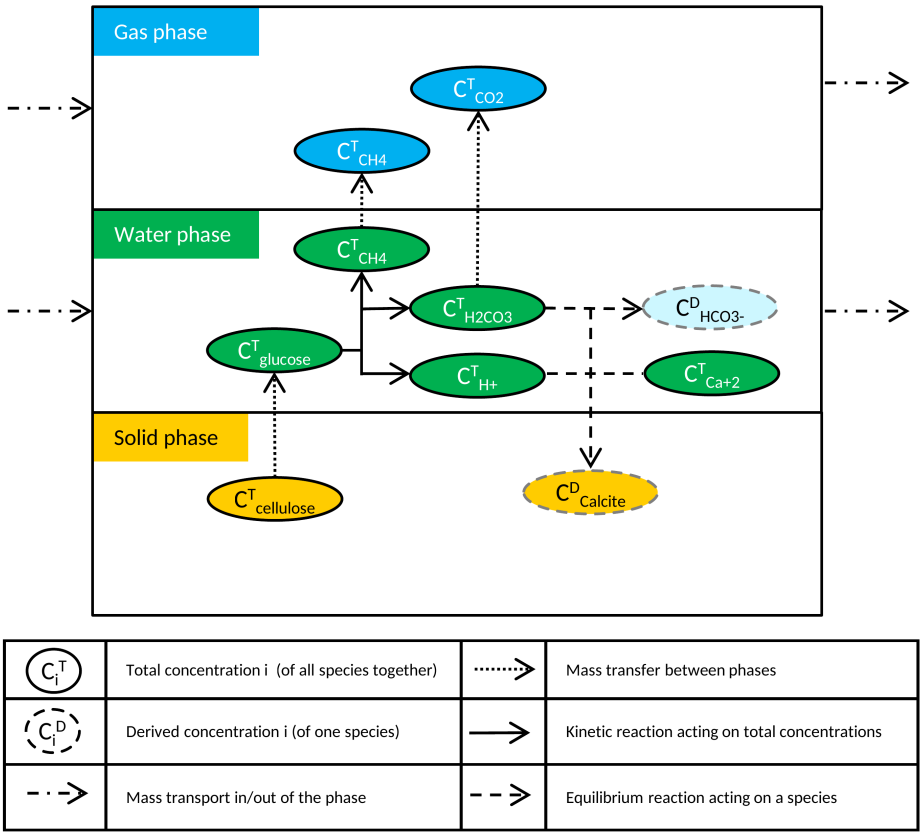

Fully coupled rate dependent and equilibrium processes

Rate dependent processes and equilibrium processes are fully coupled within the model structure. This means that all derived concentrations are automatically recalculated when the total concentrations change because of biochemistry and transport or transfer processes. For example, the total concentration of H_2CO_3 in a standard water-carbonate system (i.e. $C^T_{H_2CO_3}$, $C^T_{Ca^{+2}}$ and $C^T_{H^+}$) changes because of gas production. The model updates the $C^T_{H_2CO_3}$ and as a result the pH and concentrations of CO_3^{-2}, HCO_3^-, H_2CO_3 and $CaCO_3$ are automatically updated. Full coupling allows accurate calculation of derived concentrations and their influence on the rate dependent processes in the system. Details on how to derive concentrations from mass balances according to equilibrium reactions are given in Bethke

et al. (2008) .

Type of rate dependent processes

Biogeochemical reaction rates ($R^{\mathrm{K}}_{C_{\mathrm{i}}^{\mathrm{T}}}$) are implemented as

$$R^{\mathrm{K}}_{C_{\mathrm{i}}^{\mathrm{T}}} = \mu^{\max} \cdot C^{\mathrm{T}'} \cdot I \cdot s_{\mathrm{i}} \tag{2.1}$$

where $\mu^{\max}$ is the maximum rate, $C^{\mathrm{T}'}$ is the concentration that drives the reaction, I is the total inhibition factor ranging from 0 to 1 and s_{i} is the stoichiometry. This type of reaction supports Monod kinetics when the inhibition factor is (partly) determined by substrate limitation and the total concentration of bacteria is set as the driving concentration.

The rates of change in the liquid phase ($\mathrm{p_l}$) and the gas phase ($\mathrm{p_g}$) due to the presence of a mass transfer flux between phases are implemented as

$$F^{\mathrm{MF}}_{C_{\mathrm{i}}^{\mathrm{T,p_l}}} = k_{\mathrm{l}}a \cdot \left(C_{\mathrm{i}}^{\mathrm{p_l}'} - C_{\mathrm{i}}^{\mathrm{p_g}'} \cdot K_{\mathrm{H}} \cdot R \cdot T \right) \tag{2.2}$$

$$F^{\mathrm{MF}}_{C_{\mathrm{i}}^{\mathrm{T,p_g}}} = F^{\mathrm{MF}}_{C_{\mathrm{i}}^{\mathrm{T,p_l}}} \cdot \frac{V_{\mathrm{l}}}{V_{\mathrm{g}}} \tag{2.3}$$

where $k_{\mathrm{l}}a$ is the mass transfer constant, $C^{\mathrm{p_l}'}$ and $C^{\mathrm{p_g}'}$ are the driving concentrations (total or derived) in the water phase and the gas phase, K_{H} is the Henry coefficient, T is the temperature, R is the universal gas constant, V_{l} is the volume of the water phase and V_{g} is the volume of the gas phase.

The rate of change due to a mass transport flux ($F^{\mathrm{MT}}_{C_{\mathrm{i}}^{\mathrm{T}}}$) is implemented as

$$F^{\mathrm{MT}}_{C_{\mathrm{i}}^{\mathrm{T}}} = \frac{\phi \cdot C_{\mathrm{i}}^{\mathrm{T}}}{V} \tag{2.4}$$

where ϕ is the mass transport flow and V is the volume of the phase.

Type of equilibrium processes

Two types of equilibrium processes can be implemented in a model structure. The first type is a true equilibrium reaction relating concentrations of species according to mass action law. The second type is an equilibrium between the gas and the liquid phase. This equilibrium is implemented using mass transfer reactions (eq. 2.2) with high values for $k_{\mathrm{l}}a$.

Environmental inhibitions and limitations

Rate inhibiting and limiting reaction terms are implemented using four mechanisms of biochemical reactions taken from environmental studies (equations 2.5 to 2.8). These are substrate limitation (f^{SL}) (Monod, 1949), non-competitive inhibition (f^{NC}) (Haldane, 1930), inhibition of sulphate reduction by sulfide (f^{SS}) and inhibition of sulphate reduction by protonated Volatile Fatty Acids (VFA) (f^{SA})

(Rzeczycka and Blaszczyk, 2005). In these equations, C_{inh} is the inhibiting concentration (either a total or derived concentration), K_{inh} is the inhibition or half saturation constant and l is a shape parameter. Each mechanism gives an inhibition factor f ranging from 0 to 1. Multiplication of all inhibition factors acting on a biochemical reaction gives its total inhibition factor I (eq. 2.1).

$$f^{\mathrm{SL}}_{(C_{\mathrm{inh}})} = \frac{C_{\mathrm{inh}}}{C_{\mathrm{inh}} + K_{\mathrm{inh}}} \tag{2.5}$$

$$f^{\mathrm{NC}}_{(C_{\mathrm{inh}})} = \left(\frac{K_{\mathrm{inh}}}{K_{\mathrm{inh}} + C_{\mathrm{inh}}}\right)^{l} \tag{2.6}$$

$$f^{\mathrm{SS}}_{(C_{\mathrm{inh}})} = \left(1 - \frac{C_{\mathrm{inh}}}{K_{\mathrm{inh}}}\right)^{l} \tag{2.7}$$

$$f^{\mathrm{SA}}_{(C_{\mathrm{inh}})} = \left(1 + \left(\frac{C_{\mathrm{inh}}}{K_{\mathrm{inh}}}\right)^{l}\right)^{-1} \tag{2.8}$$

Selecting mechanistic parameter values from databases and derivation methods

Parameter values or bandwidths are entered into the spreadsheet where the model structure is defined. The geochemical parameters for the equilibrium reactions are automatically retrieved from an extensive geochemical database which is part of the Orchestra chemical equilibrium model (Meeussen, 2003). A wide variety in validated geochemical equilibria can be selected. As an option, activity correction can be calculated with the Davies equation.

Stoichiometry and rate parameters of biochemical metabolic reactions can be derived from thermodynamic principles with an additional spreadsheet. This derivation method is adapted from Kleerebezem and van Loosdrecht, (2010). It allows to constrain the model with established mechanistic information.

As an example, we illustrate the method with the derivation of a metabolic reaction for methanogenesis. Metabolism is a combination of catabolism (releasing energy) and anabolism (biological growth) which are coupled using the yield factor,

$$Y_{\mathrm{xs}} = \frac{\mathrm{CmolX}}{\mathrm{CmolS}} \tag{2.9}$$

which specifies how much growth (X) occurs from substrate (S) given the amount of energy generated by the catabolic reaction. CmolX is the number of moles of C in the biomass and CmolS is the number of moles of C in the substrate. The redox half reactions for catabolism can be written as

$$1\mathrm{C_2H_3O_2^-} + 2\mathrm{H_2O} \rightleftharpoons 2\mathrm{CO_2} + 7\mathrm{H^+} + 8\mathrm{e^-} \tag{2.10}$$

$$1\mathrm{C_2H_3O_2^-} + 9\mathrm{H^+} + 8\mathrm{e^-} \rightleftharpoons 2\mathrm{CH_4} + 2\mathrm{H_2O} \tag{2.11}$$

which combine to the following catabolic reaction:

$$1C_2H_3O_2^- + 1H^+ \rightleftharpoons 1CO_2 + 1CH_4. \tag{2.12}$$

Following the same principle, the anabolic reaction is as follows,

$$0.5C_2H_3O_2^- + 0.3H^+ + 0.2NH_4^+ \rightleftharpoons 1CH_{1.4}O_{0.4}N_{0.2} + 0.6H_2O \tag{2.13}$$

where we assume the generic molecular composition of bacteria ($CH_{1.4}O_{0.4}N_{0.2}$) to be the same as used by Henze et al. (1995).

The growth yield is calculated with the method proposed by Kleerebezem and van Loosdrecht, (2010). This is a partially empirical method based on the Gibbs reaction energy of the catabolic and anabolic reaction (Heijnen and Kleerebezem, 1999). In this case, $Y_{xs} = 0.04$ which leads to the following total metabolic reaction:

$$\begin{aligned} &12.9C_2H_3O_2^- + 12.7H^+ + 0.2NH_4^+ \rightleftharpoons \\ &\quad 1CH_{1.4}O_{0.4}N_{0.2} + 12.4CO_2 + 12.4CH_4 + 0.6H_2O. \end{aligned} \tag{2.14}$$

In addition to the stoichiometry, also the rate parameters for metabolic reactions can be estimated from thermodynamic principles (Heijnen and Kleerebezem, 1999).

Estimated parameter values can be corrected for temperature using several relations. Maximum rates, equilibrium constants and the solubility of Calcite are corrected with equations 2.15-2.17 respectively (Plummer and Busenburg, 1982, Veeken and Hamelers, 1999). In these equations, T_e is the temperature of the environment, T_r is the reference temperature of the parameter, $\triangle H^0$ is the standard enthalpy, k is 64 $\frac{kJ}{mol}$, a is -171.9065, b is 0.077993, c is 2893.319 and d is 71.595.

$$\ln(\mu_e^{max}) = \ln(\mu_r^{max}) + \ln\left(\frac{k}{R} \cdot \left(\frac{1}{T_r} - \frac{1}{T_e}\right)\right) \tag{2.15}$$

$$\ln(K_e) = \ln(K_r) + \ln\left(\frac{\triangle H^o}{R \cdot T_r^2} \cdot (T_e - T_r)\right) \tag{2.16}$$

$$\log_{10}\left(K_{eq(Calcite)}\right) = a + b \cdot T_e + \frac{c}{T_e} + d \cdot \log_{10}(T_e) \tag{2.17}$$

2.2.3. Solving the model structure with a generic matrix calculation method

The model structure is automatically assembled in to a system of ordinary differential equations (ODE) with a generic matrix calculation method adapted from Reichel et al. (2007). This system of ODEs is fully coupled with the equilibrium calculator ORCHESTRA (Meeussen, 2003). The ODEs are solved in MATLAB and the equilibrium calculator is part of the JAVA memory space of MATLAB. This makes the algorithm very efficient since both solvers use the same memory space while information about the total and derived concentrations are exchanged via a JAVA link.

The set of ODEs for each phase can be written as

$$\frac{\mathrm{d}C^{\mathrm{T,water}}}{\mathrm{d}t} - F^{\mathrm{T,water}} = R^{\mathrm{K}} \tag{2.18}$$

$$\frac{\mathrm{d}C^{\mathrm{T,gas}}}{\mathrm{d}t} - F^{\mathrm{T},gas} = 0 \tag{2.19}$$

where F^{T} are the total fluxes into the respective phase and R^{K} are the total biochemical rates. The total concentrations in the solid phase are included in the ODEs of the water phase and are expressed per volume of water phase. The total fluxes $F^{\mathrm{T},water}$, $F^{\mathrm{T},gas}$ and the total biochemical rates R^{K} are calculated by vector summation over the number of fluxes or reactions j per process,

$$R^{\mathrm{K}} = \mu^{\max} \circ C^{\mathrm{T}'} \circ I \cdot S \tag{2.20}$$

$$F^{\mathrm{T,water}} = \sum_j F^{\mathrm{MT,water}} - \sum_j F^{\mathrm{MF,water}} \tag{2.21}$$

$$F^{\mathrm{T,gas}} = \sum_j F^{\mathrm{MF,gas}} - \sum_j F^{\mathrm{MT,gas}} - x \cdot \sum \left(\sum_j F^{\mathrm{MF,gas}} - \sum_j F^{\mathrm{MT,gas}} \right) \tag{2.22}$$

where $\mu^{\max}$, $C^{\mathrm{T}'}$ and I have size $1 \times j$, $\circ$ is the symbol for element-wise multiplication, S are the stoichiometry with size $j \times n_{\mathrm{l}}$, $F^{\mathrm{MF,water}}$ and $F^{\mathrm{MT,water}}$ have size $j \times n_{\mathrm{l}}$, $F^{\mathrm{MF,gas}}$ and $F^{\mathrm{MT,gas}}$ have size $j \times n_{\mathrm{g}}$ and x are the molar fraction of the total concentrations in the gas phase. The last term in $F^{\mathrm{T,gas}}$ constrains the gas phase with a constant volume and a constant total pressure.

2.2.4. Evaluating model performance

Qualitative evaluation

Model performance is evaluated visually by automatically generated plots combining the model results with the measured data and plots of all modeled states. Because of the strong human capacity for pattern detection, these plots may indicate extreme, under- or non-modeled behavior. In addition, residuals are evaluated with QQ plots and auto-correlation plots.

Applying Bayesian inference

In order to find a model structure which provides the best fit to the data, we also evaluate the outcome of the simulation with several objective criteria. All these criteria are evaluated using the results of Bayesian inference applied to the set of most uncertain parameters (θ). The outcome of Bayesian inference,

$$p\left(\theta|\hat{y}\right) \propto p\left(\theta\right) \cdot L\left(\theta|\hat{y}\right), \tag{2.23}$$

is the joint posterior probability distribution ($p\,(\theta|\hat{y})$) of the set of parameters given the measured data. This distribution reflects the uncertainty in the different parameters. The posterior distribution is calculated from the prior distribution of the parameters ($p\,(\theta)$) and the likelihood of the parameters in light of the measured data ($L\,(\theta|\hat{y})$). The posterior distribution is obtained using an adapted version of the DREAM$_{(ZS)}$ algorithm (Laloy and Vrugt, 2012, Vrugt et al., 2003) where algorithmic settings and parameters are set to the recommended and default values.

The toolbox uses a Gaussian objective function, which includes the set of standard deviations of total error (σ) for each subset of data, to evaluate the likelihood,

$$\ln\left(L\left(\theta|\hat{y}\right)\right) = -\frac{n}{2}\cdot\ln\left(2\pi\right) - \sum\ln\left(\sigma\right) - \frac{1}{2}\cdot\sum\left(\frac{\hat{y}-y}{\sigma}\right)^2 \tag{2.24}$$

where $\mathbf{y}$ is the modeled data and $\sigma = [\sigma^{\text{subset1}}_{(m\times1)}; \sigma^{\text{subset2}}_{(m\times1)}; ...]$ with m being the size of a subset of data and all entries in $\sigma_{(m\times1)}$ have the same value σ^{subset} for that subset. Because it is often difficult to estimate the measurement error, and it is more or less impossible to estimate the model error, we chose to expand the set of uncertain parameters θ with the standard deviations σ^{subset} for each dataset.

Prior distributions of uncertain model parameters are assumed to be uniform with an initial search range that is $100\times$ wider to ensure global convergence. Prior distributions of standard deviations are also uniform ranging from $\frac{1}{5}\cdot\sigma^{\text{subset}}$ to $5\cdot\sigma^{\text{subset}}$. Ranges in the prior distributions can be different for other problems.

Quantitative criteria

The result from the Bayesian inference allows us to quantitatively compare the performance of different model structures. Since our modeling objective is to find the model structure with minimal (mechanistic) uncertainty, we implemented criteria that quantify aspects related to this. For other modeling objectives, other criteria/metrics (Bennett et al., 2013, Vrugt, 2016) may be more suited which are readily implemented.

One criterion is the difference in best fit or lowest total error (measurement error & model error) between model structures. In addition, we can also assess the probability distribution of total errors which is related to the combined probability distributions in calibrated parameters. The latter directly reflects the uncertainty of the complete model structure in light of the measured data. Even more, the uncertainty of total error per subset of data can be compared between models with the marginal probability distributions of the standard deviations.

A second criterion is the uncertainty in calibrated parameters for different model structures. Parameter uncertainty is quantified by the width of its marginal posterior distribution. A wider distribution indicates more uncertainty under the condition of the same prior distribution. For a quantitative comparison, the gain of information from marginal prior to marginal posterior for parameter i can be quantified with the Kullback-Leibler divergence (D_{KL}). This metric,

$$D_{\text{KL}} = \int\left(p\left(\theta_i|\hat{y}\right)\cdot\ln\left(\frac{p\left(\theta_i|\hat{y}\right)}{p\left(\theta_i\right)}\right)\cdot\mathrm{d}\theta_i, \tag{2.25}$$

is a non-symmetric measure of the dissimilarity between two probability distributions. Higher values of D_{KL} indicate a larger information gain and therefore less uncertainty.

A third criterion is the presence of correlations between parameters in the model structure which can be seen in the marginal posterior distributions. These correlations point to possibilities for optimizing model structure by adding restrictions or lumping of correlated parameters.

A fourth criterion is the mechanistic completeness of model structure. Mechanistic completeness is evaluated by comparing the calibrated parameter bandwidths (i.e. 5%-95% quantiles) with 'ideal' parameter values measured under non-limiting conditions. A close match between calibrated parameters and 'ideal' values indicates a mechanistically complete model structure. Parameters that strongly deviate from 'ideal' values indicate missing mechanistic processes.

A final criterion is the amount of information a model structure provides given its complexity. More complex models with a large number of parameters can be compared with simpler ones with the marginalized likelihood (L^{m}) which is the probability of the measured data given the model structure, not assuming any particular model parameters. It can be approximated with the harmonic mean of likelihoods (Newton and Raftery, 1994),

$$L^{\mathrm{m}} = \left(\frac{1}{N} \sum_{i=1}^{N} L\left(\theta|\hat{y}\right)^{-1} \right)^{-1} \tag{2.26}$$

where N is the number of likelihoods. The model structure with the highest marginal likelihood has the best balance between information content and model complexity.

2.3. Results

2.3.1. The final four evaluated biogeochemical reaction networks

The dataset we used for testing our toolbox was obtained from Roberto Valencia (Valencia et al., 2009b, Valencia Vazquez, 2008). We present the final four model structures that were the outcome of our search for an optimal model with the methodology provided by the toolbox. These four reaction networks are schematically depicted in Figure 2.3. In this figure, the most simple network 1 is presented with black lines. Our hypothesis for this network is that four kinetic reactions control the measured emissions. The first one is hydrolysis lumped with acidogenesis. It converts the available biodegradable Solid Organic Matter (SOM) into a mix of Volatile Fatty Acids ($\mathrm{VFA_{mix}}$) with hydrolysis as rate limiting step. The second one is methanogenesis which converts the $\mathrm{VFA_{mix}}$ into methane and carbon dioxide. The final two reactions are decay of the two types of bacteria involved in lumped hydrolysis and methanogenesis with rates which are 5% of the maximum growth rates (Angelidaki et al., 1999). Furthermore, only methanogenesis is influenced by substrate limitation of $\mathrm{VFA_{mix}}$. The stoichiometry of the kinetic reactions is listed

in table 3.2. We included the most common geochemical equilibrium reactions assuming a readily available excess of $\mathrm{Calcite}$ to represent the high alkalinity of MSW. In addition, we assume that the exchange between concentrations in the gas and liquid phases is instantaneous.

According to the experimental design, gas vents to the atmosphere and no other transport flows are included. Because leachate was recirculated during the experiment, we simplified the problem to ideally mixed batch conditions. Model parameters which we considered to be well known are taken from literature. These parameter values are listed in table 2.2 together with the initial experimental conditions. The model parameters which we considered to be unknown or uncertain are listed in table 2.3 together with the prior ranges found in literature. These unknown parameters in the model's reaction network are obtained via Bayesian inference which fits the model outputs to the measurements.

For reaction network 2, we increased the complexity by adding the main environmental inhibitions that are known to influence the kinetic reactions in wastewater treatment. These inhibitions are non-competitive inhibition of hydrolysis by pH and total concentration of $\mathrm{VFA_{mix}}$ and non-competitive inhibition of methanogenesis by pH and ammonia.

In reaction network 3, we further increased the complexity by adding a kinetic ammonium oxidation reaction. We implemented this reaction to find an explanation for the decreasing measured ammonium concentration in time which normally does not occur under anaerobic conditions.

Finally, network 4 extends the reaction network further in order to include sulphate and sulfide. These compounds are usually present in anaerobic environments and are known to inhibit methanogenesis and oxidize available biodegradable SOM. Adding mechanistic information about these processes may therefore optimize model performance. The following is included: 1) a kinetic sulphate reduction reaction, 2) corresponding equilibrium reactions, 3) inhibition of methanogenesis by $\mathrm{H_2S}$ and 4) inhibition of sulphate reduction by $\mathrm{H_2S}$ and protonated $\mathrm{VFA_{mix}}$.

Figure 2.3: Schematic representation of the final four reaction networks that were evaluated.

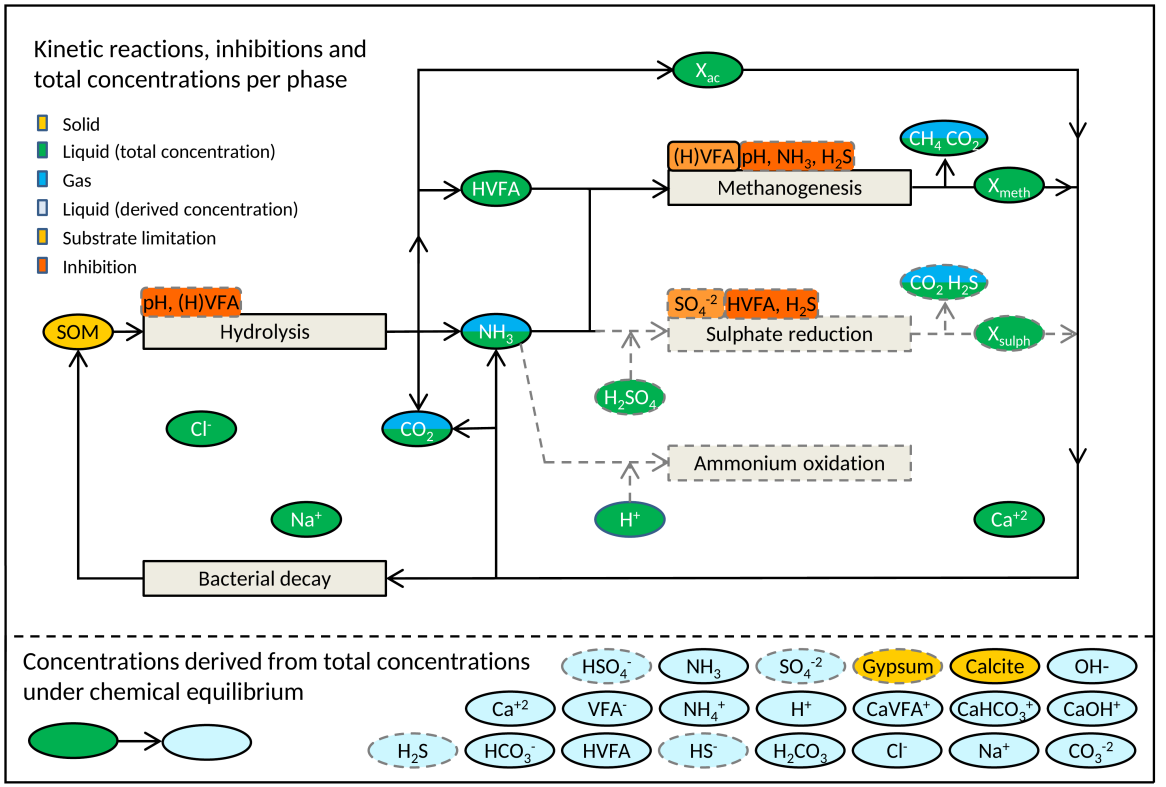

The most basic reaction network 1 is presented with the black lines. Complexity is increased stepwise from network 1-4 which is indicated by the dashed gray lines. Network 2 includes inhibition of hydrolysis by pH and $C^{T}_{VFA_{mix}}$ and inhibition of methanogenesis by pH and ammonia. In network 3, an ammonium oxidation reaction is added. Network 4 is extended with sulphate reduction for which total concentrations, derived concentrations and inhibitions are included accordingly. X represents bacterial biomass. Compounds that are in equilibrium between the gas phase and the liquid phase have two colors.

Table 2.1: Stoichiometry for the total concentrations in the biochemical reactions

	$SOM^{3)}$	$VFA_{mix}{}^{3)}$	H_2CO_3	NH_3	H_2O	CH_4	$SO_4{}^{-2}$	H_2S	X_{acid}	X_{meth}	X_{sulph}	H^+
Hydrolysis[1)]	-1	0.3	0.01	0.024	-0.088	-	-	-	0.18	-	-	-
Methanogenesis	-	-6.67	7.23	-0.2	-8.76	9.37	-	-	-	1	-	-
Decay[2)]	0.92	-	0.08	0.14	-0.42	-	-	-	(-1)	(-1)	(-1)	-
Ammonium oxidation	-	-	-	-1	-	-	-	-	-	-	-	-1
Sulphate reduction		-10.6	27.1	-0.2	-27.1		-15.3	15.3			1	-30.5

The gray cells highlight the reaction driving concentrations. 1) In this reaction, the growth yield for acidogenesis on glucose is used: $Y_{XS} = 1.09$. 2) Each bacterial biomass (X) decays individually. 3) The elemental compositions of SOM is $CH_{1.79}O_{0.63}N_{0.06}$ and VFA_{mix} is $C_{2.64}H_{5.28}O_2$ which were derived from the data measured in the lysimeter experiments.

Table 2.2: Model parameters and initial conditions

			K_{inh}	l		Initial conditions			
μ_{aci}^{max}	0.12	2)	$f_{(hyd,C_{H^+}^D)}^{NC}$	1×10^{-5}	2	3)	$C_{SOM}^{T1)}$	5.44	$C_{Cl^-}^T$	0.1
μ_{decay}^{max}	$0.05 \cdot \mu_{growth}^{max}$	2)	$f_{(hyd,C_{VFA}^T)}^{NC}$	2.34×10^{-2}	1	3)	$C_{SO_4{}^{-2}}^T$	0.16	V_g	250
K_{H,CH_4}	1.5×10^{-3}	4)	$f_{(meth,C_{H^+}^D)}^{NC}$	5×10^{-7}	2	3)	$C_{NH_3}^T$	0.065	p_{tot}	1
K_{H,NH_3}	71.4	4)	$f_{(meth,C_{NH_3}^D)}^{NC}$	1.5×10^{-3}	1	3)	$C_{H_2CO_3}^T$	1.13	T	303
K_{H,H_2S}	0.11	4)	$f_{(meth,C_{H_2S}^D)}^{NC}$	4.29×10^{-2}	1	5)	$C_{Ca^{+2}}^T$	1.16	pH	6.15
K_{H,H_2O}	2.3×10^3	4)	$f_{(sulph,C_{H_2S}^D)}^{SS}$	1.61×10^{-2}	0.401	6)	$C_{Na^+}^T$	0.2	V_l	325
K_{H,CO_2}	0.03	4)	$f_{(sulph,C_{HVFA}^D)}^{SA}$	9×10^{-4}	1.08	6)				

1) Initial concentration of SOM is taken from the total amount of carbon produced as biogas in the experiment. 2) Angelidaki et al. (1999). 3) Siegrist et al. (2002). 4) Atkins and de Paula (2011). 5) Paula Jr and Foresti (2009). 6) Rzeczycka and Blaszczyk (2005). Units of maximum rates, Henry constants, inhibition constants, concentrations, temperatures, pressures and volumes are respectively d^{-1}, $\frac{mol}{L.atm}$, $\frac{mol}{L}$, $\frac{mol}{L}$, atm, K and L. All parameter values are corrected for 303K except $K_{inh,C_{H_2S}^D}$ (298 K).

2.3.2. Outcome of the Bayesian inference applied on the four networks

The result of the Bayesian inference allows us to evaluate the quality of performance of our four model structures. We start with the most basic evaluation, visual inspection of fit. Figure 2.4 presents the modeled data with the highest likelihood (in red) and the related uncertainty bandwidths (in green) together with the measured data (in blue) for each network. Visual inspection clearly shows that some networks perform better than others. The fit for the cumulative biogas is better in networks $2-4$ and the fit for ammonium concentration is better in networks $3-4$. In addition, the uncertainty is lower in networks $2-4$ indicated by slightly narrower green bandwidths.

Visual judgment, however, reveals very little about the mechanistic correctness and parameter uncertainty in the models. The D_{KL} values in table 2.3 indicate the uncertainty of the calibrated parameters relative to the different model structures. Higher values mean lower uncertainty. The uncertainty in the calibration of $K_{\mathrm{inh},C_{\mathrm{VFA}}^{\mathrm{T}}}^{\mathrm{SL(meth)}}$, for example, is much lower for network $2-4$ than network 1. Preferably, we select a model with a low uncertainty in all calibrated parameters. The uncertainty in the total error for each subset of data is shown per network by the D_{KL} values of the standard deviations. This shows for instance that the uncertainty for the subset of ammonium is much lower in networks $3-4$ than networks $1-2$.

The posterior bandwidths ($5\%-95\%$ quantiles) in table 2.3 reveal how close the calibrated parameters are to 'ideal' values measured under non-limiting conditions. Parameters that are close are indicated in bold. Ideally for mechanistic completeness, all calibrated parameters should be close to 'ideal' values. Network $2-4$ are therefore more mechanistic correct than network 1 because the calibrated bandwidths of $\mu_{\mathrm{hyd}}^{\mathrm{max}}$ and $\mu_{\mathrm{meth}}^{\mathrm{max}}$ are closer to 'ideal' values.

Most parameters in the networks are not correlated except for the maximum rate and the half saturation constant of methanogenesis in the less complex networks. These correlations are presented in Figure 2.5. Interestingly, the correlation becomes weaker as the complexity and mechanistic information content of the model structures increases.

The log-normal marginal likelihoods-values in figure 2.4 show the performance of the networks with respect to the balance of information content (model complexity) versus model uncertainty. They show that although network 4 is most complex, the added information improves the maximum likelihood without increasing model uncertainty too much.

When evaluating model uncertainty based on statistics, it is important to check if the statistical assumptions applied are valid. This means that the probability of the residuals should be normally distributed because we apply a Gaussian likelihood. We check this with Q-Q plots and normalized autocorrelation functions (ACF) for the residuals of the best fit results of network 4 which are presented in figure 2.6. The Q-Q plots show residual quantiles (in blue) vs quantiles from the theoretical normal distribution. When the residual quantiles are normally distributed they should coincide with the theoretical red line. Apparently, not all residuals are normally distributed. Therefore, some error is present in the statistical evidence we apply to

evaluate our models. The same violation of normal distribution is indicated by the autocorrelation of the residuals. However, for the type of evaluations we apply this statistical error has minimal impact. If one is interested in a more statistical correct evaluation, we suggest to use the general likelihood function presented by Schoups and Vrugt et al. (2010).

Table 2.3: The prior ranges, posterior ranges (5% – 95% quantiles) and information gain (D_{KL}) for the inferred parameter per network

	μ_{hyd}^{max} (d^{-1})		μ_{meth}^{max} (d^{-1})		$K_{inh,C_{VFA}^{T}}^{SL(meth)}$ (mM)		$C_{X_{meth}}^{T(ini)}$ (mM)	
	quantiles	D_{KL}	quantiles	D_{KL}	quantiles	D_{KL}	quantiles	D_{KL}
Prior	0.09-0.26[1)]		0.04-0.47[2)]		0.03-420[2)]		0.27-19[3)]	
Network 1	0.004-0.0045	10.6	0.013-0.029	7.72	330-1318	2.12	**8.6-13.5**	5.70
Network 2	0.052-0.060	7.84	**0.127-0.199**	6.24	**60-152**	4.54	**8.8-12.6**	5.97
Network 3	0.056-0.069	7.30	**0.095-0.167**	6.23	**95.5-184**	4.54	**12.9-25.3**	4.83
Network 4	0.050-0.061	7.55	**0.095-0.145**	6.63	**152-259**	4.24	**14.5-25.8**	4.93

	$\mu_{NH_4}^{max}$ (d^{-1})		μ_{sulph}^{max} (d^{-1})		$K_{inh,C_{SO_4^{-2}}^{T}}^{SL(sulph)}$ (mM)		$C_{X_{sulph}}^{T(ini)}$ (mM)	
	quantiles	D_{KL}	quantiles	D_{KL}	quantiles	D_{KL}	quantiles	D_{KL}
Prior	0.001-1		0.024-2.4[4)]		0.178-0.26[5)]		0.27-19[3)]	
Network 1								
Network 2								
Network 3	0.0044-0.0052	6.94						
Network 4	0.0043-0.0052	6.84	16.47-210	0.26	952-25085	1.06	0.095-120	2.95

	σ_{biogas} (m^3)		σ_{VFA} (mM)		σ_{pH}		$\sigma_{NH_4^+}$ (mM)	
	quantiles	D_{KL}	quantiles	D_{KL}	quantiles	D_{KL}	quantiles	D_{KL}
Prior	3.41-85.2		0.05-1.24		0.16-3.95		0.005-0.136	
Network 1	4.19-5.14	8.86	0.13-0.19	7.47	0.24-0.28	8.82	0.12-0.15	5.93
Network 2	2.12-2.52	9.76	0.12-0.17	7.62	0.27-0.32	8.86	0.14-0.17	5.76
Network 3	2.19-2.62	8.68	0.12-0.17	7.65	0.27-0.32	8.18	0.029-0.036	7.24
Network 4	2.06-2.49	9.64	0.12-0.17	7.58	0.23-0.26	9.11	0.029-0.038	7.06

	σ_{pCO_2} (atm)		σ_{pCH_4} (atm)	
	quantiles	D_{KL}	quantiles	D_{KL}
Prior	0.04-1.01		0.04-1.05	
Network 1	0.12-0.14	7.99	0.11-0.13	8.10
Network 2	0.13-0.16	7.89	0.13-0.16	7.91
Network 3	0.13-0.17	7.87	0.13-0.16	7.82
Network 4	0.13-0.17	7.82	0.13-0.16	7.79

Quantiles that are comparable with 'ideal' values measured under non-limiting conditions are presented in bold. 1) Veeken and Hamelers (1999). 2) Meima et al. (2008). 3) Nopharatana et al. (2007). 4) Rzeczycka and Blaszczyk (2005). 5) Roychoudhury et al. (2003).

Figure 2.4: Measured data and best fit model results for the four reaction networks

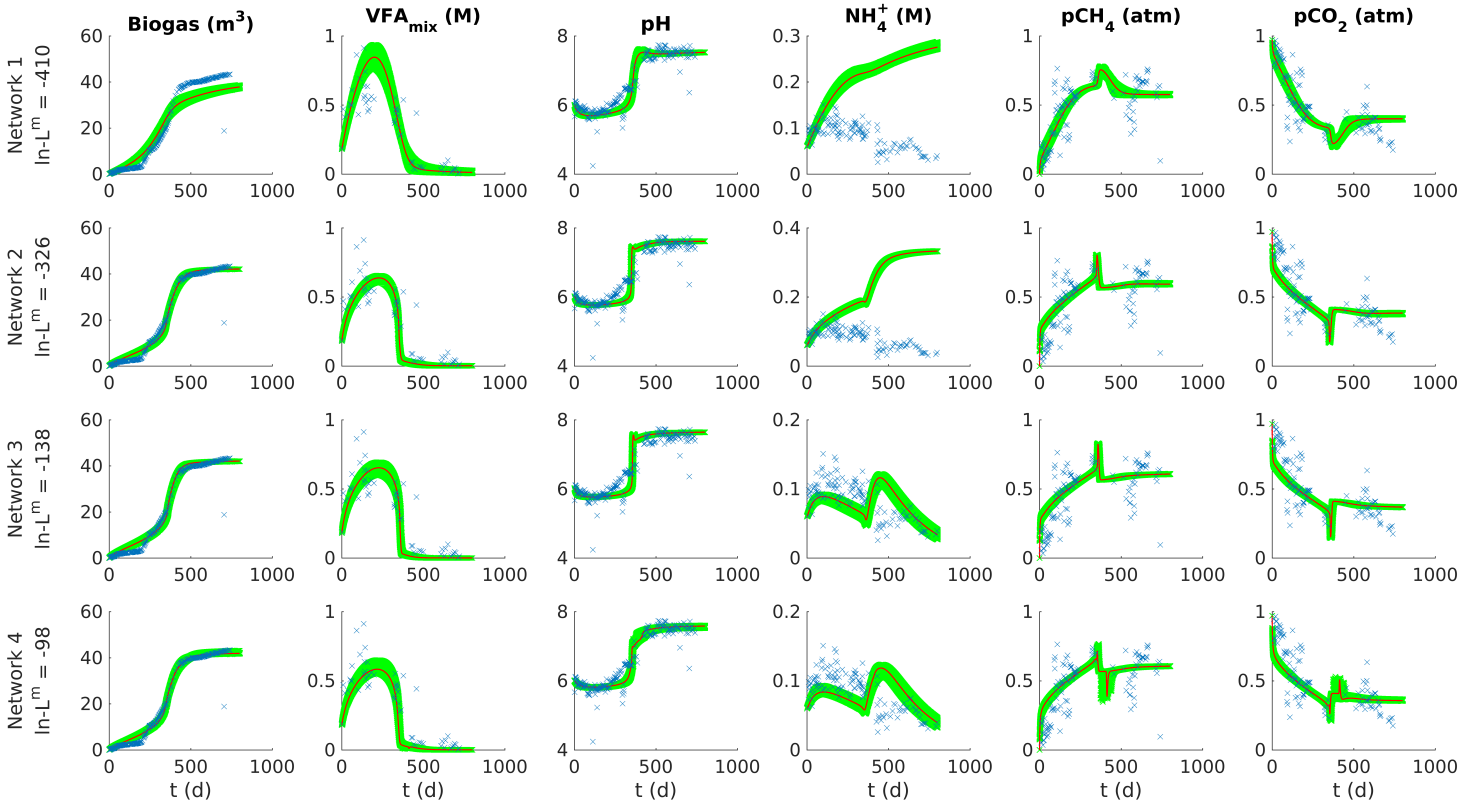

Figure 2.5: Correlations between parameters per network

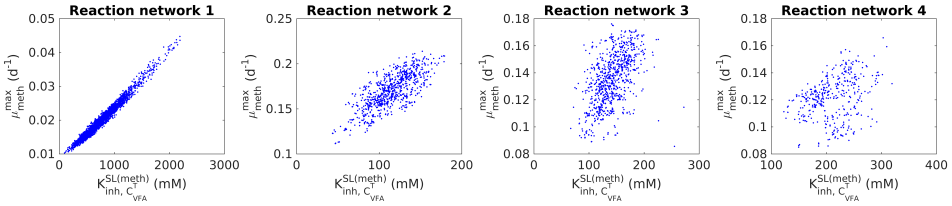

Figure 2.6: Q-Q plots and autocorrelation functions (ACF) per sub dataset of the best fit residuals of reaction network 4

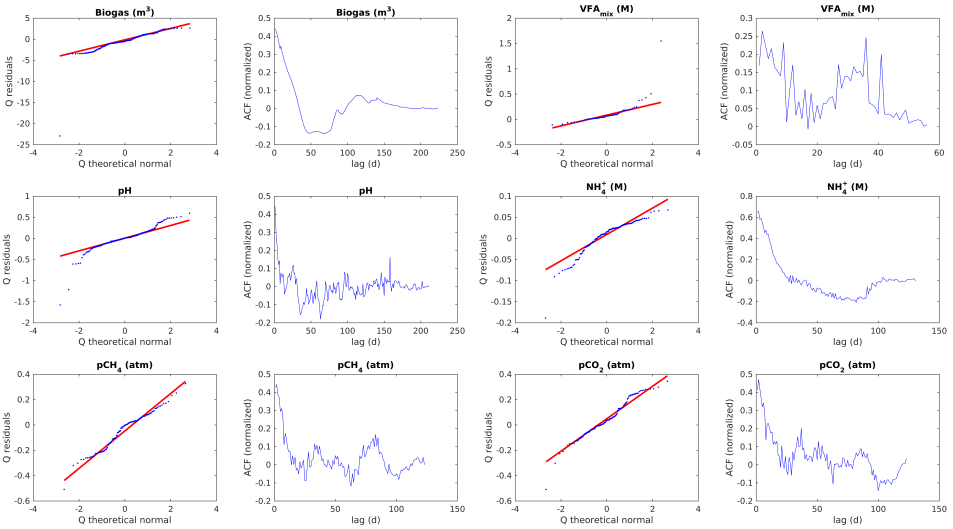

2.4. Discussion & Conclusions

The aim of the methods combined in the toolbox is to choose an optimal network with which we can describe anaerobic digestion of MSW. We believe this novel approach helps to reduce the ambiguity in model structure and calibrated parameter values reported in literature for a given environmental system. It strengthens (qualitative) judgment of model performance by providing quantitative criteria for evaluating (mechanistic) model uncertainty and it allows integrated environmental assessment. As a result, we obtain model structures which allow us to make predictions with a higher certainty because we have included more (objective) information for selecting the reaction network.

2.4.1. Performance of network 1

The most basic reaction network 1 reasonably reproduced a significant portion of the measured data (figure 2.4) with low uncertainty in total error (narrow green bandwidths). The model captures the values and trends of measured $\mathrm{VFA_{mix}}$, pH,

pCH_4 and pCO_2 in time. This good fit was achieved by selecting a set of reactions with the correct stoichiometry and parameter values from well established anaerobic reaction networks from literature, databases and derivation methods. The toolbox optimizes the implementation of such networks.

The model based on reaction network 1, however, does not provide a nice fit to all subsets of data. Using the results from the Bayesian inference, we modified the model structure in order to improve the results. Figure 2.5 shows that $K_{\text{inh},C_{\text{VFA}}^{\text{T}}}^{\text{SL(meth)}}$ is strongly correlated with $\mu_{\text{meth}}^{\text{max}}$. This suggests that both parameters can be lumped together or that another process is being compensated for by the correlation of these two parameters. The results also show that the optimized values of probability distributions of the maximum rates are low compared to 'ideal' values. We concluded that limitations or inhibitions are missing in the reaction network which reduce prediction accuracy and cause the poor fit for cumulative biogas and ammonium.

2.4.2. Performance of network 2

Network 2 is extended with reaction terms which include the main environmental inhibitions acting on hydrolysis and methanogenesis. Assessing the results for this network indicate that this extension significantly improves the model fit of the cumulative biogas. In addition the calibrated maximum rates are in closer agreement with 'ideal' values. We conclude that the mechanistic description is more correct, while all parameters are still identifiable within sharp bandwidths (although some with slightly broader probability distributions than in network 1).

Adding the inhibition terms weakened the correlation between $K_{\text{inh},C_{\text{VFA}}^{\text{T}}}^{\text{SL(meth)}}$ and $\mu_{\text{meth}}^{\text{max}}$. The value of $K_{\text{inh},C_{\text{VFA}}^{\text{T}}}^{\text{SL(meth)}}$ is still high compared to 'ideal' values which indicates that this parameter compensates for a missing mass transport limitation in the model.

The difference in calibrated values between network 1 and network 2 nicely illustrates how easily ambiguity is created in published parameter values and outcomes of models (Meima et al., 2008). By assuming a slightly different model structure, different sets of calibrated values will be reported which in turn may be used in yet again different model structures leading to wrong predictions. The only way to reduce this ambiguity is to report calibrated parameters together with the reaction networks and model structures from which they have been defined. Ideally the reactions should be mechanistically correct and the resulting parameters should be identifiable (i.e. possessing a narrow probability distribution without being correlated to other parameters). For this, statistical evaluation of model outcome and parameter distributions is necessary because basic evaluation by eye does not give the information needed to judge mechanistic correctness and identifiability.

In the case of reaction network 2, the evaluation indicates a structure that is nearly correct. However, the concentration of ammonium is still overestimated by the model. This is to be expected since hydrolysis releases ammonium and the anaerobic reaction network 2 does not include an ammonium removal process. The experimental results clearly indicate that such a process occurs in the lysimeter.

2.4.3. Performance of network 3

In network 3, a relatively simple ammonium oxidation process is added to the reaction network. As a result, the model fit of the ammonium concentration improved drastically, while the rest of the model performance stayed similar to that of network 2. The modeled pH and the calibrated parameter bandwidths are not significantly influenced. The results indicate that in this lysimeter experiment an ammonium oxidation rate of 0.0048 d^{-1} is likely. The ammonium oxidation in the experiment was most likely caused by intrusion of oxygen when leachate was recirculated.

2.4.4. Performance of network 4

Although the results of network 3 are very good, we chose to do one more iteration. The waste used in the lysimeter most probably contained a source of sulphate (gypsum from building waste). This implies that sulphate reduction can occur which may explain the delay in onset of biogas production observed in the measured data. Although neither sulphate or sulphide were measured in this experiment, the results indicate an improved fit because both the errors in the fit of cumulative biogas and pH decreased. The final parameter distributions of the other parameters remained the same as found for network 3. The calibrated parameter values for sulphate reduction have a wide range and are high compared to 'ideal' values so we have to be careful in judging the mechanistic correctness of this approach. The improved datafit can be explained by the mechanism of sulphate reduction but it just as well can be attributed to the additional degrees of freedom added by the extra reaction. Measurements of sulphate and sulphide species are necessary to make a conclusion about how to improve the reaction network.

2.4.5. Selecting the optimal model structure for anaerobic digestion of MSW

For lysimeter scale

Based on the evaluation of network performances, we choose reaction network 3 as the optimal model structure for anaerobic digestion of MSW on a lysimeter scale. All parameters are either based on thermodynamic principles, taken from well established geochemical databases or calibrated with bandwidths which are in agreement with 'ideal' values. This strong mechanistic character of the model together with its low uncertainty in calibrated parameters increases confidence in (long-term) prediction accuracy compared to other model structures.

For the value of $K^{\mathrm{SL(meth)}}_{\mathrm{inh},c^{\mathrm{T}}_{\mathrm{VFA}}}$, we suggest to either keep it as a parameter to be calibrated as a 'material property' for the system under investigation or to further extend the model with a transport limitation mechanism such as diffusion with an extra transport parameter which then needs to be calibrated.

Network 4 is not preferred over network 3 because the mechanism of sulphate reduction can not be adequately calibrated with this dataset. The improved likelihood is not guaranteed when applying this reaction network to other experiments and conditions. Calibration of network 4 with an extended measured dataset including sulphate or sulfide measurements would be very interesting.

Another interesting option would be to include the measurement error in the likelihood function. This was not possible for this dataset since the measurement error was unknown. Nevertheless, when included a distinction between model and measurement error could be made. A fully correct model would by necessity include all measured data within the green uncertainty bandwidths in figure 2.4.

For full scale

For full scale application, we select network 2 as the optimal model structure. Network 2 is preferred over network 3 because the ammonium oxidation in network 3 is modeled with a non-mechanistic first order decay function based on the observations only. In this experiment, air intrusion during recirculation of leachate is causing this degradation. This is probably not representative for large scale anaerobic digestion of waste in landfills.

2.5. Acknowledgments

This research is supported by the Dutch Technology Foundation STW, which is part of the Netherlands Organization for Scientific Research (NWO), and which is partly funded by the Ministry of Economic Affairs. We thank Roberto Valencia for providing us with the original data from his lysimeter experiments. We also thank Jasper Vrugt for providing us with a very efficient $\mathrm{DREAM_{ZS}}$ module which is included in the toolbox. Furthermore, we like to thank Jasper Vrugt and the anonymous reviewers for their comments which helped us to greatly improve the paper.

2.6. Supporting Information

The toolbox is implemented in MATLAB(MATLAB Release 2015a, 2015) and the algorithm is available at DOI: 10.4121/uuid:aefbaeb9-85be-4fa6-a29e-a9cb71d0fb3a. Here, also a detailed manual is provided on how to use the toolbox. The toolbox can be used without the requirement of special MATLAB toolboxes. Ordinary differential equations are solved with ode15s. For the Bayesian inference, an efficient submodule of DREAM_{ZS} is used and provided by Jasper Vrugt. A single integration of a network takes approximately 2.5 seconds and a Bayesian inference run with 250.000 iterations takes approximately 1 week. Inference run time can be substantially decreased ($\frac{1}{3}$) when Markov chains are run in parallel.

3

Theoretical analysis of MSW treatment by recirculation under anaerobic and aerobic conditions

Long-term emissions of Municipal Solid Waste (MSW) landfills need to be reduced to decrease the aftercare burden for future generations. Although re-circulation of leachate through the waste body reduces emissions on a lysimeter scale, effectiveness at the field scale as yet has to be demonstrated. Theoretical understanding of how re-circulation leads to improved leachate quality is important for optimizing the design of field scale applications. In this study, we present novel theoretical insights in the fundamental processes that control leachate quality of MSW in lysimeter scale experiments. Biogeochemical reaction network models were identified that describe measured data under anaerobic and aerobic conditions. These networks indicate that the major factor controlling treatment efficiency is the amount of biodegradable carbon reached by the most important reactant (i.e. oxygen or methanogenic bacteria). Biodegradable carbon removal is highest under aerobic conditions, however, the hydrolysis rate constant is lower, indicating that hydrolysis is not enhanced intrinsically in aerobic conditions. Furthermore, nitrogen removal via sequential nitrification and denitrification is plausible under aerobic conditions as long as sufficient biodegradable carbon is present in the MSW. Major removal pathways for nitrogen are N_2 emission and leachate drainage, while bacterial assimilation and ammonium stripping have a minimal impact.

This chapter has been submitted to Waste Management.

3.1. Introduction

A major challenge for this human generation, is to quickly reduce emissions from Municipal Solid Waste (MSW) landfills in order to protect human health and the environment and thereby reduce the burden of aftercare for future generations. Untreated, landfills can potentially emit gas and leachate for hundreds of years (Belevi and Baccini, 1989) because degradation processes in waste bodies are slow due to inhibitions and transport limitations (Kjeldsen et al., 2002, Laner et al., 2011, Meima et al., 2008). An approach to minimize longterm emissions via leachate and gas, is to actively treat the waste body with methods that accelerate degradation and the release of carbon and nitrogen containing compounds (Scharff et al., 2011). Accelerated release of landfill gas with a high content of methane is also economically more attractive because this gas can be utilized as an energy source.

Leachate recirculation and aeration are two treatment methods that have been shown to accelerate emission rates in lysimeter scale experiments (Bilgili et al., 2007, Brandstätter et al., 2015a,b, Erses et al., 2008, Kasam et al., 2013, Veeken et al., 2000). Leachate recirculation stimulates the mixing of solutes and bacteria within the waste body (partly) removing inhibitions and transport limitations (White et al., 2011). The stimulated degradation leads to strictly anaerobic conditions due to the fast consumption of readily available electron acceptors. It is possible to remove dissolved compounds in the leachate by bleeding the leachate stream and replacing with fresh water. Aeration by injection of air (Ritzkowski and Stegmann, 2012) has two main advantages, aerobic degradation is generally faster than anaerobic degradation (Heijnen and Kleerebezem, 1999) and ammonium can partly be removed by oxidation to nitrogen gas (Bolyard and Reinhart, 2016).

Full-scale application with these treatment methods has not yet shown to be successful in reducing longterm emissions through leachate (Benson et al., 2007, Hrad et al., 2013). We believe that increasing the level of theoretical understanding of the underlying processes is necessary for the design of successful application of these methods at the full scale. Novel insights in the fundamental factors and processes controlling treatment efficiency are essential. A good point to start is to revisit data obtained in lysimeter experiments and to explain the measurements in terms of fundamental biogeochemical reaction networks.

Fundamental modeling of environmental systems is an approach that can overcome limitations often encountered during experiments such as a limited capacity to measure certain parameters and extremely long experiment times due to slow kinetics. A mechanistic model provides insight in any specific mass balance required in context of the processes, inhibitions and limitations which are not directly measured. The challenge, however, is to identify a fundamental reaction network that optimally describes the measured data with minimal model uncertainty. In this study we use the toolbox developed by Van Turnhout et al. (2016). This toolbox supports integration of several environmental frameworks and extensive qualitative and quantitative evaluation of (fundamental) model uncertainty.

The aim of this study is to obtain novel fundamental insights into factors and processes that control the effectiveness of leachate circulation and aeration in waste

bodies. We present the biogeochemical reaction networks that give the optimal description of the measured emission data from lysimeter experiments performed by Brandstätter et al. (Brandstätter et al., 2015a,b). The results from our analysis allow us to identify the processes and factors controlling the effectiveness of the treatment method as well as the removal pathways for carbon and nitrogen compounds.

3.2. Material & Methods

3.2.1. Types of lysimeter experiments and measured data

For this study we used the data measured in two lysimeter experiments of Brandstätter et al. (2015a,b). Both experiments were based on leachate recirculation, one under anaerobic conditions and the other where recirculation is combined with continuous air injection. The experiments were carried out in duplicate on MSW (sieved to a grain size < 20 mm) taken from a 40 year old landfill. Leachate removed during sampling was replaced with distilled water (Aqua dest) to maintain the degree of water saturation. An illustration of both set-ups is presented in figure 3.1 and the initial and environmental conditions are listed in table A.1.

For each experiment, one set of time series measurements is used for model calibration and the other for validation. Time series measured are cumulative produced biogas (CO_2 and CH_4), partial pressure of CO_2, CH_4 and O_2, pH, Biological Oxygen Demand (BOD), NH_4^+ and Cl^- concentrations. BOD is assumed to consist of Volatile Fatty Acids (VFA) (i.e. Acetic Acid) and is referred from now on as VFA.

Figure 3.1: Illustration of experimental set-ups for leachate recirculation under anaerobic and aerobic conditions.

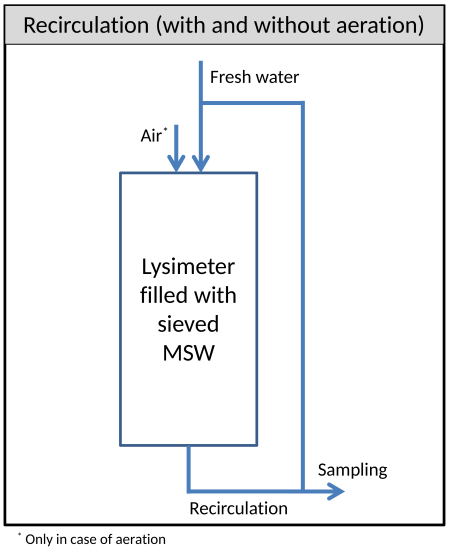

Table 3.1: Initial and environmental conditions in the duplicate experiments.

	Initial conditions					Environmental conditions					
	p_{CO_2}	NH_3	pH	Cl^-	V_{liquid}	$\phi^{in}_{waterflow}$	$\phi^{out}_{sampleflow}$	$\phi^{in}_{airflow}$	V_{gas}	p^{tot}_{gas}	T
Type of experiment	[atm]	[M]	[-]	[M]	[L]	[L d^{-1}]	[L d^{-1}]	[L d^{-1}]	[L]	[atm]	[K]
Anaerobic (calibration)	0.10	0.03	8	0.025	19.5	0.03	0.03	-	41.9	1	308.5
Anaerobic (validation)	0.10	0.03	8	0.025	19.5	0.03	0.03	-	41.9	1	308.5
Aerated (calibration)	0.41	0.025	7.25	0.025	21.24	0.0524	0.0483	56.67	38.8	1	308.5
Aerated (validation)	0.41	0.025	7.25	0.025	20.95	0.0526	0.0491	56.67	38.82	1	308.5

3

3.2.2. Biogeochemical reaction networks that optimally describe measured data

Figure 3.2: Iterative procedure to find the biogeochemical reaction network that optimally describes measured data.

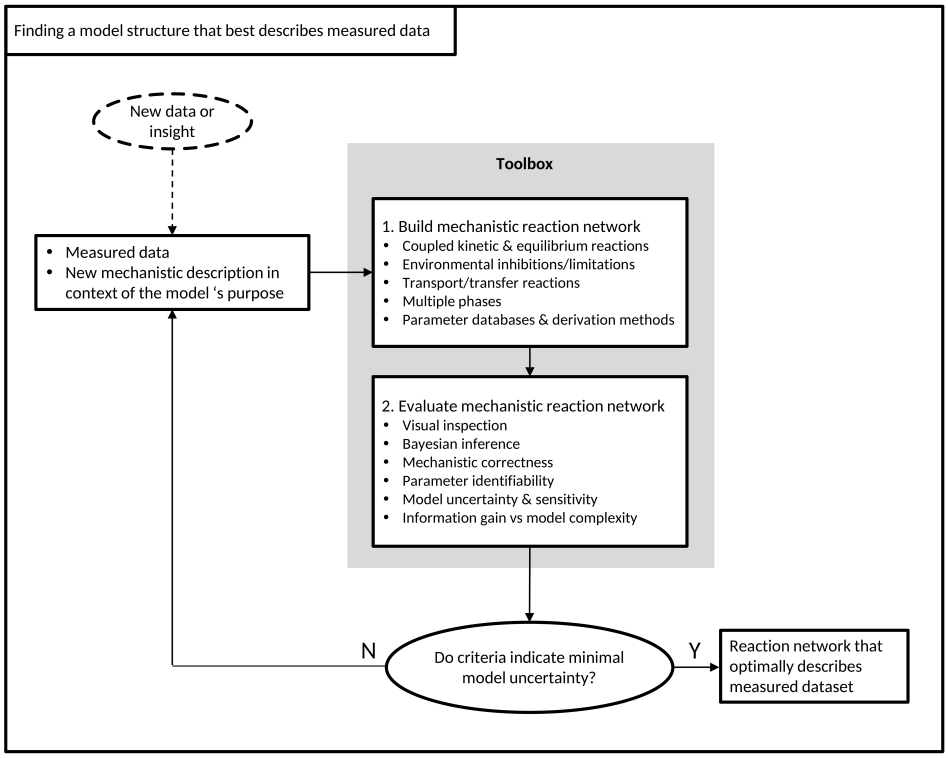

The approach to select the optimal biogeochemical reaction network that describes the measured data with the least error is shown in figure 3.2 (van Turnhout et al.,

2016). The first step is to build a model structure with the relevant kinetic, equilibrium, transfer and transport reactions together with the environmental inhibitions and limitations. The reactions occur within a multiphase environment. Fundamental parameters are obtained from an extensive geochemical database and a method to derive biochemical parameters from thermodynamic principles (Kleerebezem and van Loosdrecht, 2010). The second step is to obtain the probability distribution functions of the most uncertain parameters using a Bayesian statistical optimization method which, together with the optimal parameter set, provides an extensive set of qualitative and quantitative performance criteria which enable a detailed assessment of model performance in the third step. The aim of this analysis is to determine if the model uncertainty is small enough to be acceptable. If the result is not satisfactory, a next iteration of these three steps can be done with an alternative biogeochemical reaction network. Modifying this biogeochemical reaction network is not automated and needs to be done by the user as it requires expert knowledge.

We used the following qualitative and quantitative criteria to evaluate the (mechanistic) uncertainty of the different biogeochemical reaction networks. One criterion is the visual fit between the modeled data and the measured data. The second criterion is the practical identifiability of the calibrated parameters. This is indicated by their $5\% - 95\%$ quantile range of the posterior probability distribution. A smaller range means a better identifiability. The third criterion is the agreement between calibrated parameter ranges and the published values of these parameters measured under or estimated for non-limiting environmental conditions (e.g. perfectly mixed batch experiments without limitations/inhibitions). If all individual parameters agree with such optimal, intrinsic values this strongly indicates a fundamentally correct model structure. The closer all these criteria are met, the lower (fundamental) model uncertainty of the biogeochemical network.

3.3. Results & Discussion

3.3.1. A fundamental biogeochemical reaction network for leachate recirculation under anaerobic conditions

Figure 3.3 presents the best fit between modeled data (in red) and measured data (in blue) for leachate recirculation under anaerobic conditions based on a visual inspection. The uncertainty in the total model error is indicated with the green bandwidth surrounding the modeled data. The model is able to describe measurements for both the calibration and the validation dataset. Only the dynamics in measured NH_4^+ concentrations cannot be accurately described with this model indicating that some processes are still missing in the model. Such a process could be adsorption of NH_4^+ to the MSW which can control the measured concentration of NH_4^+ significantly. However, the total mass balance in the measured and modeled NH_4^+ are in agreement.

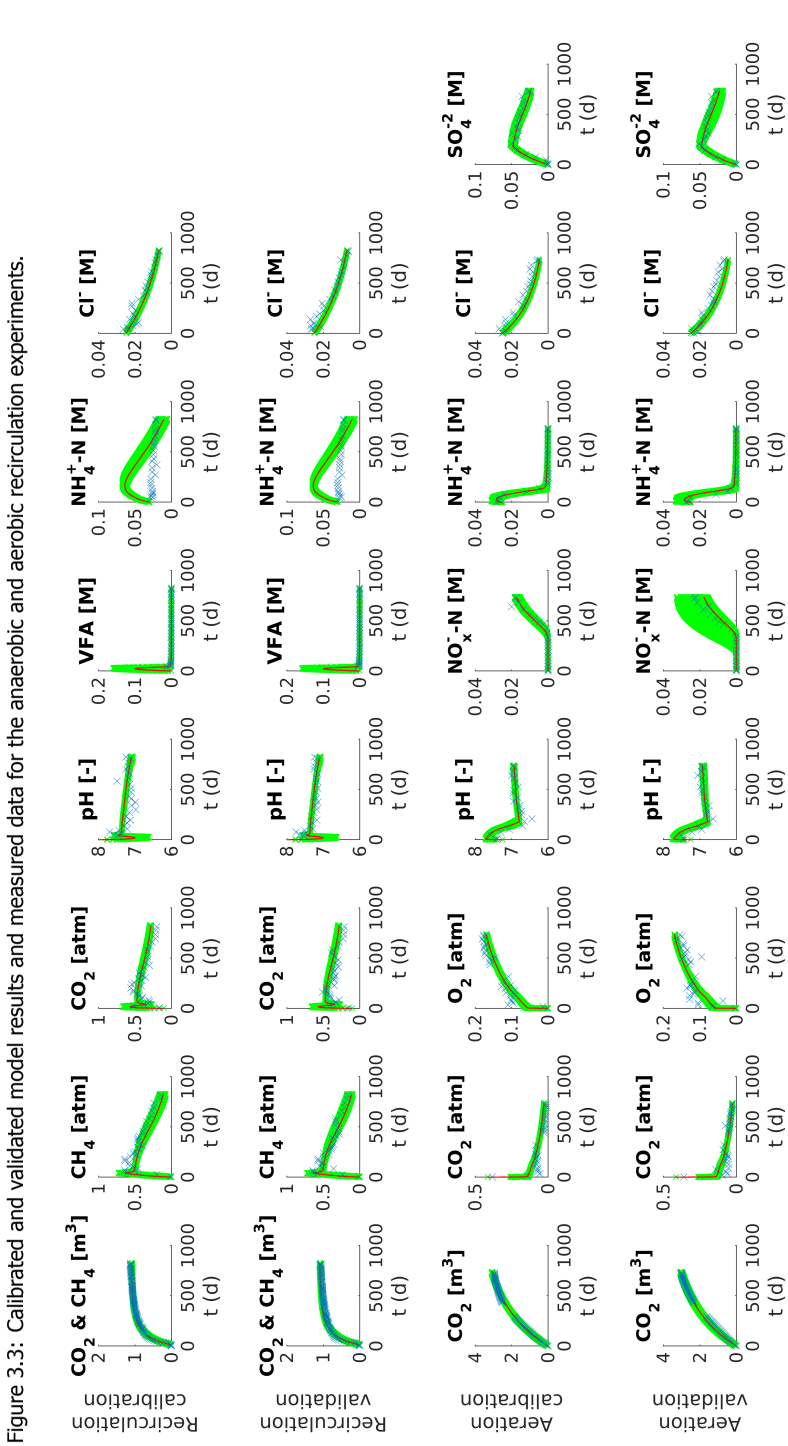

Figure 3.3: Calibrated and validated model results and measured data for the anaerobic and aerobic recirculation experiments.

The biogeochemical reaction network generating these modeled data is shown in figure 3.4 with the corresponding stoichiometry listed in table 3.2. The reaction network is based on five kinetic reactions: the first is a lumped hydrolysis/acidogenesis reaction that converts the biodegradable solid organic matter (SOM) into acetic acid and ammonium (with hydrolysis as rate limiting step); the second is a methanogenesis reaction that converts the acetic acid into biogas (i.e. CH_4 and CO_2) and methanogenic bacterial biomass; the third and fourth are reactions for decay of bacterial biomass where $\mu^{\max}_{\text{decay}} = 0.05 \cdot \mu^{\max}_{\text{growth}}$; and the fifth is a lumped nitrification/denitrification reaction with nitrification as rate limiting step. The oxygen for the nitrification reaction comes from a small leakage flow of air. Assuming this leakage enabled us to simulate both the observed loss in total nitrogen and decrease in partial pressures of CH_4 and CO_2.

The stoichiometry of the kinetic reactions is derived from thermodynamic principles (Kleerebezem and van Loosdrecht, 2010). Only the release of ammonium in the hydrolysis reaction was estimated from the measured amounts of removed organic carbon and organic nitrogen in the solid phase.

The reaction network also includes a set of equilibrium reactions (i.e. speciation, complexation, precipitation and gas-liquid transfer reactions) controlling the concentrations of the species shown in the bottom part of figure 3.4. Changes in the concentrations of equilibrium species are calculated from total concentrations which change due to the kinetic reactions. The calculations are based on the mass action laws and equilibrium constants from readily available thermodynamic databases. Including these equilibrium reactions is essential for describing the measured pH. The high alkalinity of leachate is included in the model assuming a sufficient amount of readily available Calcite.

In order to fit the models to the measured data, we calibrate the parameters with the highest uncertainty in the reaction network. The $5 - 95\%$ quantiles of the optimized posterior bandwidths of these parameters are presented in Table 4.1 together with the initial prior (search) ranges and (published) values which were measured under or estimated for non-limiting environmental conditions. The small range of all posterior quantiles indicate that all parameters are identifiable from the information present in the measured data set. More interesting, however, is the fact that although a relatively simple reaction network was used, most calibrated bandwidths fall in the range of the reference values measured under non-limiting conditions. We believe that this indicates that the reaction network includes most fundamental reactions and processes controlling the emissions. Calibrated bandwidths of maximum rates are a bit lower than the reference values presumably due to mass transport limitations in our experiments which have not been included in the model. The network closely resembles the network identified for a similar type of lysimeter experiment by van Turnhout et al. (2016). The main difference is that we did not include environmental inhibition relations because concentrations of potential inhibitors remained low.

An interesting parameter obtained from the calibration step is the amount of organic carbon in the MSW ($C^{\text{ini}}_{\text{SOM}}$) that could be removed under the experimental conditions. In the optimization procedure this parameter is only determined from

Figure 3.4: Biogeochemical reaction networks for anaerobic (top) and aerobic (bottom) recirculation treatment on a lysimeter scale.

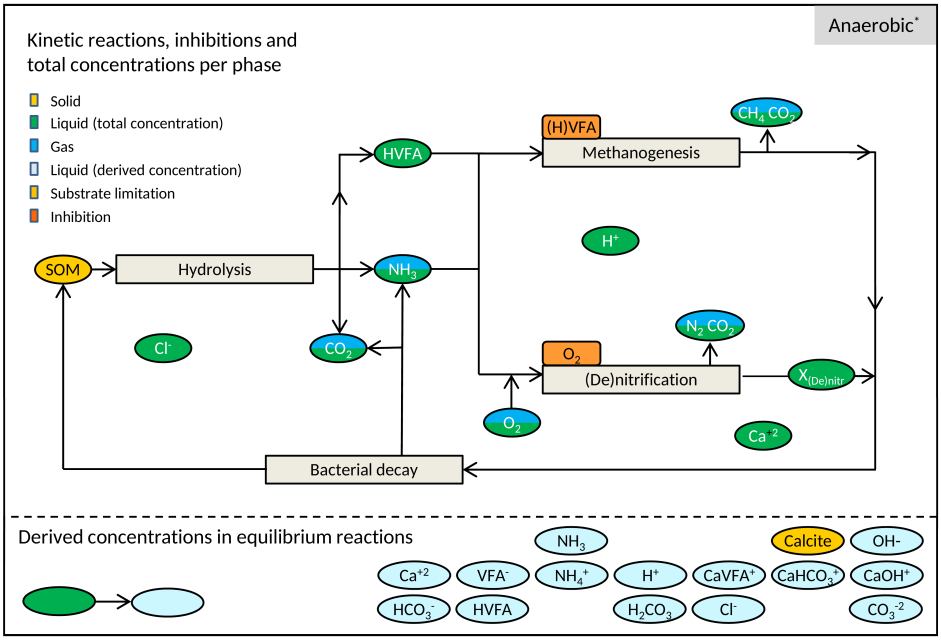

*with some oxygen present due to leakage

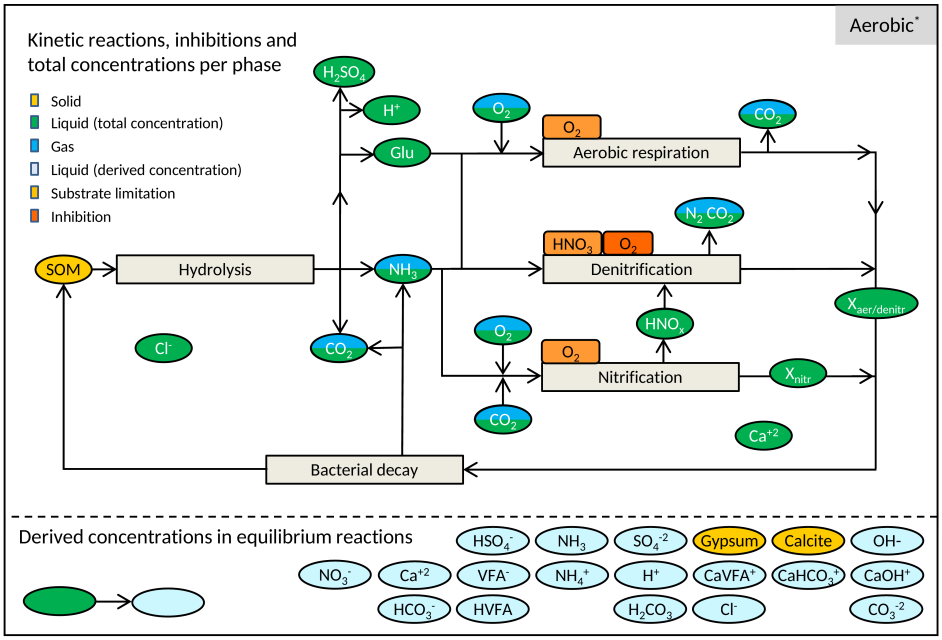

*with remaining anaerobic pockets because air is transported through preferential flow paths

measured emissions leading to a mean value of $2.3\ \frac{\text{Cmol}}{\text{L}}$ ($= 0.018\ \frac{\text{kgSOM}}{\text{kgdrywaste}}$). This value is comparable with the total carbon removed at the end of the experiment measured by MSW sampling. This indicates that the amount of biodegradable or potentially emitted carbon can be reasonably estimated from the emission data by inverse modeling without sampling of MSW. For further study, it would be even more interesting to predict the amount of carbon that is removed over longer time periods or under different experimental conditions. However in order to extrapolate the model, first processes have to be included that relate the amount of SOM that is hydrolyzed with the total amount of organic matter present in the MSW.

The model results provide insight into the mass balances of carbon and nitrogen per phase during the experiment. Figure 3.5 presents the change with time in mass percentage of organic carbon and nitrogen in MSW, solutes, bacteria, sampled leachate, CO_2(gas), CH_4(gas), N_2(gas) and NH_3(gas) during the experiment. Most of the organic carbon and nitrogen ($85\% - 83\%$) in the MSW is unaffected by the treatment. The model outcome indicates that removal of carbon and nitrogen is mainly limited by the transport of important reactants (e.g. oxygen or methanogenic bacteria) to the biodegradable fraction of MSW because the network gives a good fundamental description and the optimal parameter values do not indicate any severe biochemical rate limitations or inhibitions. The residual unaffected carbon may not have been removed because of strong transport limitations and/or because it was (partly) not biodegradable.

It seems that in order to optimize degradation, we need a treatment that allows for a thorough mixing of electron acceptor or other important reactants (such as the methanogenic bacteria) throughout the MSW. It is, however, questionable if an improved distribution throughout the waste body at field scale can be achieved that is comparable with the distribution achieved in the lysimeter experiments considering that mixing in the latter case is already close to optimal due to recirculation. Optimizing treatment approaches at full scale is an important and challenging research topic.

Figure 3.5 furthermore shows that carbon is mainly removed via the gas phase and nitrogen is mainly removed via leachate sampling. Bacterial assimilation and ammonia stripping have a minimal impact on the decrease of total nitrogen. The main removal pathways indicate the important fluxes to measure on a full scale in order to successfully monitor the efficiency of the treatment methods. Inconclusive field scale results so far, may be (partially) caused by incomplete monitoring.

Table 3.2: Stoichiometry & kinetics of the biogeochemical reaction networks.

Stoichiometry for the recirculation experiment under anaerobic conditions [mol]												Kinetics[c]
	SOM[a]	Acetic Acid	CO_2	NH_3	CH_4	H_2O	H^+	$X^{b)}_{meth}$	$X_{(de)nitr}$	O_2	N_2	
Hydrolysis	−1	0.5	0	0.036	0	−0.172	0	0	0	0	0	$k_{hyd} \cdot C^T_{SOM}$
Methanogenesis	0	−12.91	12.41	−0.2	12.41	0.6	0	1	0	0	0	$\mu^{max}_{meth} \cdot C_X \cdot f^{SL}_{C^T_{Ac}} \cdot f^{SL}_{C^T_{NH_3}}$
Bacterial decay [d]	0	0.5	0	0.2	0	−0.6	0	(−1)	0	0	0	$0.05 \cdot \mu^{max}_{meth} \cdot C_X$
(De)nitrification	0	−0.12	0.39	−0.54	0	1.5	0	0	1	−0.63	0.17	$\mu^{max}_{(de)nitr} \cdot C_X \cdot f^{SL}_{C^T_{O_2}} \cdot f^{SL}_{C^T_{NH_3}}$

Stoichiometry for the recirculation experiment under aerobic conditions [mol]												Kinetics
	SOM	Glucose	CO_2	NH_3	H_2O	H^+	$X_{aer\text{-}denitr}$	O_2	SO_4^{-2}	NO_3^-	X_{nitr}	N_2	
Hydrolysis	−1	0.167	0	0.032	−0.172	ν_{H^+}	0	0	0.03	0	0	0	$k_{hyd} \cdot C^T_{SOM}$
Aerobic respiration	0	−0.23	0.39	−0.2	0.99	0	1	−0.39	0	0	0	0	$\mu^{max}_{aer} \cdot C_X \cdot f^{SL}_{C^T_{Glu}} \cdot f^{SL}_{C^T_{O_2}} \cdot f^{SL}_{C^T_{NH_3}}$
Nitrification	0	0	−1	−11.42	10.82	11.22	0	−21.44	0	11.22	1	0	$\mu^{max}_{nitr} \cdot C_X \cdot f^{SL}_{C^T_{NH_3}} \cdot f^{SL}_{C^T_{CO_2}}$
Denitrification	0	−0.24	0.42	−0.2	2.62	−0.33	1	0	0	−0.33	0	0.17	$\mu^{max}_{denitr} \cdot C_X \cdot f^{SL}_{C^T_{Glu}} \cdot f^{SL}_{C^T_{NO_3^-}} \cdot f^{SL}_{C^T_{NH_3}} \cdot f^{NC}_{C^T_{O_2}}$
Bacterial decay [d]	0	0.17	0	0.2	−0.6	0	(−1)	0	0	0	(−1)	0	$0.05 \cdot \mu^{max} \cdot C_X$

a) SOM is the biodegradable fraction of Solid Organic Matter in MSW modeled as cellulose. Its value is different for anaerobic and aerobic conditions. b) X are species of bacteria with the elemental composition $CH_{1.4}O_{0.4}N_{0.2}$ taken from Henze et al. (1995) . c) Substrate limitation factors (f^{SL}) and inhibition factors (f^{NC}) range between 0 and 1 (van Turnhout et al., 2016). Half saturation constants which are not optimized have relatively very low values, primarily included as switch factors. They do not significantly influence the model outcome. d) Bacterial biomass decay is included as a separate process.

Table 3.3: Prior ranges, 5%−95% quantiles of posterior ranges and reference ranges measured under or estimated for non-limiting environmental conditions.

Anaerobic recirculation experiment

	prior	posterior	reference		prior	posterior	reference
k_{hyd} [d^{-1}]	$0.0005 - 0.15$	$0.0094 - 0.0104$	$0.09 - 0.26$[1)]	X_{meth} [mM]	$0.005 - 15$	$0.59 - 11$	$0.27 - 19$[3)]
$\mu^{\mathrm{max}}_{\mathrm{meth}}$ [d^{-1}]	$0.01 - 3$	$0.04 - 0.12$	0.8[2)]	$X_{(\mathrm{de})\mathrm{nitr}}$ [mM]	$0.015 - 15$	$1.2 - 14$	$0.27 - 19$[3)]
$\mu^{\mathrm{max}}_{(\mathrm{de})\mathrm{nitr}}$ [d^{-1}]	$0.001 - 1$	$0.11 - 0.96$	1.4[2)]	$K^{\mathrm{meth}}_{\mathrm{s},C^{\mathrm{T}}_{\mathrm{Ac}}}$ [mM]	$1 - 1000$	$5.5 - 16.7$	$0.03 - 420$[4)]
$\phi_{\mathrm{in,air}}$ [Ld^{-1}]	$0.005 - 1.5$	$0.12 - 0.19$	–	$C^{\mathrm{ini}}_{\mathrm{SOM}}$ [M]	$2 - 3$	$2.27 - 2.33$	–

Aerated recirculation experiment

	prior	posterior	reference		prior	posterior	reference
k_{hyd} [d^{-1}]	$0.00024 - 0.026$	$0.0021 - 0.0023$	$0.09 - 0.26$[1)]	X_{nitr} [mM]	$0.09 - 110$	$1.1 - 2.7$	$0.27 - 19$[3)]
$\mu^{\mathrm{max}}_{\mathrm{aer}}$ [d^{-1}]	$1.2 - 121$	$25.6 - 118$	57[2)]	$X_{\mathrm{aer-denitr}}$ [mM]	$7 - 800$	$9.5 - 35.4$	$0.27 - 19$[3)]
$\mu^{\mathrm{max}}_{\mathrm{nitr}}$ [d^{-1}]	$0.003 - 0.31$	$0.01 - 0.02$	1.4[2)]	$K^{\mathrm{nitr}}_{\mathrm{s},C^{\mathrm{T}}_{\mathrm{NH_3}}}$ [mM]	$0.9 - 110$	$1.6 - 7.1$	0.04[5)]
$\mu^{\mathrm{max}}_{\mathrm{denitr}}$ [d^{-1}]	$2 - 201$	$6.4 - 198$	54[2)]	$K^{\mathrm{denitr}}_{\mathrm{i},C^{\mathrm{T}}_{\mathrm{O_2}}}$ [mM]	$0.005 - 0.6$	$0.047 - 0.093$	–
$C^{\mathrm{ini}}_{\mathrm{SOM}}$ [M]	$5 - 7$	$6.2 - 6.5$	–	$\nu^{\mathrm{hyd}}_{\mathrm{H^+}}$ [mol]	$0 - 0.06$	$0.037 - 0.041$	–

1) Veeken and Hamelers (1999) 2) Kleerebezem and van Loosdrecht (2010) 3) Nopharatana et al. (2007) 4) Meima et al. (2008) 5) Kantartzi et al. (2006)

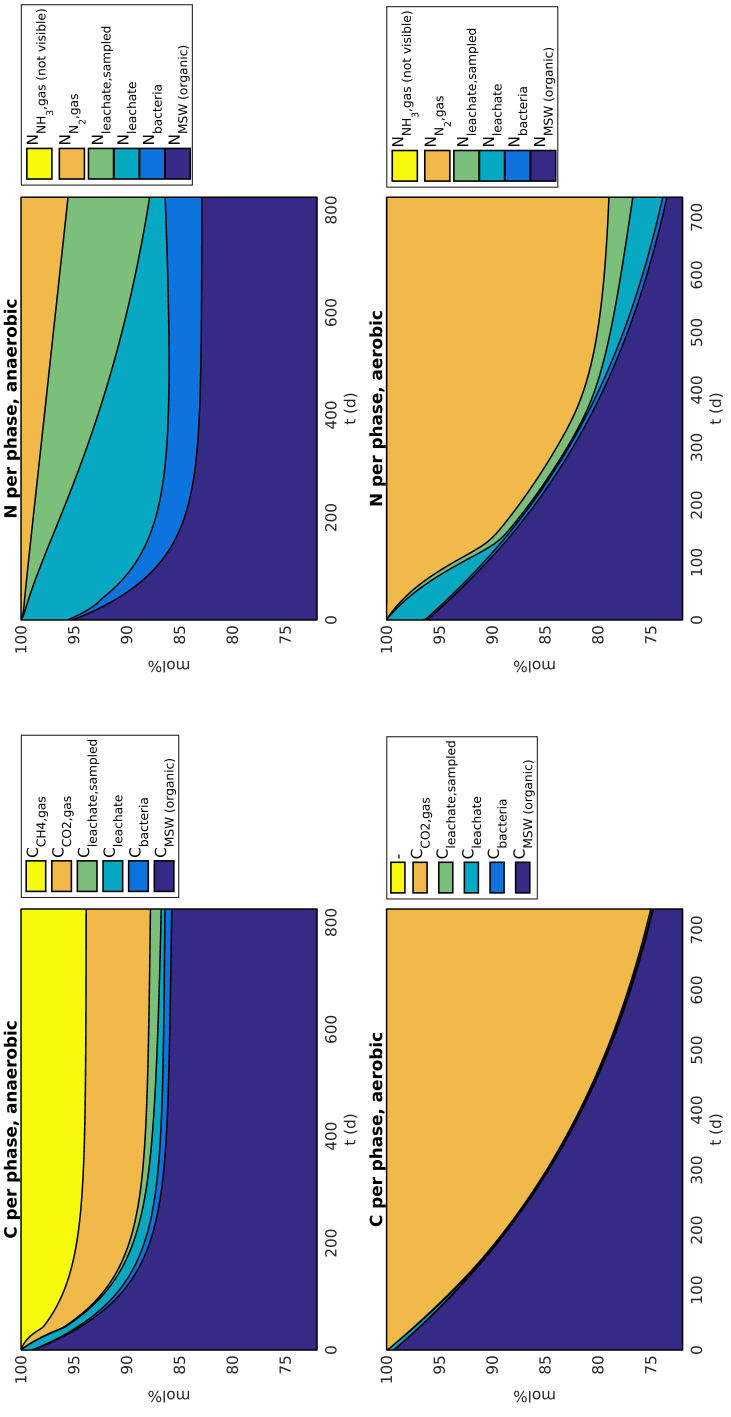

Figure 3.5: Variation of mol percentage of carbon and nitrogen in the different phases during both experiments

3.3.2. A fundamental biogeochemical reaction network for leachate recirculation under aerobic conditions

Figure 3.3 also presents the best visual fit between modeled and measured data for leachate recirculation under aerobic conditions. Again all model results are in good agreement with the measured data for both the calibration dataset and the validation dataset.

Six kinetic reactions are included in this reaction network (figure 3.4 and table 3.2). The first is hydrolysis of SOM to glucose, ammonium and sulphate. The second is aerobic respiration of glucose into CO_2 and bacterial biomass. The third and fourth are nitrification and denitrification. The fifth and sixth are bacterial decay reactions. The stoichiometry for nitrogen and sulfur release in hydrolysis is derived from the measured ratio between total removed solid carbon and nitrogen/sulfur. The sulfur/carbon ratio suggests that gypsum is co-dissolved during hydrolysis because it is too high to be explained solely by protein hydrolysis. The amount of protons released per sulfate (ν_{H^+}) is calibrated on the measured data. The mean calibrated value (table 4.1) indicates mainly release of HSO_4^-.

The set of equilibrium reactions (figure 3.4) is identical to that used for modeling the the anaerobic experiment except that sulphate speciation and gypsum precipitation are included as well. Inclusion of the chemical equilibrium allowed the model to reproduce the dynamics in measured pH and dissolved sulphate.

The consumption of ammonium by sequential nitrification and denitrification suggests the presence of anaerobic pockets in the MSW during air injection. This implies that air is transported through preferential flow paths which is reasonable given the strong heterogeneity of the MSW. Figure 3.6 schematically explains how nitrification and denitrification can occur simultaneously because of concentration gradients between preferential flow paths and the bulk of the waste. With sufficient biodegradable carbon available the oxygen is readily consumed near the channels. The produced nitrate diffuses into the anaerobic bulk of the waste where it is used as electron acceptor to oxidize carbon. However, when in time the concentration of biodegradable carbon decreases, oxygen penetrates deeper into the waste outcompeting nitrate as electron acceptor for the oxidation of the remaining carbon. As a consequence concentrations of nitrate/nitrite increase when SOM depletes which is also observed in the measured data (figure 3.3). The inhibition of denitrification by oxygen is included in the reaction network with the relation:

$$f^{\mathrm{NC}}_{C^{\mathrm{T}}_{\mathrm{O}_2}} = \left(\frac{K_{\mathrm{inh}}}{K_{\mathrm{inh}} + C^{\mathrm{T}}_{\mathrm{O}_2}} \right)^6 \tag{3.1}$$

where K_{inh} is the inhibition constant and $f^{\mathrm{NC}}_{\mathrm{denitr},C^{\mathrm{T}}_{\mathrm{O}_2}}$ ranges from 0 to 1. This type of ammonium removal mechanism has two main characteristics. First, nitrate removal by denitrification is always slowed down by mass transport of nitrate from the aerobic to the anaerobic region. Second, denitrification fails when little biodegradable carbon is left in the MSW leading to high concentrations of nitrate.

Our mechanism that facilitates denitrification generalizes the one proposed by Brandstätter et al. (2015b) . They propose that denitrification mainly occurred at

the bottom of the reactor where leachate remained anaerobic and had a long retention time. We believe that oxidation of carbon by nitrate that is transported to an anaerobic region applies everywhere near aerobic preferential flowpaths. However, the existence of the large anaerobic region at the bottom of the reactor could have amplified the chances for denitrification.

The parameters in the aerobic reaction network with the highest initial uncertainty were calibrated using the measured data (table 4.1). The quantiles of the posterior distributions show that the identifiability of most calibrated parameters is good. Only the maximum rates of aerobic respiration and denitrification have a wide distribution with high values which is reasonable because these reactions are limited by the rate of oxygen or nitrate supply. Therefore, any high value for these maximum rates gives a satisfying model result. Most posterior ranges fall close to the reference values, but similar to the findings for the anaerobic case, slightly lower. As mass transport limitations in the experiments are not included in the model these slightly lower values include these limitations. The high posterior range of initial concentration of aerobic respirators seems to compensate for a high initial growth rate which was not recorded due to too large measurement intervals. Based on these results we conclude that the calibrated parameter ranges indicate that fundamental model uncertainty is relatively small.

Figure 3.5 shows the mass percentages of organic carbon and nitrogen in MSW, solutes, bacteria, sampled leachate, CO_2(gas), CH_4(gas), N_2(gas) and NH_3(gas) during the aerobic experiment. The main removal pathway for carbon and nitrogen is via the gas phase as CO_2 and N_2. Clearly, more carbon is removed in the aerobic experiment ($\sim 25\%$) than in the anaerobic one with only recirculation ($\sim 14\%$). Apparently, during aeration the electron acceptor (i.e. oxygen) was better mixed throughout the waste and/or the fraction of biodegradable carbon was higher under aerobic conditions. In addition, more nitrogen is removed under aeration i.e. $\sim 27\%$ against $\sim 17\%$ for the anaerobic case. However, the amount of carbon and nitrogen removed is still quite small compared with the total amount in MSW. Therefore, we have the same conclusion for the aerobic recirculation treatment as for the anaerobic one: optimal electron acceptor distribution throughout the waste-body at field scale is a main issue to be tackled.

Interestingly, the hydrolysis constant (i.e. the rate constant of generally the slowest step in biodegradation) is lower under aerobic conditions. Stripping of water may have decreased the amount of water per surface area of MSW which resulted in the lower hydrolysis constant. This indicates that aeration should not always be the preferred option to enhance the intrinsic degradation mechanism. It is, however, important to note that absolute rates of carbon removal can still be high with a low hydrolysis constant as long as the fraction of biodegradable carbon is high. An optimal treatment strategy could be to treat the waste body in a cyclic fashion where a phase of anaerobic recirculation is followed by a drainage step which then is followed by a subsequent aeration phase etc.

Adopting a different after-care perspective (and corresponding treatment goals) for landfills also increases the efficiency of possible treatment methods. Rather than aiming to completely remove all biodegradable carbon and nitrogen in the waste

body, it may be sufficient to reduce the long-term emissions to low levels. Given that gas and leachate are transported by preferential flow-paths throughout the waste-body, acceptably low emissions may already be established by removing the carbon and nitrogen in the proximity of the preferential pathways. In such a case, slow diffusion from the bulk of the waste and the continuing degradation in the close vicinity of the preferential pathways jointly contribute to maintaining low emission levels. Follow up studies must however show that preferential flow-paths are stable over long time periods.

Figure 3.6: Concentration gradients for carbon rich and carbon depleted scenarios.

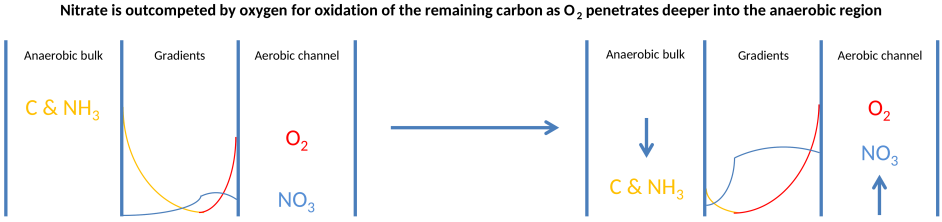

3.4. Conclusions

This paper discusses factors and processes that control the effectiveness of leachate recirculation treatment under anaerobic and aerobic conditions. Fundamental reaction networks were found which closely reproduce the measured data from experiments at the lysimeter scale (Brandstätter et al., 2015a,b). Using qualitative and quantitative criteria (van Turnhout et al., 2016), we also indicate that the (fundamental) uncertainty in these models is small.

The model results indicate that efficiency of treatment is mainly controlled by how much of the carbon and nitrogen is reached by the electron acceptor or dominant reactant (i.e. oxygen or the methanogenic bacteria) and biodegradability. A higher fraction of carbon and nitrogen is removed under aerobic conditions than under anaerobic conditions, for carbon $\sim 25\%$ vs $\sim 14\%$ and for nitrogen $\sim 27\%$ vs $\sim 17\%$. Surprisingly, the model results indicate that the intrinsic rate of biodegradation is not enhanced under aerobic conditions because the rate constant for hydrolysis is lower than under anaerobic conditions. Nevertheless, the absolute rate of hydrolysis is still higher because it also depends on the fraction of biodegradable carbon reached.

To maximize degradation of organic matter in waste bodies at full-scale, a challenge is to maximize distribution of the electron acceptors and other reactants throughout the waste-body. It is, however, doubtful if a higher removal rate than established in the lysimeter experiments is achievable since distribution at full-scale will always be less optimal. A more realistic goal is to remove biodegradable carbon and nitrogen in the proximity of the preferential flow-paths to such extent that the emissions from the rest of the bulk are limited by diffusion and degradation and therefore low.

The main removal pathways to be monitored for carbon and nitrogen under anaerobic conditions are CO_2/CH_4 via the gas phase and NH_4^+ in the leachate, under aerobic conditions these are CO_2 and N_2 in the gas phase. The N_2 in the gas phase is, however, difficult to monitor due to the very high background concentration in the atmosphere. Removal of carbon and nitrogen by bacterial assimilation and NH_3 stripping was minimal for the lysimeter experiments analyzed.

The reaction networks indicate that denitrification during aeration is possible because air flows through preferential flow-paths which keeps the domains in the waste-body without flow anaerobic. However, sufficient biodegradable carbon must be available for nitrate to out-compete oxygen as oxidizer. Otherwise, the concentration of nitrate increases in the leachate.

The amount of biodegradable carbon potentially released during the treatment is inferred from the measured emissions and is comparable with solid sampling estimations. Estimating the amount of biodegradable carbon from emission measurements rather than solid samples substantially reduces measurement costs. However, the models are not yet capable of predicting the amount of carbon that is removed over longer time periods or under different experimental conditions. In order to extrapolate, processes must be included that relate hydrolysis to the amount of total biodegradable SOM present in the MSW. We believe this is the most important step to take in further model development.

3.5. Acknowledgments

This research is supported by the Dutch Technology Foundation STW, which is part of the Netherlands Organization for Scientific Research (NWO), and which is partly funded by the Ministry of Economic Affairs.

4

Coupled model of water flow, mass transport and biogeochemistry to predict emission behavior of landfills

Accurate predictions of long-term emissions from landfills are important to estimate the investment and time required for (shortening) after-care; this to limit the burden of after-care for future generations to protect the environment. Available models do no provide accurate predictions. They are mainly hampered by two limitations: 1) they only extract information from one type of measured data and/or 2) the many assumptions made in the more complex, coupled models are difficult to quantify. This paper presents a model to predict long-term emissions from waste bodies which optimally uses the measured data and the fundamental insights available, thereby utilizing multiple data sources. Processes of water flow, mass exchange and biodegradation are coupled within the framework. After calibration, the results show that the modeling approach is well-suited for reproducing leachate discharge and the dynamics in concentration of chloride, sodium and ammonium in the leachate. A major benefit of the presented approach is that after calibration, the modeled states provide insight in the (reduction of) emission behavior of the landfill. We illustrate this by showing the reduction in leachable masses of chloride, sodium, ammonium, solid organic matter and biogas production rate. Modeled concentrations in addition indicate (emerging) inhibition of biodegradation processes and therefore reduction of emission potential. The main sources of model uncertainty and further developments to minimize them are discussed.

4.1. Introduction

Landfill operators need an accurate prediction of the amount of leached chemicals and biogas generated by a landfill over time. This gives good indications on how much investment and time is required for after-care of the landfill and how much income can be generated from the produced biogas (i.e. the produced methane). It also gives the regulators sufficient confidence to release the landfill from after-care when emissions are low enough (Berge et al., 2009, Scharff, 2014). The intention is to limit the burden of after-care for future generations to protect the environment from emissions from our waste (Hoornweg and Bhada-Tata, 2012, Laner et al., 2012).

Accurate prediction of emission behaviour from a landfill for long time periods is not an easy task because of the highly heterogeneous nature of waste bodies which also strongly limits the options for measurements. Collecting sufficient samples from the solid waste for a statistically sound prediction is very costly. A cheaper option is therefore to base prediction on the quality and quantity of produced leachate and gas. However, current models used for predictions of leachate and gas emissions are mainly based on empirical relations which extrapolate measured data (Fellner et al., 2009, Gönüllü, 1994, Kamalan et al., 2011, Karaca and Özkaya, 2006, Ozkaya et al., 2007, Scharff et al., 2011), leading to long term predictions with large uncertainties, an inherent property of empirical approaches.

The models available are mainly hampered by two limitations. The first is that models are often focused on one particular process in the landfill such as leaching, biodegradation or gas production. They only extract information about the landfill behaviour from one type of often very limited data. Because it is well known that all processes in landfills are coupled, a better approach would be to use a coupled model that enables to extract information from all data available. Such models also exist (Garcia de Cortazar and Monzon, 2007, Gawande et al., 2010, Kouzeli-Katsiri et al., 1999, McDougall, 2007, Reichel et al., 2007, White et al., 2004), however, the second limitation is that many of the assumptions made in these coupled models are difficult to quantify. Some processes in these models are based on well understood fundamental concepts whereas other processes are based on simplified approximations. Finding the proper balance in where to apply fundamentals and where approximations is crucial for the application of models based on coupled processes. Too much complexity leads to large uncertainty because of over-parametrization while over-simplification leads to loss of fundamental information that can constrain the models (Bennett et al., 2013, Kelly et al., 2013).

Our aim is to present a model to predict long-term emissions from waste bodies which optimally uses the measured data and the fundamental insights available. This model couples the processes of water flow, mass exchange and biodegradation and can, therefore, be calibrated on both leachate and gas measurements. We choose to simulate water flow stochastically because of the large scale of a waste-body and the associated complexity of calibrating a dual permeability Richards' equation in order to describe preferential flow. The biodegradation reactions in the model on the other hand are based on fundamental concepts, using previously established knowledge on stoichiometry, kinetics and limitations can restrict the

parameter ranges. Mass exchange between stagnant water and mobile water in the waste body is simulated as a diffusion type of exchange.

We show the information that the model can provide about the emission behavior of a landfill. Furthermore, model uncertainty is indicated and prediction accuracy and future developments are discussed.

Figure 4.1: Concept of the coupled model.

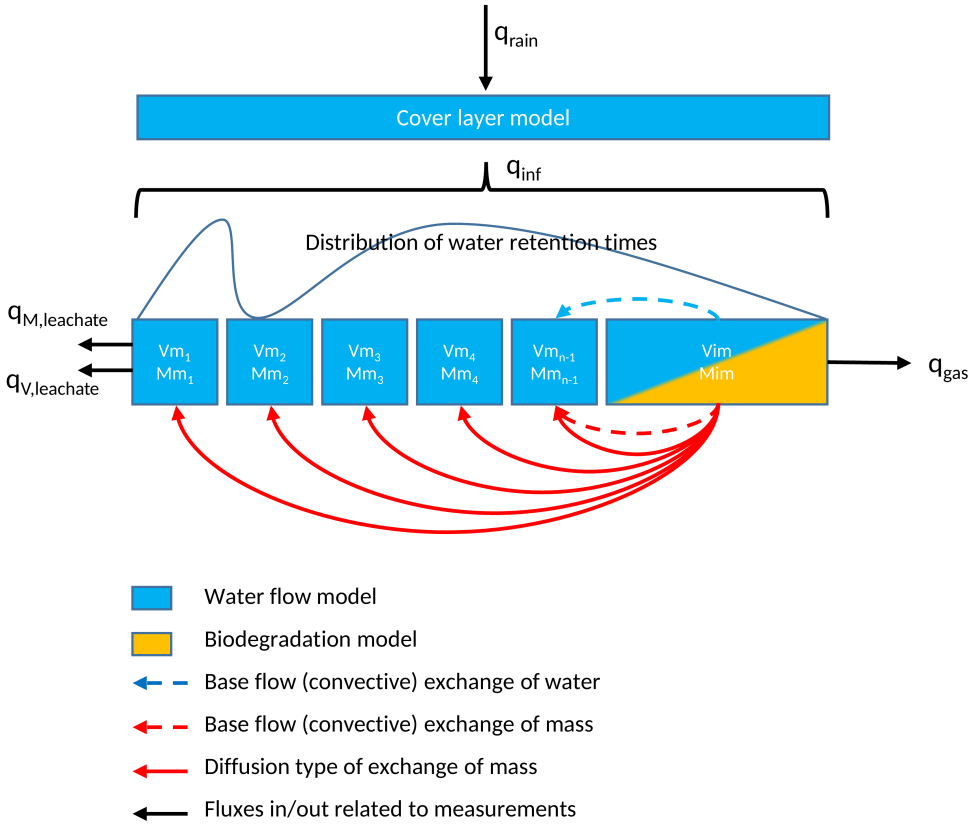

4.2. Theory

4.2.1. The conceptual framework of the coupled model

Figure 4.1 presents the conceptual framework of the coupled model where we consider three main processes, the flow of water, conversion of mass and the exchange of mass within the waste body. Water enters the landfill as rain (q_{rain}) at the surface of the cover layer. The flux of water entering the waste-body (q_{inf}) is calculated from the mass balance between rainfall, evapo-transpiration, infiltration and storage in the cover layer. Water flow and storage in the waste body is simulated with a stochastic approach where the residence time of water is assumed to follow a

bimodal log normal distribution. This stochastic residence time model is discretised by assuming n_{res} 'cells' which represent the time a certain water volume present in the waste body will need to drain towards the pump pit in the landfill where it will be extracted as leachate. Because a finite amount of 'cells' is used, a base flow is required to drain the water from the bulk of the wastebody (i.e. the $n_{\mathrm{res}}^{\mathrm{th}}$ 'cell' with immobile water) towards the flowing water present in the other 'cells'. The pump pit is the boundary of the model and it is assumed that all water present in the pump pit is immediately removed by the pump. Every time step, the simulation proceeds by shifting all cells towards the pump pit, where the water volume in the first cell corresponds with the daily produced leachate.

Changes to the composition of organic matter within the waste body are calculated assuming that reactive mass ($\mathrm{M_{im}}$) in contact with the water volume present in the bulk of the waste body (or immobile water $\mathrm{V_{im}}$) undergoes transitions according to the biodegradation processes. The model simulates the dissolution of mass from the solid phase to the water phase, the conversion of mass in the water phase and the production of gas (q_{gas}). The reaction network, consisting of kinetic and equilibrium reactions, inhibition and limitation mechanisms, transfer and transport reactions, is described in van Turnhout et al. (2016). Inert mass such as chloride is unaffected by the biodegradation model.

Transport of the dissolved mass from the immobile water volume to the water volumes present in the mobile cells is based on a diffusion type of exchange between a number of mobile cells (i.e. for $n_{\mathrm{res}} = 1 : n_{\mathrm{ex}}$) and the immobile bulk. Each time step, this transport flux is proportional to the gradient between the concentration of immobile mass and the concentration of mass in a respective mobile water volume ($\mathrm{C_{im}}$ and $\mathrm{C_m}$) and an exchange rate constant. We assume a single value for the exchange rate constants for all cells and it is therefore a transport related property of the waste-body. In addition, mass is also advectively transported from the immobile water to its adjacent mobile water volume with the base flow. The daily discharge with leachate corresponds the amount of mass present in the first cell ($q_{\mathrm{M,leachate}}$).

4.2.2. Mathematics of the cover layer

The rate of change of the water content in the cover layer is based on the following mass balance,

$$\frac{d\theta}{dt} = \frac{q_{\mathrm{rain}} - q_{\mathrm{inf}}}{\Delta z_{\mathrm{root}}} - \frac{q_{\mathrm{evap}}}{\Delta z_{\mathrm{root}}} \tag{4.1}$$

where the flux of rain (q_{rain}) is taken from measurements as a boundary condition, Δz_{root} is the depth of the root layer, q_{inf} is the infiltration flux into the waste-body and q_{evap} is the flux of evaporation calculated with:

$$q_{\mathrm{evap}} = Ev_{\mathrm{pot}} \cdot f_{\mathrm{crop}} \tag{4.2}$$

where Ev_{pot} is the potential evaporation flux taken from the Royal Dutch Meterological Institute (KNMI) and f_{crop} is the crop factor. The infiltration flux in to the

waste body is estimated with a free drainage type relation:

$$q_{\mathrm{inf}} = -K_{\mathrm{sat}}^{\mathrm{inf}} \cdot \left(\frac{\theta_{\mathrm{cover}} - \theta_{\mathrm{r,cover}}}{\theta_{\mathrm{cover}} - \theta_{\mathrm{s,cover}}} \right)^{m_{\mathrm{inf}}} \tag{4.3}$$

where $K_{\mathrm{sat}}^{\mathrm{inf}}$ is the hydraulic conductivity of the cover layer, $\theta_{\mathrm{r,cover}}$ is the residual water content and $\theta_{\mathrm{s,cover}}$ is the saturated water content and m_{inf} is an empirical shape parameter.

4.2.3. Mathematics of the water retention time model

Because of the very complex nature of water flow in the heterogeneous waste body we chose to model the flow with a stochastic stream tube model where the residence time of water in the stream tubes is described with a bimodal lognormal distribution similar to Jury and Roth, (1990). The flux of produced leachate ($q_{\mathrm{V,leachate}}$) is calculated from the probability distribution of retention times of the water inside the waste-body with:

$$q_{\mathrm{V,leachate}}(t) = A_{\mathrm{lf}} \cdot \int_0^t q_{\mathrm{inf}}(t-\tau) \cdot f(\tau) d\tau \tag{4.4}$$

were A_{lf} is the area of the landfill, t is the time at a given moment and τ is the retention time of the water in the waste-body. The probability distribution of retention times, $f(\tau)$ is a bimodal lognormal distribution describing how water is retained in preferential fast flow paths and slow more immobile flow paths within the waste-body:

$$f(\tau) = \frac{\beta}{\tau\sigma_{\mathrm{fast}}\sqrt{2\cdot\pi}} e^{\frac{-(\ln\tau-\mu_{\mathrm{fast}})^2}{2\sigma_{\mathrm{fast}}^2}} + \frac{1-\beta}{\tau\sigma_{\mathrm{slow}}\sqrt{2\pi}} e^{\frac{-(\ln\tau-\mu_{\mathrm{slow}})^2}{2\sigma_{\mathrm{slow}}^2}} \tag{4.5}$$

where β is the fraction between fast and slow moving water and μ and σ are the mean and standard deviation of the fast moving or slow moving water residence times.

The integral in equation 4.4 is solved by assuming n discrete cells in the waste body each containing a volume water that is n-days from draining in to the pump pit. In other words, the index of each cell is the residence time in days for the volume of water present in the cell. Each time step, the daily volume of water infiltrating in to the waste body is distributed over all cells based on the distribution given in 4.5. As there are a limited number of cells, all remaining water (obtained from the cumulative distribution of 4.5) is added to the bulk waste:

$$V_{\mathrm{im,added}}^{t} = A_{\mathrm{lf}}\, q_{\mathrm{inf}}(t) \int_{\tau}^{\infty} f(\tau)) \tag{4.6}$$

where $f(\tau)$ is the pdf from 4.5. In order to maintain the water balance, water needs to be able drain to the mobile cells. This base flow is described with a free drainage type of relation:

$$q_{\mathrm{base}}^{\mathrm{water}} = -A_{\mathrm{lf}}\, K_{\mathrm{sat}}^{\mathrm{base}} \left(\frac{\theta_{\mathrm{b}} - \theta_{\mathrm{bres}}}{\theta_{\mathrm{bsat}} - \theta_{\mathrm{bres}}} \right)^{m_{\mathrm{base}}} \tag{4.7}$$

where $K_{\mathrm{sat}}^{\mathrm{base}}$ is a the saturated hydraulic conductivity in the bulk waste, θ_{b} is the volumetric water content of the bulk waste, $\theta_{\mathrm{b_{sat}}}$ and $\theta_{\mathrm{b_{res}}}$ are the saturated and residual water contents of the bulk waste respectively. Finally, m_{base} is an empirical shape parameter. It is important to realise that addition of this base flow to the model is a consequence of the discretization of the water residence times. If n is a very large number, for instance $>= 10.000$ days, the accumulation would be insignificant and the base flow could be neglected in the model.

4.2.4. Mathematics of the biodegradation model

We assume that the reactive mass in the bulk of the waste body degrades in time according to a set of dominant fundamental reactions and processes which are implemented in the biodegradation model. We implemented reaction network 2 from Turnhout et al. (2016), which is described in detail Chapter 2. In chapter 2 we showed that this reaction network gives an accurate description of anaerobic degradation of MSW in a waste-body at the landfill scale. To summarize, the biodegradation model keeps track of all mass changes in solid, water and gas phases with respect to kinetic and chemical equilibrium reactions, inhibition and limitation mechanisms and transfer processes. Consequently, it also calculates the amount of produced biogas in time. Inert mass such as chloride is not affected by the biodegradation model.

4.2.5. Mathematics of mass transport within the waste-body

Each time step, mass is exchanged between the immobile water volume and each mobile water volume cell i, assuming a first order exchange mechanism:

$$F_{\mathrm{m},i}^{\mathrm{transport}} = -k_{\mathrm{ex}} \left(C_{\mathrm{m},i} - C_{\mathrm{im}} \right) \tag{4.8}$$

and

$$F_{\mathrm{im}}^{\mathrm{transport}} = \sum_{\mathrm{i}=1}^{\mathrm{n}-1} k_{\mathrm{ex}} \left(C_{\mathrm{m},i} - C_{\mathrm{im}} \right) \tag{4.9}$$

where k_{ex} is the exchange constant, $C_{\mathrm{m},i}$ is the concentration in the mobile water volume present in cell i and C_{im} is the concentration in the immobile water volume present in the bulk of the waste body. In addition, mass is convected together with the base flow of water from the immobile water volume to the cell $n-1$ according to:

$$q_{\mathrm{base}}^{\mathrm{mass}} = q_{\mathrm{base}}^{\mathrm{water}} C_{\mathrm{im}} \tag{4.10}$$

4.3. Results & Discussion

4.3.1. Model calibration

The coupled model is calibrated in two steps. First, the parameters in the water flow model and exchange processes for conservative compounds are found by fitting the model results to measured time series of cumulative produced leachate

and chloride concentration in the leachate. The parameter optimization is performed using the Bayesian inference scheme implemented in the DREAM algorithm (Vrugt, 2016). The best fit is determined with a sum of squares criterion weighted by the standard deviation of the noise which is jointly optimized together with the parameters (van Turnhout et al., 2016, Vrugt, 2016). As a further check for the reliability of the optimized parameters, values obtained are compared with physical realistic values although we are very aware of the fact that this model is a severe simplification of reality and to a large extent empirical.

Figure 4.2 presents the measured data of cumulative produced leachate and chloride concentrations in the leachate together with the simulated results obtained with the optimal parameters. Figure 4.3 shows the measured and simulated data of the leachate discharge rate which is calculated from the cumulative leachate production. Both figures show that modelled and measured data agree well, the model captures the dynamics in leachate discharge (rates) and chloride concentrations. The $5\% - 95\%$ quantile ranges of the probability distributions of the optimized parameters are listed in table 4.1 together with the initial conditions. Most optimized parameter ranges compare reasonably well with physical realistic values which can be seen as an indication that the modelled processes make sense. Interestingly, the optimized exchange rate values give physical realistic estimates of the diffusion length ($= 0.053 - 0.071\,\mathrm{m}$) when compared to the diffusion constant for chloride in water ($D_{\mathrm{Cl}^-} = 1.73\mathrm{x}10^{-4}\,\frac{\mathrm{m}^2}{d}$) following:

$$dx_{\mathrm{diff}} = \sqrt{\frac{D_{\mathrm{Cl}^-}}{\mathrm{k_{ex}}}}. \tag{4.11}$$

In the second calibration step, the initial sodium concentration in leachate and three parameters of the biogeochemical reaction network are optimized by fitting the simulated results to the measured data of sodium and ammonium concentrations in the leachate. Also, four initial conditions are set differently than described in van Turnhout et al (2016) in order to mimic the conditions in the landfill from which the measured data were taken. The initial concentration of SOM is $0.02\,\frac{\mathrm{kg}}{\mathrm{kg\ drymatter}}$ and the initial concentrations of $\mathrm{NH_3}$, $\mathrm{Acetate}$ and methanogenic bacteria are low, resembling newly landfilled waste.

Modelled and measured data are presented in figure 4.3. The results show that the dynamics of ammonium concentration in the leachate can be described with this coupled water/exchange and biodegradation model calibrated on lysimeter data by re-fitting the hydrolysis constant and the stoichiometry of N ($s^{\mathrm{hyd}}_{\mathrm{NH_3}}$ and $s^{\mathrm{hyd}}_{\mathrm{C_X}}$) in the hydrolysis:

$$\mathrm{SOM} + 0.13\mathrm{H_2O} \rightleftharpoons 0.31\mathrm{VFA_{mix}} + 0.04\mathrm{CO_2} + s_{\mathrm{NH_3}}\mathrm{NH_3} + s_{\mathrm{C_X}}\mathrm{C_X} \tag{4.12}$$

A lower hydrolysis constant for the field scale case is reasonable since transport limitations between regions of hydrolysis and methanogenesis become more prominent than in the relatively well mixed lysimeter case. The influence of these transport limitations on the processes of hydrolysis and methanogenesis may be estimated

Table 4.1: 5% – 95% posterior quantiles or optimal values of the calibrated parameters and initial conditions.

Water flow model & exchange model							
Δz_{root} [m]	1.07 – 1.53	f_{crop} [−]	1.01 – 1.03	β [−]	0.53 – 0.60	$K_{\mathrm{sat}}^{\mathrm{base}}$ [$\frac{\mathrm{m}}{\mathrm{d}}$]	0.0001 – 61.03
$\theta_{\mathrm{r,cover}}$ [−]	0.00001 – 0.0035	$\theta_{\mathrm{s,cover}}$ [−]	0.29 – 0.36	m_{base} [−]	0.18 – 4.90	$\theta_{\mathrm{r,im}}$ [−]	0.18 – 0.47
$K_{\mathrm{sat}}^{\mathrm{inf}}$ [$\frac{\mathrm{m}}{\mathrm{d}}$]	0.016 – 0.048	m_{inf} [−]	4.24 – 4.65	A_{lf} [ha]	5.8 – 5.9	k_{ex} [d^{-1}]	0.034 – 0.062
μ_{fast} [d]	2.77 – 2.97[1)]	σ_{fast} [d]	1.26 – 1.74	$C_{\mathrm{im}}^{\mathrm{Cl}^-}$ [$\frac{\mathrm{kg}}{\mathrm{m}^3}$]	3.07 – 4.31	$f_{\mathrm{w}}^{\mathrm{ini}}$ [$\frac{\mathrm{kg\ water}}{\mathrm{kg\ dw}}$][2)]	0.30 – 0.47
μ_{slow} [d]	5.67 – 5.72[1)]	σ_{slow} [d]	0.35 – 0.42	n_{res} [−]	1250	n_{ex} [−]	365
Biodegradation model (with concentrations per volume of water)							
$C_{\mathrm{Na^+}}^{\mathrm{im}}$ [$\frac{\mathrm{kg}}{\mathrm{m}^3}$]	2.47	$s_{\mathrm{NH_3}}^{\mathrm{hyd}}$ [−]	0	$s_{\mathrm{C_x}}^{\mathrm{hyd}}$ [−]	0.15	k_{hyd} [d^{-1}]	0.001
$K_{\mathrm{s}}^{\mathrm{meth}}$ [M]	0.001						
Initial conditions (with concentrations per volume of water)							
$W_{\mathrm{lf}}^{\mathrm{wet}}$ [ton kg]	429	V_{lf} [ton m^3]	478	$C_{\mathrm{SOM}}^{\mathrm{im}}$ [$\frac{\mathrm{kg}}{\mathrm{kg\ dm}}$][2)]	0.02	$C_{\mathrm{Xmeth}}^{\mathrm{im}}$ [$\frac{\mathrm{kg}}{\mathrm{m}^3}$]	0.023
$C_{\mathrm{NH_4^+}}^{\mathrm{im}}$ [$\frac{\mathrm{kg}}{\mathrm{m}^3}$]	0	$C_{\mathrm{Ac}}^{\mathrm{im}}$ [$\frac{\mathrm{kg}}{\mathrm{m}^3}$]	0				

1) The optimized values of the bimodal water retention time distribution correspond to an average mean residence time of 54 days for fast flowing water and 320 days for slow flowing water. 2) Abbreviations dw and dm stand for dry waste and dry matter.

from gas and leachate emission measurements as described in Appendix A of this thesis. The stoichiometry of $\mathrm{NH_3}$ is very site-specific, depending on the composition of (organic) waste deposited. For this waste-body, the optimization indicates that the N content in SOM is lower than in the MSW used in the lysimeter experiments. As a consequence, it also indicates that the yield of $\mathrm{CO_2}$ is higher and the SOM is less reduced ($= \mathrm{CH_{1.58}O_{0.63}N_{0.03}}$) after balancing of the oxidation states.

In addition the good fit of ammonium and the similarity between the dynamics of ammonium, sodium and chloride, also indicate that the concentrations in the leachate are dominated by dilution with water with a relatively short residence time in the waste body. The concentrations are to a large extent controlled by the the same slow exchange mechanism; the same rate constant as calibrated for chloride works well. This especially holds for other non-reactive compounds such as sodium. For ammonium, production by hydrolysis in the immobile water is another important process dominating its concentration measured in the leachate. Optimized parameter values are listed in table 4.1. Estimates of the initial concentrations of chloride and sodium are in agreement with measured values from solid waste samples.

Figure 4.2: Measured and modelled time series of cumulative leachate production and concentration of chloride in the leachate used for calibration of the waterflow and exchange mechanism.

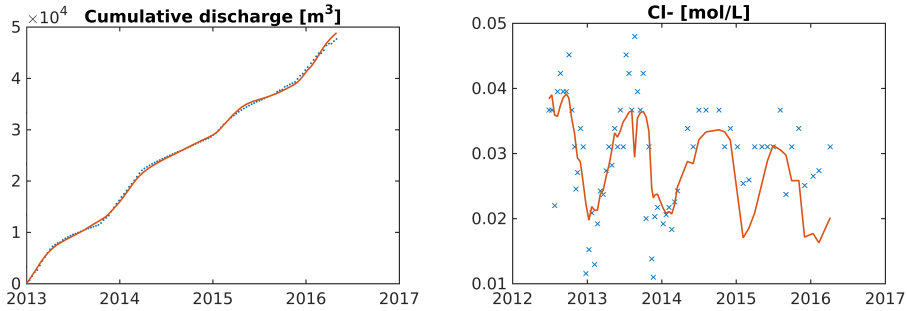

Figure 4.3: Measured and modelled time series of the leachate production rate and concentrations of sodium and ammonium in the leachate.

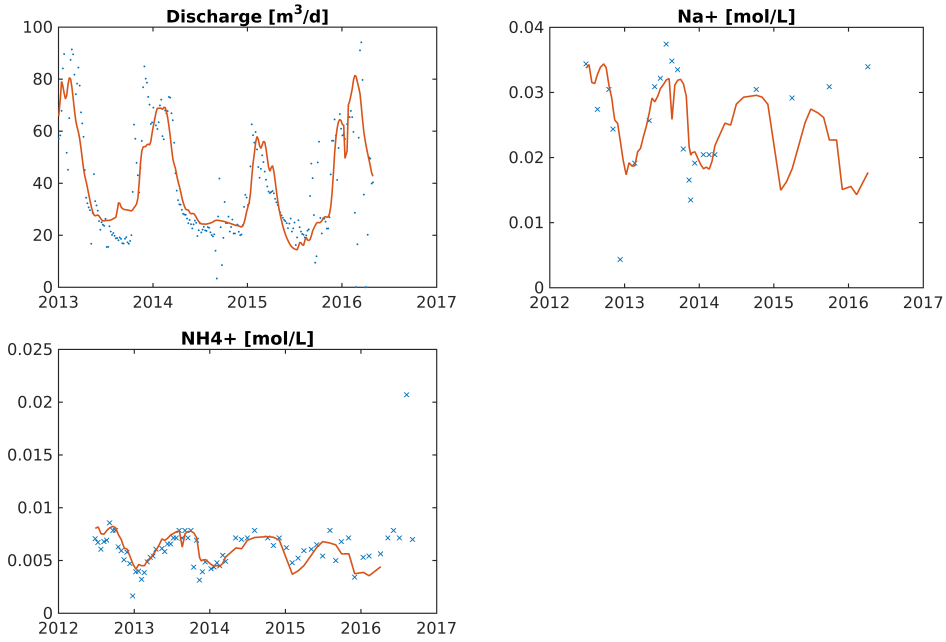

4.3.2. Information on emission potential and its uncertainty

A major benefit of this model is that after calibration, we can look at additional modelled states to obtain insights in to the potential emission behaviour of the landfill. Figure 4.4 shows a selection of masses and concentrations of compounds in the immobile water volume. The concentrations fluctuate because of the change in immobile water volume in time presented in figure 4.5. The masses indicate i.a. the amount of chloride and sodium left that potentially will leach out because this amount is in contact with water (the masses therefore do not represent the total amount in the waste-body). Their amounts are also decreasing indicating reduction of emission potential. The same reasoning holds for ammonium, except that it also is produced by hydrolysis and decay of bacteria (C_X). Both leaching and production of ammonium explains the relative less steep trend in ammonium concentration observed in the leachate compared to the chloride and sodium concentration. The decrease in emission potential of ammonium is less steep because it is also released from the solid phase. In conclusion, a first step towards quantification of the emission potential of a landfill is made.

The concentrations in the immobile water volume furthermore can indicate (emergence of) possible inhibition or limitations of the processes in the waste-body. For instance, a low pH results in slower inhibited hydrolysis which has a major impact on the reduction of emission potential of ammonium but also biogas (i.e. CO_2 and CH_4); the rate of biogas production is directly related to the rate of SOM hydrolysis. Because these are directly related, the amount of emitted biogas and reversely the emission potential of biogas in the form of organic carbon in SOM can also be predicted. Figure 4.4 shows that the mass of SOM decreases in time. The related modeled rate of biogas production in time is presented in figure 4.5 which is similar to those commonly observed at landfills after the filling phase has been completed.

In future studies it is very interesting to also calibrate the coupled model to other measured data. Biogas production on a field scale can reduce the uncertainty in the model states of emission potential of SOM, biogas, ammonium and likely also other states or parameters such as the hydrolysis constant and the half saturation constant for methanogenesis (K_S^{meth}). Other measured concentrations in the leachate can also reduce uncertainty. In this model for instance, the value of K_S^{meth} was set a bit lower than in the original network in order to establish a low acetate concentration which is common for mature leachates. In the same line of reasoning, settlement measurement data can also provide input to reduce overall model uncertainty when a proper mechanism of settlement in landfills is available.

Model calibration is now focused on the behavior of chloride and ammonium which are the two main problematic emitted compounds in landfills. However, because the model also provides information about SOM degradation, pH and other concentrations (e.g. H_2CO_3, HCO_3^-, CO_3^{-2} and Calcite) the model can easily be extended with mechanisms of e.g. dissolved organic matter (DOM) development, metal complexation or degradation of organic micros.

A first step is made in developing a framework to estimate remaining emission potential in landfills. However, some modeled states such as the immobile water volume are still very uncertain and have a major impact on the model outcome. It is

therefore needed to further develop this framework such that model error is further reduced. Minimizing error can be facilitated in several ways. One is (stochastically) simplifying or fundamentally intensifying the implemented processes to optimally use the prior and measured information available without over-parametrization. A second is adding processes to utilize more available measured data. A third is intensifying or testing new measurement techniques to further investigate the implemented processes. Another is to extend the modeling approach with data assimilation methods such as particle filtering which minimizes error in modeled states by correcting them with information in measured data.

4.4. Conclusions

This paper presents a model to predict long-term emissions from waste-bodies which optimally uses the measured data and fundamental insights available. Results from the first calibration step showed that the simplified, stochastic approach for modeling water flow is well-suited to reproduce measured data of leachate discharge. They also showed that dynamics in chloride concentration in the leachate can be explained with a diffusion type of compound exchange between mobile water and the immobile water volume. Moreover, results from the second calibration step showed that also the concentrations of sodium and ammonium in the leachate can be reproduced with this exchange mechanism with the same rate constant. The less steep trend in ammonium concentration compared with sodium and chloride is explained by simultaneous production of ammonium in the immobile water by hydrolysis and bacterial decay.

The major added value of this modeling approach is that after calibration, it also provides information about the potential emission behavior of the landfill through its modelled states. The amounts of all masses and their concentrations in contact with the immobile water, representing the leachable amounts, are available. We illustrated this by showing the reduction in emission potential of chloride, sodium and ammonium, but also SOM and the biogas production rate. In addition, modeled concentrations such as pH also indicate (emergence of) important inhibitions of biogeochemical processes potentially leading to delayed reduction of emission potential. Calibration of the model was focused on chloride and ammonium, however, the framework can easily be extended with mechanisms for other important pollutants such as DOM, metals or organic micros. In conclusion, the modeling approach presented provides a first step towards quantifying the emission potential of a landfill.

For further studies, it would be very interesting to reduce the uncertainty in modeled states and certain parameters by also calibrating the model with other measured data such as produced biogas. A modeled state with high uncertainty and a major impact on the model outcome is the immobile water volume. Suggestions for development to minimize uncertainty are o.a. simplifying or fundamentally intensifying the modeled processes, adding more processes to utilize more measured data, intensifying or testing new measurement techniques or applying data assimilation techniques such as particle filtering.

Figure 4.4: Modeled masses and concentrations of compounds in (contact with) the immobile water volume.

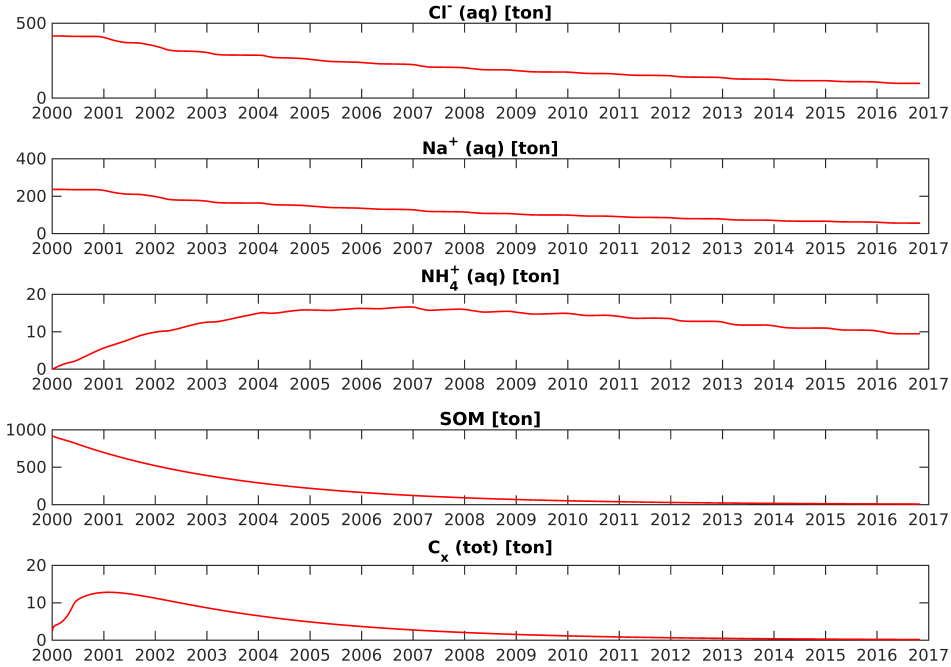

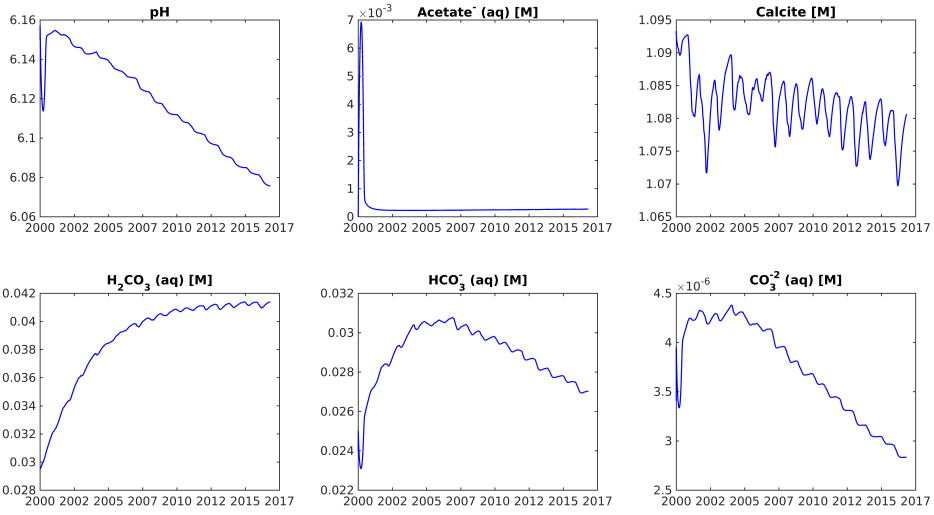

Figure 4.5: Modelled state of immobile water volume and gas production rate.

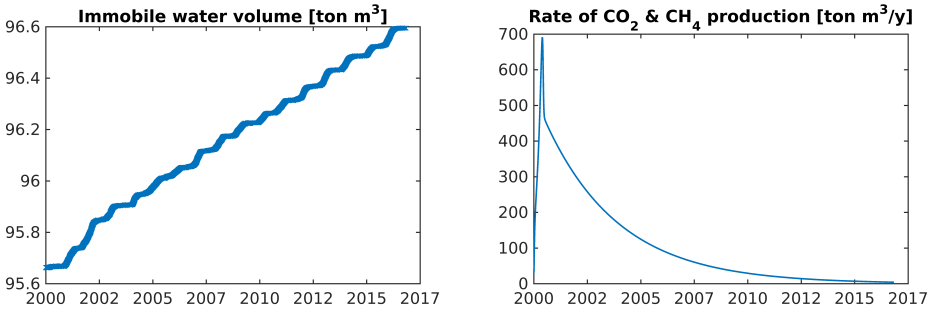

5

Optimizing landfill aeration strategy with a 3-D multiphase model

In order to reduce the environmental and financial burden for future generations, approaches are needed to improve and shorten after-care of Municipal Solid Waste (MSW) landfills. Aeration of the waste body is a promising approach, however, the poor understanding of gas and water through a waste-body makes it difficult to design an effective aeration strategy. This study presents a 3-D multiphase model to compare aeration strategies based on the air distribution they generate. The implemented theory is based on parameter values obtained from (laboratory) experiments performed under conditions which are similar to those in a full-scale landfill. Calibration with field scale gas extraction data shows that the model gives a good description of the average gas flow under extraction. Scenario analyses indicate that injection strategies reach a larger volume fraction of waste with a higher air flow compared with extraction strategies, especially at the bottom of the landfill. Extraction, however, supplies oxygen more homogeneously through-out the waste. Another important design criteria is the separation of the wells. Too large distances lead to ineffective treatment because too large volumes of waste/leachate remain untreated. For our case study Wieringermeer, a combination of (alternating) injection and extraction wells which are maximum 16.5 m *apart seems to be the optimal strategy.*

5.1. Introduction

Dutch operators and regulators seek approaches to shorten the aftercare of Municipal Solid Waste (MSW) landfills in order to reduce the environmental and financial burden of future generations. Essential to such an approach is a fast removal of compounds from the waste-body to such extent that the concentrations in remaining emissions are and remain acceptable (Laner et al., 2012, Scharff et al., 2011). The main challenge in developing these approaches is to accelerate the removal mechanisms in a waste-body which are severely inhibited and/or mass transport limited due to heterogeneity (Kjeldsen et al., 2002, Laner et al., 2011, Meima et al., 2008).

Aeration is an approach that showed promising results in lysimeter scale experiments. Injection of air into the waste-body leads to accelerated release of carbon and nitrogen to the leachate and gas phases (Brandstätter et al., 2015a,b, Erses et al., 2008). In general, aeration causes oxidation of many problematic compounds which are non-reactive under anaerobic conditions such as NH_4^+ (Bolyard and Reinhart, 2016) and oxidation can lead to immobilization of compounds that co-precipitate with oxidized dissolved organic matter (DOM). It has also been tested on a field scale (Ritzkowski and Stegmann, 2012), however, it has yet to be proven successful for reducing long-term emissions through leachate (Benson et al., 2007, Hrad et al., 2013).

A key factor influencing the effectiveness of aeration at the lysimeter scale is the amount of biodegradable carbon reached by the electron acceptor or main reactant (see chapter 3). Apparently, the most important factor for optimal aeration on a field scale is the distribution of air throughout the waste-body. As a consequence, knowing which aeration strategy yields the optimal distribution of air given the available energy resources and infrastructure is crucial for designing full-scale aeration projects.

Air flow through a waste-body at the field scale is not well understood. Field scale measurements and experiments are very scarce which limits the development of validated conceptual models (Hrad et al., 2013, Ritzkowski et al., 2006, Ritzkowski and Stegmann, 2012). Also, extensive numerical models (Fytanidis and Voudrias, 2014) are over-parametrized which results in poor calibration and therefore prediction. Although such models are interesting for fundamental insights, it is questionable if they give very realistic simulations of field scale conditions. As a result, a thorough quantitative comparison of different aeration strategies is currently missing in literature.

The aim of this paper is to compare different aeration strategies for the distribution of air they generate within a full scale waste-body. For this, we use a 3-D model based on fundamental principles from multiphase flow theory in porous media in which the liquid and gas phase pressures are coupled. The implemented theory is kept as simple as possible to limit over-parametrization. Material properties are obtained from literature data for lab scale experiments performed under conditions similar to those found in full scale landfills (Powrie and Beaven, 1999, Stoltz et al., 2010a,b, 2012). Data obtained from gas extraction measurements at the field scale are used for calibration.

Four common extraction/injection strategies with a relatively large well distance are compared with each other: 1) extraction near the bottom with short filters; 2) injection with long filters; 3) combined extraction (short filters) and injection (long filters); and 4) combined extraction near the bottom and injection near the surface with short filters (Hupe et al., 2003, Ritzkowski and Stegmann, 2012). In addition to the above four scenarios, we also presents a comparison of four different well separations. The criterion we chose to assess aeration effectiveness is the minimum air flow rate achieved in a certain volume percentage of the waste-body.

5.2. Material & Methods

5.2.1. Site characteristics, calibration, validation and scenarios

To illustrate the comparison of aeration strategies, we focus on finding an optimal aeration strategy for the Dutch pilot site Wieringermeer (Scharff and Jacobs, 2006). At this pilot site, one landfill cell has been selected to carry out a full-scale aeration pilot. The cell has a height of $12\ \mathrm{m}$ and an area of $2.6\ \mathrm{ha}$. Its waste-body has an estimated wet density of $1.28\ \frac{\mathrm{ton}}{\mathrm{m}^3}$ and approximately $19\ \mathrm{kg}$ biodegradable carbon left per m^3 of waste (van Vossen and Heyer, 2009). The landfill operator aims to convert 80% of the remaining carbon within 8 years via aeration. Based on the stochiometry this requires approximately $21.5\ \frac{\mathrm{m}^3_{\mathrm{air}}}{\mathrm{m}^3_{\mathrm{waste}} \cdot \mathrm{y}}$ if we assume an oxygen consumption of 80% and a conversion of $2.67\ \mathrm{kg}\ \mathrm{O}_2$ per $\mathrm{kg}\ \mathrm{C}$. Considering the inevitable heterogeneous distribution of air throughout the waste-body, an additional target is to achieve this $21.5\ \frac{\mathrm{m}^3_{\mathrm{air}}}{\mathrm{m}^3_{\mathrm{waste}} \cdot \mathrm{y}}$ in at least $85\%\ \frac{v}{v}$ of the waste-body. Especially, the lower part of the waste-body must receive sufficient air because we assume that the quality of leachate that can potentially infiltrate in to the sub-surface is mainly determined by processes at this depth. Finally, an important operational restriction for the implementation of the pilot is that pressure differences at the injection or extraction wells should not exceed $50\ \mathrm{mbar}$.

The numerical model (described in detail in section 2.2) is calibrated using measured flow rates during a gas extraction experiment carried out at the pilot site. Gas flow was measured through a single gas well during low pressure extraction. Details of this experiment are listed in table 5.1. To fit the modelled data to the measured data, a value for the parameter m of the water retention curve was selected which falls within the range measured in the experiments performed by Stoltz et al. (2012). All other parameters were obtained from experiments on MSW performed under landfilled conditions. The calibrated model was validated by comparison of simulations for other extraction experiment with measured data. For the validation scenario, the well separation, the well radius and the length of the well screens were smaller compared with the experiment used for calibration (table 5.1).

Aeration strategies are compared in two steps. In the first step, four injection/extraction strategies are compared based on the air distributions they generate. These strategies are: 1) air extraction with short, deep filters (inspired by the CDM system), 2) air injection with long filters (inspired by the IFAS system), 3)

Table 5.1: Specifications of the gas extraction experiments and modeled scenarios. R_{well}: radius of the well, L_s: filter screen length, $z_{\text{well}}^{\text{bottom}}$: bottom of well screen, D_{space}: well spacing

	R_{well} [m]	L_s [m]	$z_{\text{well}}^{\text{bottom}}$ [m]	type[1)]	D_{space} [m]
Calibration	0.5	7	−10	extracion	60
Validation	0.0315	0.9	−10	extraction	10
S1 $_{D10}$	0.0315	0.9	−10	extraction	10
S2 $_{D10}$	0.0315	5	−10	injection	10
S3 $_{D10}$	0.0315	[2 x 0.9 2 x 6.4][2)]	−10	extraction−injection	10
S4 $_{D10}$	0.0315	0.9	[2x − 10 2x − 2.9][3)]	extraction−injection	10
S3 $_{D16.5}$	0.0315	[2 x 0.9 2 x 6.4][2)]	−10	extraction−injection	16.5
S3 $_{D20}$	0.0315	[2 x 0.9 2 x 6.4][2)]	−10	extraction−injection	20
S3 $_{D30}$	0.0315	[2 x 0.9 2 x 6.4][2)]	−10	extraction−injection	30

1) for each type, a pressure difference is applied between either the extraction/injection well and the environment or between the extraction and injection wells. 2) the long filters are used for injection, the short filters for extraction. 3) the injection wells are shallow and the extraction wells deep.

combination of air injection with long filters and air extraction with short, deep filters and 4) combination of air injection with short, shallow filters and air extraction with short, deep filters. In the second step, the best injection/extraction strategy is evaluated with four well distances. Details of all scenarios are listed in table 5.1.

5.2.2. Model implementation

Governing equations

The implemented theory is based on Darcy's law for two-phase flow coupled in a 3-dimensional porous media which gives the flux for a phase α:

$$q_\alpha = -\nabla \frac{\kappa k_{r\alpha}}{\mu_\alpha} \left(\nabla p_\alpha + \rho_\alpha g \nabla z\right), \tag{5.1}$$

where α denotes the phase (w for water and g for the gas phase), q is the flux [m/s], κ is the permeability of the porous medium [m^2], $k_{r\alpha}$ is the relative permeability, μ_α is the viscosity [Pa s], p_α is the pressure [Pa], ρ the density, g the gravitational constant and z the vertical spatial coordinate. The mass balance equations for both phases are given by:

$$\frac{\partial \theta_\alpha \rho_\alpha}{\partial t} + \nabla \cdot \rho_\alpha q_\alpha + R_\alpha = 0, \tag{5.2}$$

where θ_α is the volumetric fraction of phase α [-], t the time [s] and R_α is the local production term of phase α [$\frac{kg}{m^3 s}$]. The mass balance equations for both phases can be coupled using the capillary pressure which is defined as the difference between the non-wetting and the wetting phase:

$$p_c = p_g - p_w. \tag{5.3}$$

If we then define the phase saturation as the ratio of the volumetric fraction of phase α to the porosity (ϕ [-]):

$$S_\alpha = \frac{\theta_\alpha}{\phi}, \tag{5.4}$$

we can then relate the two phase saturations with:

$$S_w + S_g = 1. \tag{5.5}$$

We use the van Genuchten equation (van Genuchten, 1980) to calculate the effective water saturation (S_e) from the capillary pressure:

$$S_e = \left(1 + (\alpha p_c)^{\frac{1}{1-m}}\right)^{-m} \text{ for } p_c > 0,\ S_e = 1 \text{ for } p_c =< 0, \tag{5.6}$$

where

$$S_e = \frac{S_w - S_{wr}}{1 - S_{wr}}. \tag{5.7}$$

Combining all above leads to two equations which describe the coupled rate of change in the pressures in both the water and the gas phase:

$$\phi\rho_w \left(S_w\beta_w - C_p\right)\frac{\partial p_w}{\partial t} + \nabla \cdot \rho_w q_w = -\phi\rho_w C_p \frac{\partial p_g}{\partial t} - R_w \tag{5.8}$$

and

$$\phi\rho_g \left(S_g\beta_g - C_p\right)\frac{\partial p_g}{\partial t} + \nabla \cdot \rho_g q_g = -\phi\rho_g C_p \frac{\partial p_w}{\partial t} - R_g, \tag{5.9}$$

where β_α is the compressibility for phase α and C_p is the specific moisture capacity which is defined as:

$$C_p(p_c) = \frac{\partial S_w(p_c)}{\partial p_c} = (1 - S_w)\frac{\partial S_e(p_c)}{\partial p_c} \tag{5.10}$$

Material properties

The properties of landfilled MSW are obtained from either data from lab scale experiments performed under conditions similar to landfilled conditions found in the literature or measurements performed at the field site under investigation. We assume that the porosity in the waste body decreases with depth:

$$\phi = \mathrm{a} + \frac{z}{\mathrm{b} - \mathrm{cz}}, \tag{5.11}$$

where the range is taken from Stoltz et al. (2010a) and the curvature is taken from White et al. (2014). The porosity along the depth (z) presented in figure 5.1 with a = 0.6125, b = 133.84 and c = 5.258.

The van Genuchten parameters in equation 5.6 are obtained from measurements performed by Stoltz et al. (2010, 2012). The water retention curve and the specific moisture capacity are shown in figure 5.1.

Figure 5.1: The porosity profile in depth (left), the water retention curve (middle) and the specific moisture capacity (right)

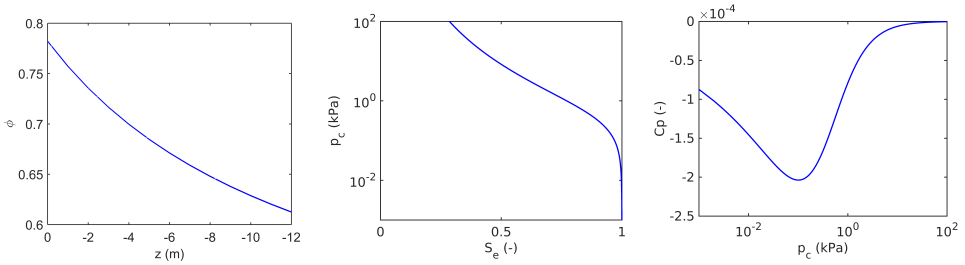

The relative permeabilities for the water and gas phase are calculated with:

$$k_{rw} = S_e^{L_w}\left(1-\left(1-S_e^{\frac{1}{G_w}}\right)^{G_w}\right)^2 \tag{5.12}$$

and

$$k_{rg} = (1-S_e)^{L_g}\left(1-S_e^{\frac{1}{G_g}}\right)^{2G_g,}, \tag{5.13}$$

where L_w and G_w are taken from White et al. (2014) and L_n and G_n are taken from Stoltz et al. (2010b). Intrinsic permeability is derived from the porosity with a power law fitted by Stoltz et al. (2010b) on measured data:

$$\kappa = 3.82\text{x}10^{-8}\cdot n^{18.13}. \tag{5.14}$$

The permeability of the waste body is anisotropic (Powrie and Beaven, 1999). Its value from equation 5.14 is therefore taken 2 x higher in the horizontal direction and 2 x lower in the vertical direction. Profiles of κ along the depth and kr_w and kr_n with respect to S_e are shown in figure 5.2.

Figure 5.2: The profiles for permeability (left), relative permeability of water (middle) and relative permeability of the gas(right)

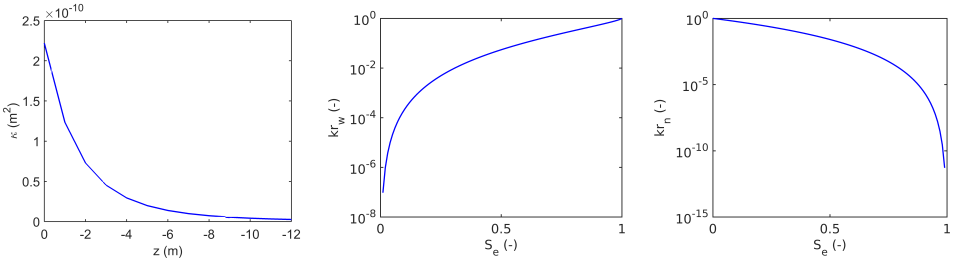

The density and compressibility of the gas phase are calculated from the ideal gas law as:

$$\rho_g = \frac{p_g M_g}{RT} \tag{5.15}$$

and

$$\beta_g = \frac{1}{\rho_g}\frac{\partial \rho_g}{\partial p_g} = \frac{M_g}{RT\rho_g} \tag{5.16}$$

where M_g is the molar mass of the gas phase, R is the universal gas constant and T is the ambient temperature [K]. All parameters related to material properties are listed in table 5.2. The gas production rate (R_g) was measured at the landfill site under investigation. We assumed that the water production rate within the waste body was zero.

Table 5.2: Parameters related to material properties and environmental conditions

T	298	K	R	8.31	$\frac{\text{J}}{\text{mol}\cdot\text{K}}$	p_{atm}	1	bar	ρ_w	1000	$\frac{\text{kg}}{\text{m}^3}$
z^{top}	12	m	z^{bot}	0	m	μ_w	0.001	Pa·s	μ_g	1.81×10^{-5}	Pa·s
β_w	4.55×10^{-10}	$\frac{1}{\text{Pa}}$	M_g	28.97	$\frac{\text{g}}{\text{mol}}$	z^{wt}	0.5	m	S_{wr}	0.4	–
m	0.26	–	α	0.0025	$\frac{1}{\text{Pa}}$	L_w	0.5	–	G_w	0.7	–
L_g	5.2	–	G_g	0.3	–	R_g	0.292	$\frac{\text{g}}{\text{m}^3\cdot\text{h}}$	K_{res}	0.01	m
F_w^{top}	0.001	$\frac{m}{d}$									

Geometry, boundary and initial conditions

The waste-body is modelled as a block with periodic, continuous boundary conditions at its sides. The size of the block and the placing of the wells depend on the type of aeration strategy. In Figure 5.3, two geometries for air extraction with different well spacing and filter lengths are shown together with the mesh.

Figure 5.3: Conceptualization of the block of a waste-body for 2 types of model domains/meshes. The left domain represents a single well extraction strategy, whereas the right domain represents extraction/injection with an evenly spaced grid of wells throughout the waste-body.

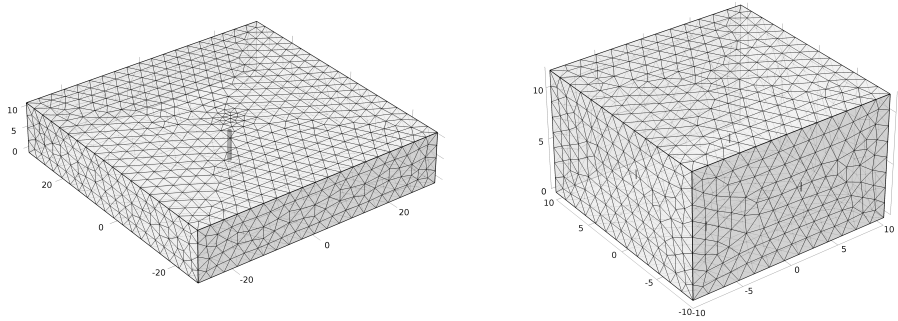

The top boundary condition for the water phase is given by an infiltration flux

(F_w^{top}) and for the gas phase by a Dirichlet condition:

$$p_g^{top} = p_{atm} e^{\frac{M_g g\left(z^{wt} - z^{top}\right)}{RT}} \tag{5.17}$$

where p_{atm} is the atmospheric pressure, z^{wt} is the height of the water table and z_{top} is the height of the waste-body. The bottom boundary condition for the water phase is a drainage flux given by:

$$F_w^{bot} = \rho_w \frac{k_{rw} Ks}{\mu_w} \left(\frac{p_{atm} + \left(z^{wt} - z^{bot}\right) \rho_w g}{K_{res}} \right) \tag{5.18}$$

where z^{bot} is the height of the bottom of the landfill and K_{res} is the resistance in the drainage layer. For the gas phase the bottom boundary condition is a Dirichlet condition:

$$p_n^{bottom} = p_{atm} e^{\frac{M_g g\left(z^{wt} - z^{bot}\right)}{R \cdot T}}. \tag{5.19}$$

5

The boundary conditions at the filters for the gas phase are Dirichlet conditions which impose pressure differences in relation to the atmosphere. The wells are assumed to be impermeable for water.

The initial water and gas pressure distribution in the model domain are assumed to be controlled by hydrostatic conditions:

$$p_w^{ini} = p_{atm} + \rho_w g \cdot \left(z^{wt} - z\right) \tag{5.20}$$

and

$$p_g^{ini} = p_{atm} e^{\frac{M_n g\left(z^{wt} - z\right)}{RT}}, \tag{5.21}$$

where we assume water to be incompressible.

Model resolution

The model is implemented in COMSOL 5.2 using two Coefficient Form PDE coupled modules. The mesh size is automatically generated with the option size fine. An example of the mesh size is given in figure 5.3. Equations are solved with the stationary solver (standard settings). A parametric sweep is used to investigate the steady state of the wetting phase and the gas phase pressures for a given series of gas pressure differences at the well boundaries.

5.3. Results & Discussion

The aim of is to find the best aeration strategy to generate an optimal air distribution throughout the waste-body for the Wieringermeer case. An optimal scenario was defined to have a minimum flow rate of 21.5 m^3 air per m^3 MSW per year in at least $85\%(v/v)$ of the waste-body while the gas pressure differences in the injection and/or extraction filters are less than $50\,\mathrm{mbar}$. In addition, the aim is to have good aeration in the lower parts of the waste body.

5.3.1. Calibration & validation

The agreement between simulated and measured flow rates at the extraction well for calibration data-set are shown in black in figure 5.4. The results show that the model is capable of reproducing the average behaviour of gas extraction through a single well at field scale using parameter values which are all retrieved from (laboratory) measurements under landfilled conditions. The fitted value of the van Genuchten parameter ($m = 0.26$) also falls in the range measured by Stoltz et al. (2012). The wide spread in measured flows per well, however, indicates that heterogeneity still has a significant impact on the gas extraction. Because we assume a homogeneous model domain we can only estimate the average flow behaviour. However, we believe that this model can be used to compare the performance of the aeration strategies because we want to do an overall, averaged comparison between scenarios.

In order to validate our model, we applied the calibrated model to simulate a second type of field scale experiment where completely different types of filters were used. Figure 5.4 presents also the modelled and measured data for this extraction experiment (in red) in which well dimensions and distances were smaller compared with the first experiment. In the left graph, extraction flow through a single well is presented. In the right graph, the pressure drop in filters nearby the extraction filter are presented. The fact that there is an agreement between the modelled and measured pressure drops in nearby wells gives us confidence in the plausibility of the modelled gas permeability throughout the waste-body.

Figure 5.4: Results of model calibration (in black) & validation (in red) on gas extraction data at different wells (W). The left graph shows the agreement between modelled and measured extraction flows through single wells. The right graph shows the agreement between modelled and measured pressures measured at wells surrounding the well from which air is extracted.

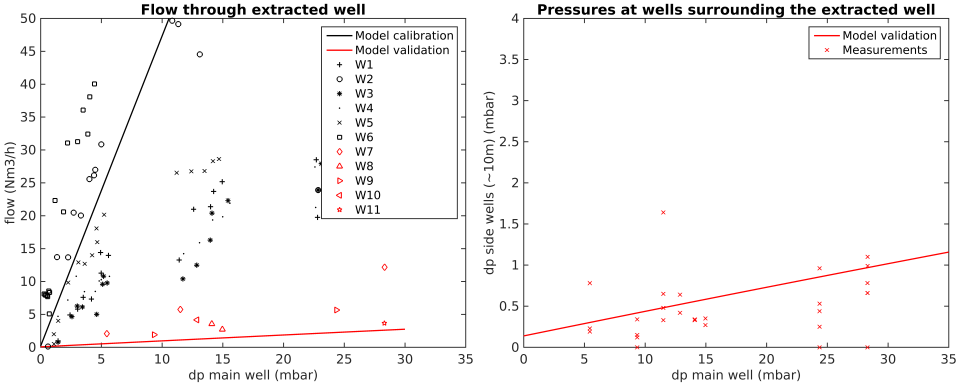

5.3.2. Optimal aeration strategy

Four different aeration scenarios were compared with each other using the calibrated model. Figures 5.5 and 5.6 present the air distribution generated by these four strategies through-out the block of waste at a pressure difference of $50\,\mathrm{mbar}$. Volumes with high flow rates are red and volumes with low flow rates are blue. Clearly, the injection strategy (S2) generates the highest flow rates in the largest volume of the waste block. It therefore produces the most optimal air distribution at a set pressure difference compared with the other strategies. Even more, the S2 strategy also produces the highest flow rates near the bottom of the landfill where most oxygen is needed because leachate accumulates here.

However, a strategy based on the extraction of gas may have a benefit compared with injection only because of how oxygen depletes as air travels through the waste. With injection, most of the oxygen is depleted near the filters where flow rates are also highest. As a result, the treatment of waste which is positioned further away from the filters may be poor because it receives little air with limited amounts of oxygen. In the extraction scenario air flow converges towards the filters thereby balancing oxygen depletion in the air by concentrating the air flow. Therefore, extraction scenarios provide both low flow regimes (near the surface) and high flow regimes (near the filters) with an approximately equal amount of oxygen.

A combined strategy of injection and extraction as in strategy S3, may therefore optimally distribute oxygen through-out the waste. While the distribution of air is best because of injection, the oxygen supply throughout the waste is more homogeneous because of extraction. However, it matters how both are combined as shown by the performance of strategy S4. The type of combination applied in this strategy is definitely not preferred because a large volume of the waste bottom is poorly aerated. For further study, we recommend to add convection of compounds in the non-wetting phase to the implemented model theory.

5.3.3. Optimal well spacing

Another important aspect that influences air distribution is the distance between the filters. We investigated the impact of four well spacings on the air distribution for aeration strategy S3 which performed best. Figures 5.7 and 5.8 present the air flow with well spacings of 10m, 16.5m, 20m and 30m. It shows that well distances must be small enough to treat a significant volume of waste with a significant flow of air. This means that the effectiveness of aeration treatment is highly dependent on the well distance applied. A too large distance may result in large volumes of untreated waste which after treatment still significantly contribute to the emitted concentrations via leachate.

To find the optimal well distance for aeration at Wieringermeer, we investigated the volume fraction reached by an air flow rate larger than $21.5\frac{\mathrm{m^3_{air}}}{\mathrm{m^3_w \cdot y}}$ under different applied pressures for each distance. The results are presented in figure 5.9. In order to treat at least $85\%\,(\frac{v}{v})$ of the waste-body, the maximum well spacing can be approximately $20\,\mathrm{m}$. A smaller well spacing is not preferred because investment costs are higher. Interestingly, in all four scenarios there is also some air flow

generated without applied pressure difference (indicated by the intersection of the results with the y-axis at 0 dp, figure 5.9). Apparently, natural convection is stimulated by perforation of the waste-body and enhances with smaller well distances.

In general, care must be taken with estimating optimal values for well distances with this homogeneous modeling approach. Although relatively a well distance may be optimal, in practice, heterogeneity has a significant impact on gas permeability. Therefore, modeled minimal flows achieved in a specific volume fraction may be overestimated as well as the effectiveness of the aeration strategy. For further model development, the addition of a simplistic mechanism for heterogeneity in permeability may already significantly improve prediction accuracy.

Figure 5.5: Airflow ($\frac{m}{h}$) through the domains for strategy S1-S2 at 50 mbar pressure difference and a well distance of 10 m. Volumes with high flow rates are red and volumes with low flow rates are blue.

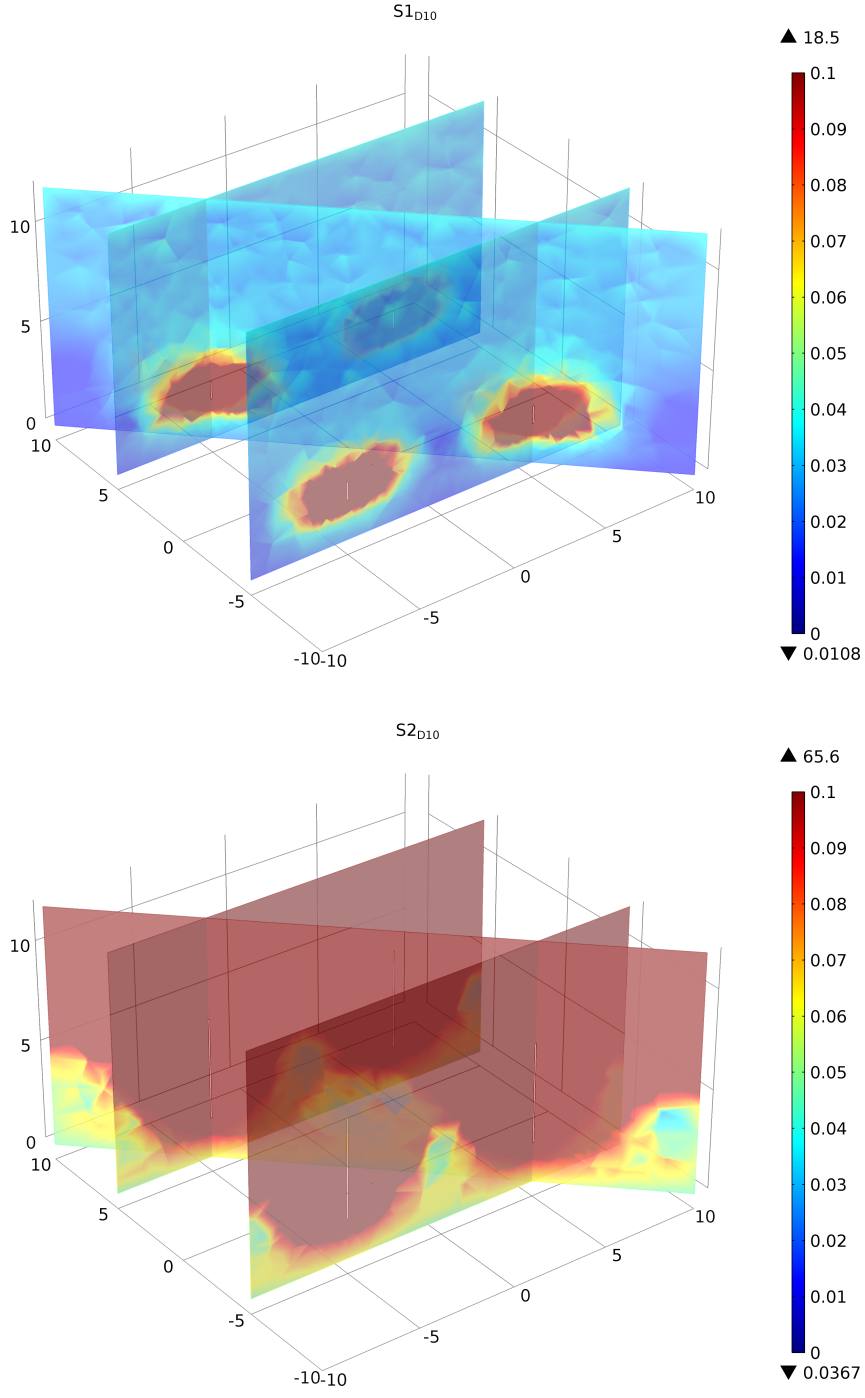

Figure 5.6: Airflow ($\frac{m}{h}$) through the domains for strategy S3-S4 at 50 mbar pressure difference and a well distance of 10 m. Volumes with high flow rates are red and volumes with low flow rates are blue.

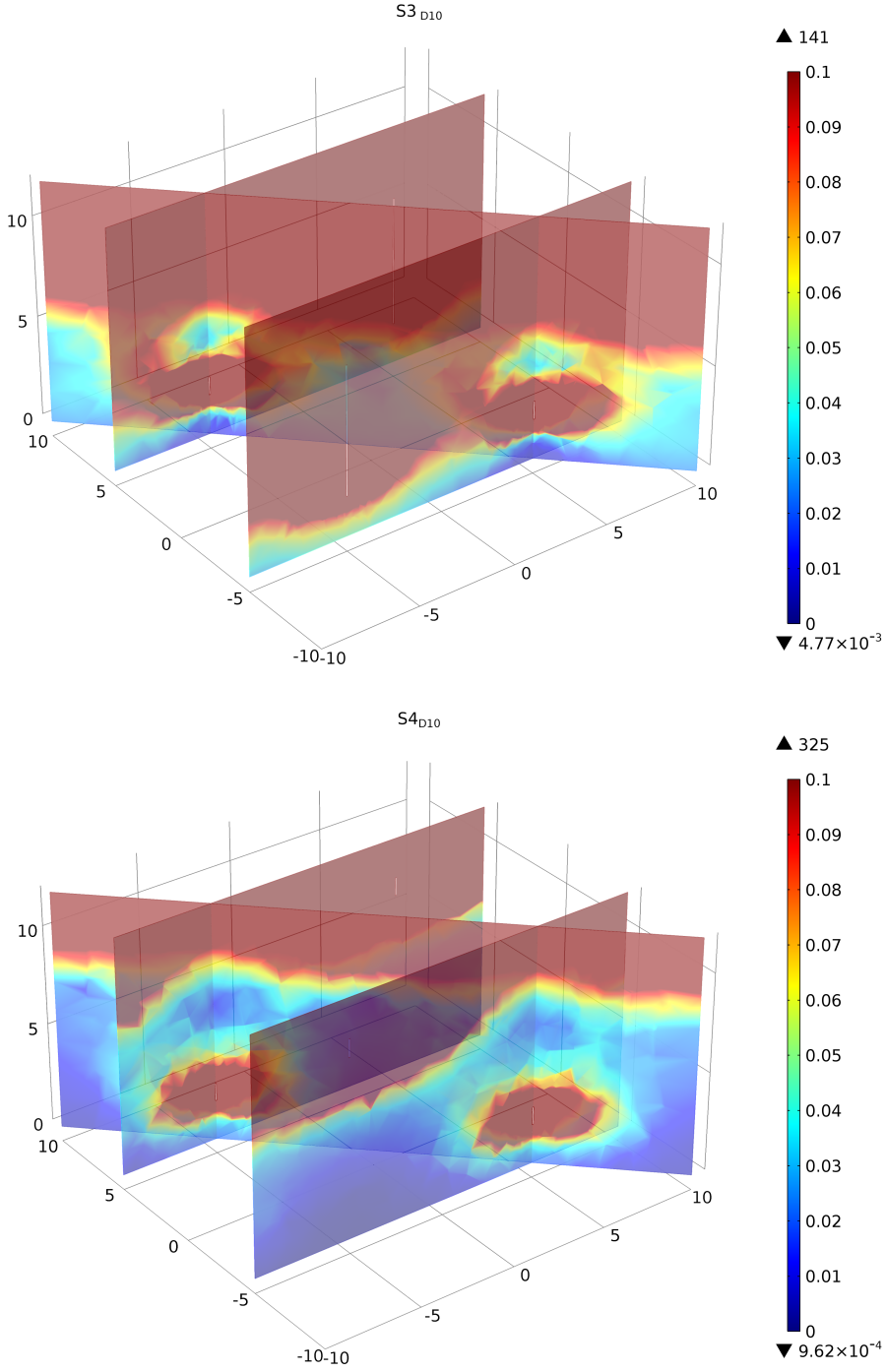

Figure 5.7: Airflow ($\frac{m}{h}$) through the domains for strategy S3 with well spacings D10-D16.5 at 50 mbar. Volumes with high flow rates are red and volumes with low flow rates are blue.

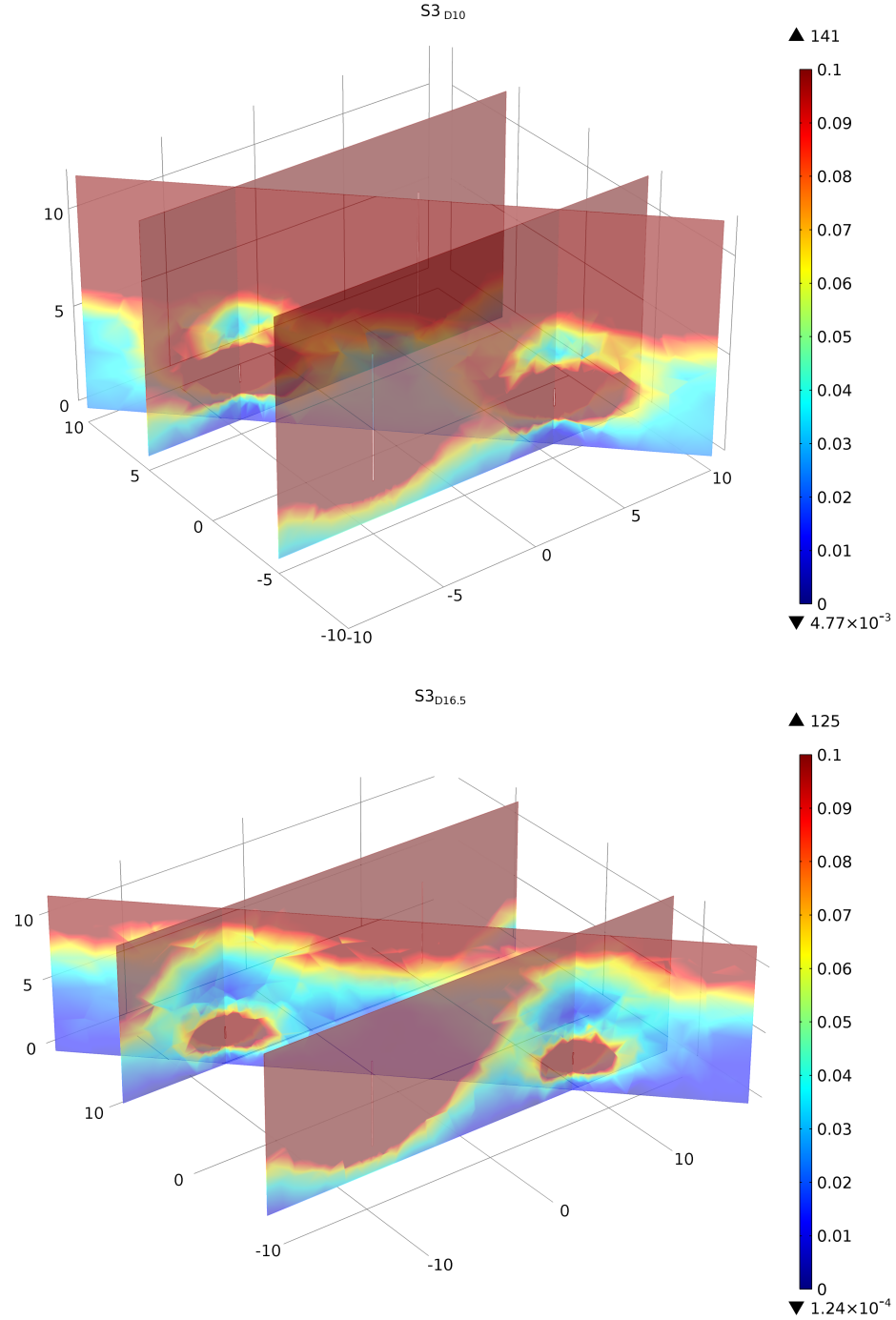

Figure 5.8: Airflow ($\frac{m}{h}$) through the domains for strategy S3 with well spacings D20-D30 at 50 mbar. Volumes with high flow rates are red and volumes with low flow rates are blue.

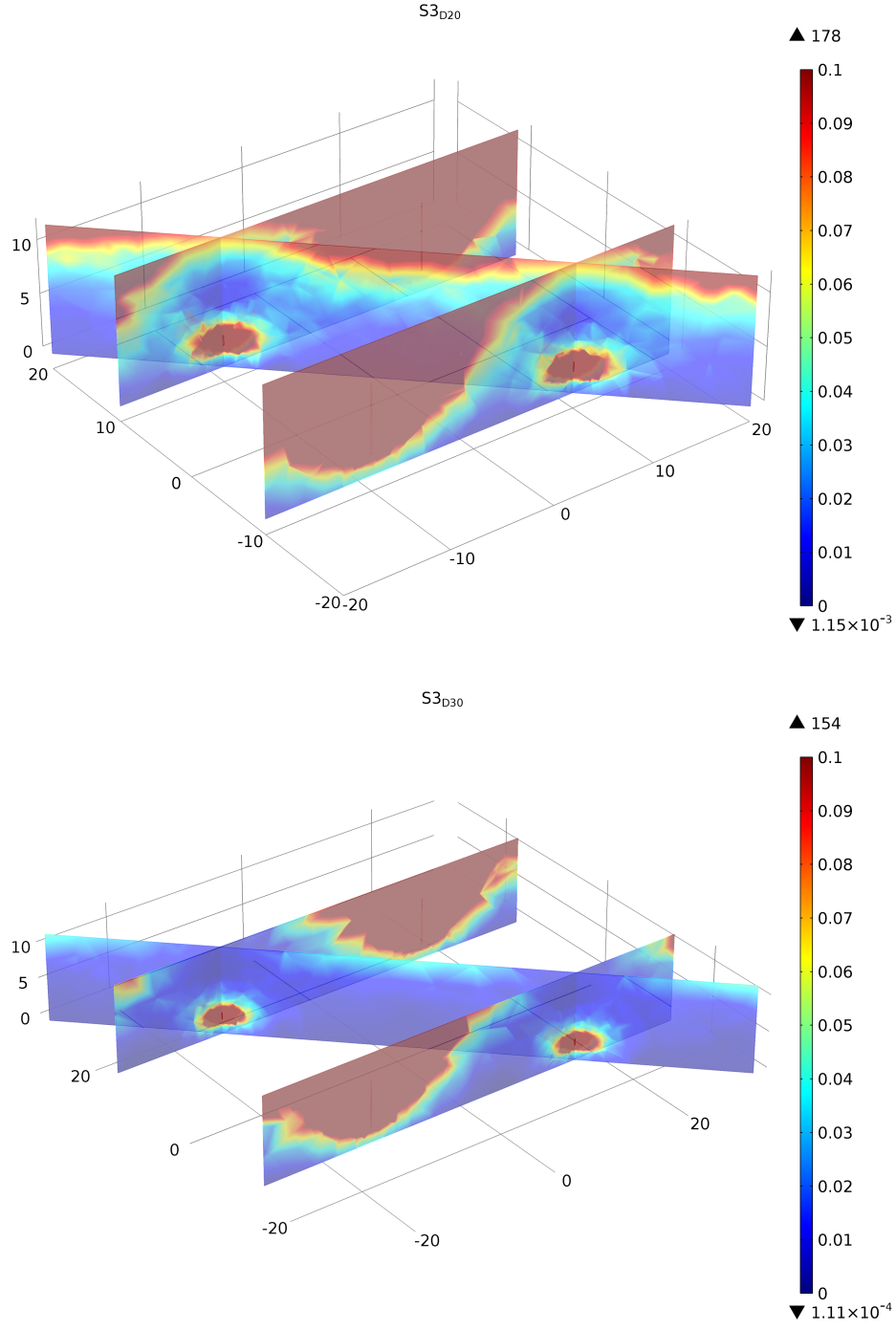

5

Figure 5.9: Percentage ($\frac{v}{v}$) of waste that receives an air flow rate larger than $21.5\,\frac{m^3_{air}}{m^3_w \cdot y}$ vs applied pressure difference for the well distances 10, 16.7, 20 and 30 m and aeration strategy S3.

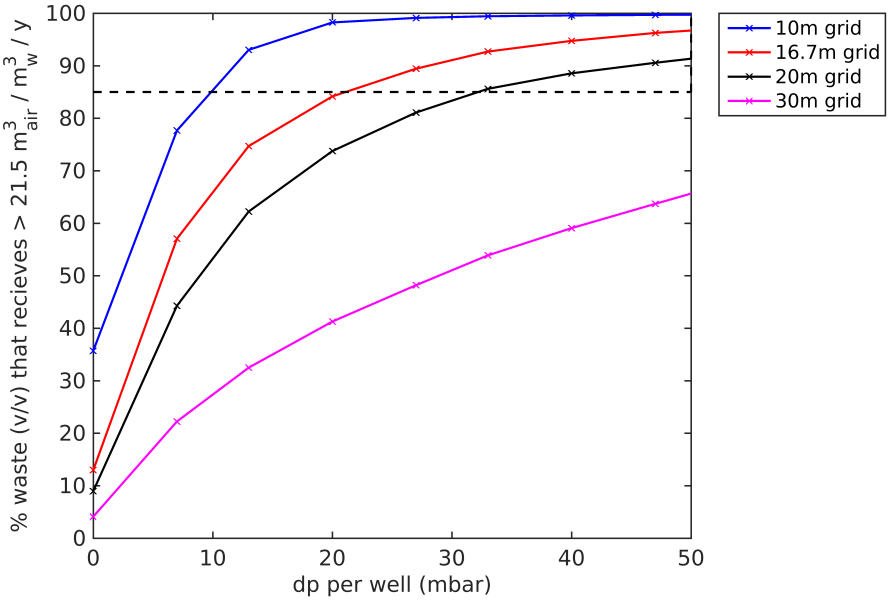

5.4. Conclusions

A 3-D multiphase model was developed to compare the effectiveness of different aeration strategies at the field scale. Model calibration & validation resulted in good agreement between modelled and measured field scale extraction data. The fundamental nature of the model which is based on material properties obtained from laboratory experiment under landfilled conditions gives confidence in the plausibility of the modelled scenarios and comparison of aeration strategies.

Four aeration strategies are compared based on the distribution of air they generate through out the waste-body. Injection generates the highest air flow in the largest volume of the waste-body. It also distributes most air towards the bottom of the waste-body. Extraction, however, provides a more homogeneous distribution of oxygen throughout the waste because oxygen depletion in the transported air is balanced by convergence of flow towards the wells. A combination of (alternating) extraction and injection wells may be most efficient.

A comparison of scenarios with different well spacings indicates that the distance between injection/extraction wells must be small enough for effective treatment. The risk of using a too large well distance is that a large volume of the waste-body and leachate will remain untreated. Interestingly, small well distances stimulate natural convection of air through out the waste-body because of perforation.

The optimal aeration strategy for our case study, Wieringermeer, is a combina-

tion of injection and extraction with a well distance of $20\,\mathrm{m}$. However, these design criteria must be interpreted with care because heterogeneity of the waste body is not included in the model. Most likely, the model overestimates the effectiveness of all aeration strategies.

6

Conclusions

The long-term emissions of leachate and gas from landfills pose a long time threat to human health and the environment. To understand which mechanisms control these emissions, many properties of and processes in landfills have been investigated through modeling and experiments. However, an important question remains unanswered. Which properties and processes dominate the emitted gas and leachate flows observed from the black box, the landfill? Or in other words, what defines the emission potential of a landfill? This thesis presents a quantifiable concept of emission potential by characterizing those processes within a landfill that control emissions and at the same time giving insight in to which processes are best to manipulate with treatment methods. The consequences and major uncertainties related to this novel concept of emission potential are now discussed.

6.1. Consequences of the insights obtained

6.1.1. Analysis of emission potential on a lysimeter scale

With the toolbox developed in chapter 2, we characterized the set of fundamental biogeochemical processes that controlled a.o. emission of biogas (i.e. CO_2 and CH_4), ammonium and pH at the lysimeter scale. This showed that, although the processes were not limited or inhibited, less than 25% of organic carbon and nitrogen is emitted under conditions of anaerobic leachate recirculation or aeration. This implies that most organic material left was not degradable or not reached by the main reactants needed for degradation such as O_2, methanogenic bacteria or water. This is very significant for how we define emission potential. It means that not all material within a waste-body poses a threat to the environment, but only that amount of the material that is able to react and is emitted/transported out at a sufficiently high enough rate. On a full scale, this amount is likely to be even smaller because environmental conditions are less ideal than in lysimeters.

But then, which processes control the release of compounds? For the lysimeter scale, we can simulate emissions that can reproduce measurements from initial

conditions with a small set of fundamental dominant kinetic biochemical reactions, equilibrium reactions and inhibitions/limitations. This set of processes enables us therefore to predict the emission potential within the boundaries of these processes. As example, the pH is correctly modeled by fundamental processes which provides insight in important potential inhibitions of biodegradation and also the leaching potential of metals in relation with Dissolved Organic Matter (DOM). Even more, via inverse modeling we can estimate the emission potential left in the waste-body from measured gas and leachate emissions. The set of processes also allows us to predict the impact of treatment methods applied to accelerate emissions.

6.1.2. Analysis of emission potential on a full scale

We extrapolated these findings to a data set obtained from full-scale waste bodies in chapter 4 and 5. Chapter 4 presented an approach in which the distribution of retention times of water within the waste-body is the main scale factor. It is modeled stochastically with a probability distribution. In water with long residence times in the landfill, organic matter is considered to be degraded according to the set of fundamental processes found at the lysimeter scale. The model assumes that dissolved compounds are transported from immobile water in the bulk of the waste to more mobile water (with lower residence times) according to a diffusional exchange mechanism. Water with the lowest residence time represents the leachate discharged from the landfill. This approach enabled us to reproduce full scale emissions of organic and inorganic compounds. Even more, the modeled states give us a first insight in to the quantifiable emission potential at the full scale: an estimate of the mass of biodegradable and leachable compounds present in the waste-body. Rather than total amounts present in the waste-body, these states represent the total amounts degradable or leachable under the prevailing environmental conditions.

Chapter 5 fundamentally investigated the distribution of water and gas at the full scale in order to study the impact of treatment methods on these distributions. Fundamental processes and material properties were taken from laboratory experiments performed under conditions found in full-scale waste bodies and biogeochemical processes were not considered. Comparison with gas extraction data measured in full-scale waste bodies showed that the material properties measured in the lab can explain the flow of gas at a full scale. Results furthermore showed that leachate recirculation with higher rates than precipitation rates do not cause ponding. The wettest regions of the waste-body are located near the bottom. The area of influence of aeration wells is likely overestimated in the model because preferential flow is missing. However, the scenarios show that wells have to be placed close enough together and near the bottom in order to achieve a sufficient distribution of oxygen for effective leachate treatment.

6.2. Uncertainties leading to new research proposals

6.2.1. Release mechanism of ammonium (proposal 1)

Some major uncertainties remain in the presented quantifiable concept of emission potential which when resolved can substantially improve model performance. One uncertainty is the release mechanism of ammonium under anaerobic conditions, especially the mechanism for the sink of ammonium observed in the experiments. Multiple fundamental mechanisms may be responsible for the ammonium removal. One is oxidation of ammonium into nitrogen by some oxidator present or leaking into the waste-body. Other plausible mechanisms are adsorption, inclusion of ammonium into DOM or slow transport of ammonium from a bulk of hydrolyzed ammonium to the leached water. As ammonium is one of the most important emitted compounds to be reduced, further investigation into its dominant release mechanism is very important. Several measurements can be used to falsify or confirm proposed mechanisms. For instance, the ratio of stable isotopes in leached ammonium could indicate the occurrence of oxidation of ammonium within the waste-body.

6.2.2. Development of DOM over time (proposal 2)

Another remaining uncertainty in the model is the development of DOM over time. In our approach, the amount of DOM is the fraction of carbon which remains in solution, not converted into biogas or bacterial biomass. Although this allows to estimate the total amount of DOM produced over time, it does not characterize the (change in) functional properties of DOM over time. Whereas, it are the functional properties of DOM which determine its adsorption, complexation and precipitation capacity with e.g. metals and organic micro pollutants. Recently, it has been proposed that the change in composition and functionality of DOM is caused by the change in its micro-constituents. In further research, it would be very interesting to include this fundamental principle of aging of DOM in the model and link this with the major knowledge base on DOM functionality developed over the past decade. A better understanding of DOM behavior would lead to improved estimation of o.a. metal and organic micro pollutant emissions.

6.2.3. Full scale water retention times (proposal 3)

A major uncertainty in the upscaled modeling approach is the volume of immobile water present in a landfill. This uncertainty dominates the uncertainty in modeled states of biodegradable, leachable masses in contact with the immobile water, i.e. the modeled emission potential. The key for further research is to develop new measurement techniques for landfills to obtain more insight in uncertain modeled states such as the residence times of water. A first suggestion is to apply a range of tracer tests on a waste-body. This can directly give information about residence times of water and to what extent mass and water travels through preferential flowpaths and is exchanged with immobile water. Another suggestion is time-lapse electrical resistivity tomography (ERT) which correlates to differences in water distribution via Archie's law. The information obtained from ERT can be translated into water

retention probabilities when also the in and outflow of water at the landfill is closely monitored. Improved calibration of water retention times may also be achieved by obtaining more information about biochemical activity because activity occurs only at sufficiently wet locations. Biochemical activity can be further investigated with distributed temperature sensing which allows to monitor temperature changes within the waste-body correlated with enthalpy production. Even settlement measurements can be very valuable once a mechanism is included in the model which relates settlement with biodegradation and indirectly measured gas emissions.

6.2.4. Delay in biogas production

Another uncertainty is the mechanism responsible for the delay in biodegradation or biogas production on a full scale. The prevailing hypothesis is that delay is caused by diffusional transport of Volatile Fatty Acids produced during hydrolysis/fermentation to methanogenic bacteria which results in pH inhibited hydrolysis and substrate limited methanogenesis. Interestingly if correct, the degree of delay should be correlated to the diffusion length of the transport and therefore directly characterizable from measured gas and leachate production. Appendix A describes first steps towards identification of the diffusion length responsible for delay in biogas production from emission measurements. Characterization of typical diffusion lengths for landfills can significantly enhance gas prediction models by identifying the main limiting step.

Overall, a first quantifiable concept of emission potential has been presented which when the main uncertainties are reduced can become a powerful tool to grasp the emission potential of MSW landfills.

Bibliography

Angelidaki, I., Ellegaard, L., and Ahring, B. K. (1999). A comprehensive model of anaerobic bioconversion of complex substrates to biogas. *Biotechnology and bioengineering*, 63(3):363–72.

Atkins, P. and de Paula, J. (2011). *Physical chemistry for the life sciences*. Freeman, W.H.

Batstone, D. J., Keller, J., Angelidaki, I., Kalyuzhnyi, S. V., Pavlostathis, S. G., Rozzi, A., Sanders, W. T. M., Siegrist, H., and Vavilin, V. A. (2002). The IWA Anaerobic Digestion Model No 1 (ADM1). *Water science and technology : a journal of the International Association on Water Pollution Research*, 45(10):65–73.

Belevi, H. and Baccini, P. (1989). Long-term behavior of municipal solid waste landfills. *Waste Management & Research*, 7:43–56.

Bennett, N. D., Croke, B. F. W., Guariso, G., Guillaume, J. H. A., Hamilton, S. H., Jakeman, A. J., Marsili-Libelli, S., Newham, L. T. H., Norton, J. P., Perrin, C., Pierce, S. A., Robson, B., Seppelt, R., Voinov, A. A., Fath, B. D., and Andreassian, V. (2013). Characterising performance of environmental models. *Environmental Modelling & Software*, 40:1–20.

Benson, C. H., Barlaz, M. A., Lane, D. T., and Rawe, J. M. (2007). Practice review of five bioreactor/recirculation landfills. *Waste management (New York, N.Y.)*, 27(1):13–29.

Berge, N. D., Reinhart, D. R., and Batarseh, E. S. (2009). An assessment of bioreactor landfill costs and benefits. *Waste Management*, 29(5):1558–1567.

Bethke, C. (2008). *Geochemical and biogeochemical reaction modeling*. Cambridge University Press, Cambridge U.K.

Bilgili, M. S., Demir, A., and Ozkaya, B. (2007). Influence of leachate recirculation on aerobic and anaerobic decomposition of solid wastes. *Journal of Hazardous Materials*, 143(1-2):177–183.

Bolyard, S. C. and Reinhart, D. R. (2016). Application of landfill treatment approaches for stabilization of municipal solid waste. *Waste Management*, 55:22–30.

Brandstätter, C., Laner, D., and Fellner, J. (2015a). Carbon pools and flows during lab-scale degradation of old landfilled waste under different oxygen and water regimes. *Waste Management*, 40:100–111.

Brandstätter, C., Laner, D., and Fellner, J. (2015b). Nitrogen pools and flows during lab-scale degradation of old landfilled waste under different oxygen and water regimes. *Biodegradation*, 26(5):399–414.

Dijkstra, J. J., Van Der Sloot, H. A., and Comans, R. N. J. (2006). The leaching of major and trace elements from MSWI bottom ash as a function of pH and time. *Applied Geochemistry*, 21(2):335–351.

Erses, A. S., Onay, T. T., and Yenigun, O. (2008). Comparison of aerobic and anaerobic degradation of municipal solid waste in bioreactor landfills. *Bioresource technology*, 99(13):5418–26.

Fellner, J., Döberl, G., Allgaier, G., and Brunner, P. H. (2009). Comparing field investigations with laboratory models to predict landfill leachate emissions. *Waste management (New York, N.Y.)*, 29(6):1844–51.

Fytanidis, D. K. and Voudrias, E. A. (2014). Numerical simulation of landfill aeration using computational fluid dynamics. *Waste Management*, 34(4):804–816.

Garcia de Cortazar, A. L. and Monzon, I. T. (2007). MODUELO 2: A new version of an integrated simulation model for municipal solid waste landfills. *Environmental Modelling & Software*, 22(1):59–72.

Gawande, N. A., Reinhart, D. R., and Gour-Tsyh, Y. (2010). Modeling microbiological and chemical processes in municipal solid waste bioreactor, Part II: Application of numerical model BIOKEMOD-3P. *Waste management (New York, N.Y.)*, 30(2):211–8.

Gönüllü, M. (1994). Analytical modelling of organic contaminants in leachate. *Waste management & research*, 12:339–350.

Haldane, J. (1930). Enzymes. *Journal of the Society of Chemical Industry*, 49:919–920.

Heijnen, J. J. and Kleerebezem, R. (1999). *Bioenergetics of microbial growth*.

Henze, M., Harremoes, P., Jansen, J., and Arvin, E. (1995). Wastewater Treatment - Biological and Chemical Processes.

Hoornweg, D. and Bhada-Tata, P. (2012). What a Waste, A Global Review of Solid Waste Management. *Urban development series*, 15.

Hrad, M., Gamperling, O., and Huber-Humer, M. (2013). Comparison between lab- and full-scale applications of in situ aeration of an old landfill and assessment of long-term emission development after completion. *Waste Management*, 33(10):2061–2073.

Hupe, K., Koop, A., and Ritzkowski, M. (2003). The low pressure aeration of landfills: experience, operation and costs. In *Proceedings Sardinia 2003, Ninth International Waste Management and Landfill Symposium*, number 9. CISA, Environmental Sanitary Engineering Centre.

Jury, W. A. and Roth, K. (1990). *Transfer functions and solute movement through soil: theory and applications.* Birkhäuser Verlag AG, Basel, Switzerland.

Kamalan, H., Sabour, M., and Shariatmadari, N. (2011). A review on available landfill gas models. *Journal of Environmental Science and Technology*, 4:79–92.

Kantartzi, S. G., Vaiopoulou, E., Kapagiannidis, A., and Aivasidis, A. (2006). Kinetic Characterization of Nitrifying Pure Cultures in Chemostate. *Global NEST Journal*, 8(1):43–51.

Karaca, F. and Özkaya, B. (2006). NN-LEAP: A neural network-based model for controlling leachate flow-rate in a municipal solid waste landfill site. *Environmental Modelling & Software*, 21(8):1190–1197.

Kasam, S., Syamsiah, S., and Prasetya, A. (2013). Effect of Leachate Recirculation on Characteristics of Leachate Generation of Municipal Solid Waste from Landfill Lysimeter. *Journal of Chemistry and Chemical Engineering*, 7:456–461.

Kelly, R. A., Jakeman, A. J., Barreteau, O., Borsuk, M. E., ElSawah, S., Hamilton, S. H., Henriksen, H. J., Kuikka, S., Maier, H. R., Rizzoli, A. E., van Delden, H., and Voinov, A. A. (2013). Selecting among five common modelling approaches for integrated environmental assessment and management. *Environmental Modelling & Software*, 47:159–181.

Khalid, A., Arshad, M., Anjum, M., Mahmood, T., and Dawson, L. (2011). The anaerobic digestion of solid organic waste. *Waste Management*, 31(8):1737–1744.

Kjeldsen, P., Barlaz, M., Rooker, A. P., Ledin, A., and Christensen, T. H. (2002). Present and Long-Term Composition of MSW Landfill Leachate: A Review. *Critical Reviews in Environmental Science and Technology*, 32(4):297–336.

Kleerebezem, R. and van Loosdrecht, M. C. M. (2010). A Generalized Method for Thermodynamic State Analysis of Environmental Systems. *Critical Reviews in Environmental Science and Technology*, 40(1):1–54.

Kouzeli-Katsiri, A., Bosdogianni, A., and Christoulas, D. (1999). Prediction of leachate quality from sanitary landfills. *Journal of Environmental Engineering*, 125(October):950–958.

Kumar, S., Chiemchaisri, C., and Mudhoo, A. (2011). Bioreactor landfill technology in municipal solid waste treatment: An overview. *Critical Reviews in Biotechnology*, 31(1):77–97.

Laloy, E. and Vrugt, J. A. (2012). High-dimensional posterior exploration of hydrologic models using multiple-try DREAM (ZS) and high-performance computing. *Water Resources Research*, 48(1):W01526.

Laner, D., Crest, M., Scharff, H., Morris, J. W. F., and Barlaz, M. A. (2012). A review of approaches for the long-term management of municipal solid waste landfills. *Waste management (New York, N.Y.)*, 32(3):498–512.

Laner, D., Fellner, J., and Brunner, P. H. (2011). Future landfill emissions and the effect of final cover installation–a case study. *Waste management (New York, N.Y.)*, 31(7):1522–31.

Macklin, Y., Kibble, A., and Pollitt, F. (2011). Impact on Health of Emissions from Landfill Sites: Advice from the Health Protection Agency. Technical report, Health Protection Agency.

MATLAB Release 2015a (2015). The MathWorks, Inc.

McDougall, J. (2007). A hydro-bio-mechanical model for settlement and other behaviour in landfilled waste. *Computers and Geotechnics*, 34(4):297–320.

Meeussen, J. C. L. (2003). ORCHESTRA: an object-oriented framework for implementing chemical equilibrium models. *Environmental science & technology*, 37(6):1175–82.

Meima, J. A., Naranjo, N. M., and Haarstrick, A. (2008). Sensitivity analysis and literature review of parameters controlling local biodegradation processes in municipal solid waste landfills. *Waste management (New York, N.Y.)*, 28(5):904–18.

Monod, J. (1949). The growth of bacterial cultures. *Annual Reviews in Microbiology*, (x):371–394.

Newton, M. A. and Raftery, A. E. (1994). Approximate Bayesian Inference with the Weighted Likelihood Bootstrap. *Journal of the Royal Statistical Society*, 56(1):3–48.

Nopharatana, A., Pullammanappallil, P. C., and Clarke, W. P. (2007). Kinetics and dynamic modelling of batch anaerobic digestion of municipal solid waste in a stirred reactor. *Waste management (New York, N.Y.)*, 27(5):595–603.

Ozkaya, B., Demir, A., and Bilgili, M. (2007). Neural network prediction model for the methane fraction in biogas from field-scale landfill bioreactors. *Environmental Modelling & Software*, 22(6):815–822.

Paula Jr, D. R. and Foresti, E. (2009). Sulfide toxicity kinetics of a uasb reactor. *Brazilian Journal of Chemical Engineering*, 26(04):669–675.

Plummer, L. N. and Busenburg, E. (1982). The solubilities of calcite, aragonite and vaterite in CO2-H2O solutions between 0 and 90 C, and an evaluation of the aqueous model for the system CaCO3-CO2-H2O. *Geochimica et cosmochimica acta*, 46.

Powrie, W. and Beaven, R. (1999). Hydraulic properties of household waste and implications for landfills. *Proceedings of the ICE - Geotechnical Engineering*, 137(4):235–247.

Reichel, T., Ivanova, L. K., Beaven, R. P., and Haarstrick, A. (2007). Modeling Decomposition of MSW in a Consolidating Anaerobic Reactor. *Environmental Engineering Science*, 24(8):1072–1083.

Ritzkowski, M., Heyer, K.-U., and Stegmann, R. (2006). Fundamental processes and implications during in situ aeration of old landfills. *Waste management (New York, N.Y.)*, 26(4):356–72.

Ritzkowski, M. and Stegmann, R. (2012). Landfill aeration worldwide: concepts, indications and findings. *Waste management (New York, N.Y.)*, 32(7):1411–9.

Roychoudhury, A. N., Van Cappellen, P., Kostka, J. E., and Viollier, E. (2003). Kinetics of microbially mediated reactions: dissimilatory sulfate reduction in saltmarsh sediments (Sapelo Island, Georgia, USA). *Estuarine, Coastal and Shelf Science*, 56(5-6):1001–1010.

Rzeczycka, M. and Blaszczyk, M. (2005). Growth and activity of sulphate-reducing bacteria in media containing phosphogypsum and different sources of carbon. *Polish Journal of environmental studies*, 14(6):891–895.

Scharff, H. (2014). Landfill reduction experience in The Netherlands. *Waste Management*, 34(11):2218–2224.

Scharff, H. and Jacobs, J. (2006). Applying guidance for methane emission estimation for landfills. *Waste management (New York, N.Y.)*, 26(4):417–29.

Scharff, H., van Zomeren, A., and van der Sloot, H. A. (2011). Landfill sustainability and aftercare completion criteria. *Waste management & research : the journal of the International Solid Wastes and Public Cleansing Association, ISWA*, 29(1):30–40.

Schoups, G. and Vrugt, J. A. (2010). A formal likelihood function for parameter and predictive inference of hydrologic models with correlated, heteroscedastic, and non-Gaussian errors. *Water Resources Research*, 46(10):531.

Siegrist, H., Vogt, D., Garcia-Heras, J. L., and Gujer, W. (2002). Mathematical model for meso- and thermophilic anaerobic sewage sludge digestion. *Environmental Science and Technology*, 36(5):1113–23.

Stoltz, G., Gourc, J. P., and Oxarango, L. (2010a). Characterisation of the physico-mechanical parameters of MSW. *Waste Management*, 30(8-9):1439–1449.

Stoltz, G., Gourc, J. P., and Oxarango, L. (2010b). Liquid and gas permeabilities of unsaturated municipal solid waste under compression. *Journal of Contaminant Hydrology*, 118(1-2):27–42.

Stoltz, G., Tinet, A., Staub, M. J., Oxarango, L., and Gourc, J. (2012). Moisture Retention Properties of Municipal Solid Waste in Relation to Compression. *Journal of Geotechnical and Geoenvironmental Engineering*, 138(April):535–543.

Valencia, R., den Hamer, D., Komboi, J., Lubberding, H. J., and Gijzen, H. J. (2009a). Alternative treatment for septic tank sludge: Co-digestion with municipal solid waste in bioreactor landfill simulators. *Journal of Environmental Management*, 90(2):940–945.

Valencia, R., van der Zon, W., Woelders, H., Lubberding, H. J., and Gijzen, H. J. (2009b). Achieving "Final Storage Quality" of municipal solid waste in pilot scale bioreactor landfills. *Waste management (New York, N.Y.)*, 29(1):78–85.

Valencia, R., van der Zon, W., Woelders, H., Lubberding, H. J., and Gijzen, H. J. (2009c). The effect of hydraulic conditions on waste stabilisation in bioreactor landfill simulators. *Bioresource Technology*, 100(5):1754–1761.

Valencia, R., Zon, W. V. D., Woelders, H., Lubberding, H. J., and Gijzen, H. J. (2011). Anammox: an option for ammonium removal in bioreactor landfills. *Waste management (New York, N.Y.)*, 31(11):2287–93.

Valencia Vazquez, R. (2008). *ENHANCED STABILISATION OF MUNICIPAL SOLID WASTE IN BIOREACTOR LANDFILLS*. PhD thesis, Wageningen University and UNESCO IHE Institute for Water Education, Delft.

van Genuchten, M. T. (1980). A Closed-form Equation for Predicting the Hydraulic Conductivity of Unsaturated Soils1. *Soil Science Society of America Journal*, 44(5):892.

van Turnhout, A. G., Kleerebezem, R., and Heimovaara, T. J. (2016). A toolbox to find the best mechanistic model to predict the behavior of environmental systems . *Environmental Modelling & Software*, 83:344–355.

van Vossen, W. and Heyer, K. (2009). Feasibility study sustainable emission reduction at the existing landfills Kragge and Wieringermeer in the Netherlands. Technical Report March, Royal Haskoning.

Vavilin, V. A., Rytov, S. V., Lokshina, L. Y., Pavlostathis, S. G., and Barlaz, M. A. (2003). Distributed model of solid waste anaerobic digestion: effects of leachate recirculation and pH adjustment. *Biotechnology and bioengineering*, 81(1):66–73.

Veeken, A. H. and Hamelers, B. (1999). Effect of temperature on hydrolysis rates of selected biowaste components. *Bioresource technology*, 69:249–254.

Veeken, A. H. and Hamelers, B. (2000). Effect of substrate-seed mixing and leachate recirculation on solid state digestion of biowaste. *Water science and technology : a journal of the International Association on Water Pollution Research*, 41(3):255–62.

Veeken, A. H., Kalyuzhnyi, S., and Scharff, H. (2000). Effect of pH and VFA on hydrolysis of organic solid waste. *Journal of Environmental Engineering*, 06:1076–1081.

Vrugt, J. A. (2016). Markov chain Monte Carlo simulation using the DREAM software package: Theory, concepts, and MATLAB implementation. *Environmental Modelling & Software*, 75(x):273–316.

Vrugt, J. A., Gupta, H. V., Bouten, W., and Sorooshian, S. (2003). A Shuffled Complex Evolution Metropolis algorithm for optimization and uncertainty assessment of hydrologic model parameters. *Water Resources Research*, 39(8).

White, J., Robinson, J., and Ren, Q. (2004). Modelling the biochemical degradation of solid waste in landfills. *Waste management (New York, N.Y.)*, 24(3):227–40.

White, J. K., Beaven, R. P., Powrie, W., and Knox, K. (2011). Leachate recirculation in a landfill: some insights obtained from the development of a simple 1-D model. *Waste management (New York, N.Y.)*, 31(6):1210–21.

White, J. K., Nayagum, D., and Beaven, R. P. (2014). A multi-component two-phase flow algorithm for use in landfill processes modelling. *Waste Management*, 34(9):1644–1656.
library

Acknowledgments

Many people supported me during my first steps into research over the past years. I want to thank all of you for the small and big impacts you made. Here, I highlight some of you.

Timo, thank you for giving me the opportunity to do a PhD under your supervision. It greatly inspires me how you create new insights and solutions by combining a wide variety of scientific disciplines. Thank you for giving me all the freedom to explore my ideas and especially for showing me how to sort my chaotic thoughts into more organized, persuasive reasoning and writing. Robbert, thank you for your critical and practical view on our research. It made me realize that a significant scientific contribution always should answer a question in a logically derived, quantifiable, reproducible and preferably practical manner. Often, it left me struggling with distilling the practical meaning from my research but it also showed me the importance of benchmarking modeling with experimental data and vice versa.

Cristian, thank you for sharing your passion for numerical modeling with me. I learned many basic, convenient and advanced numerical tricks from you. Mark, thank you for giving me the chance to do research for my master in your group while always keeping an eye on the bigger and practical picture. Olga, thank you for supervising me during an educational and enjoyable MSc thesis period. You made me realize that science is much more fun and efficient when ideas are shared and developed together. Shiva, thank you for supervising me during my internship. Your enthusiasm, openness to people and non-conformative ideas are inspirational. Our combination in research approaches, practical vs theoretical, proved to be very productive. Erik, thank you for our collaboration and friendship during our master. It helped me to manage the many projects and the stress that came along with them.

Roberto, thank you for sharing all the data measured during your PhD project with us. It was essential fuel for me to start modeling biogeochemical processes in solid waste. Christian, thank you for warmly welcoming me to Vienna and sharing your experimental data. Blending my modelers, process perspective with your experimental, ecological perspective really expended my view. Hans and Jasper, thank you for sharing your software with me. These were essential in the development of my toolbox and thesis and besides that, were really fun to play with.

Heijo, Hans, Hans, Hans, Rob, André, Nanne and Adrie thank you for the feedback on the project drawn from your many years of experience in the field. It was essential for tuning my research to a product with practical value. Regulators and STW, thank you for making it possible to do a challenging PhD project about landfills and their emission potential.

Han, Jens, Hans, Sylwia, Marc, Karel, Jolanda, Arno, Jan, Henk, Alber, Richard, Lisa and John thank you for your support in the laboratory, on the field and by

providing data. Putting science into practice would be impossible without your practical experience and convenient tricks. Also, Marlijn, Hannie, Marijke, Ralf and Lianne thank you for arranging all the administration that is needed to do a PhD.

The students I worked with: Deniz, Tiziano, Barend, Jiani, Geert, Remco, Marilou, Zhoujang, Ioannis, Juan and Rahul. I very much enjoyed working together with each of you. Your fresh views, dedication and final results really enabled us to extend our research into many interesting branches. You also showed me a broad spectrum of motivations for and methods to practice science through your diversity in skills and attitudes. It taught me a lot about supervising students which I hope to improve with every new student.

My colleagues, thank you for making the office both a stimulating and pleasant environment. Luke thanks for being a good friend in and outside the office. Shirish, Andriy, Laura, Michael, Jiao, Vinh, Jiani, Susanne, Dianne, Nor, Poly, Divya, Chiara, Ivo and Ali thanks for the many laughs, lunches, diners and cool travels. And also for the many interesting discussions about research and all kind of other stuff. Also Ngan, Dominique, Roderick, Tom, Arash, Leon, Amin, Phil, Federico, Cristina, Stefano, Haoyuan, Weiyuan, Bram, Elahe and Hongfen, thank you for the short, enjoyable coffee breaks throughout the days.

My friends, thanks for giving me a fun, warm world completely unrelated to science to, so to say, reboot the system every once in a while. It gave me the proper balance to not get swallowed by the lonely, stressful world that PhD can be sometimes. It has already been over 20 years in which we shared many great experiences but also helped each-other through more difficult times. I remember with pleasure the music we made and enjoyed, the gigs we did, (road) trips we made, houses and parties and the food we shared. Mark, Erik, Tim, Sander, Rick, Emiel, Harold, Thierry, Eelco, Jasper, Marijke, Iris, Patty, Patty and the rest of the 'gang', you mean a lot to me. Also, Erik thanks for being my statistical help from time to time. Harold thanks for the awesome thesis cover. And Mark, lets never agree to disagree, it would mean the end of many interesting discussions.

My beautiful girlfriend Sabrina, thank you for all your love, support and adventures we experienced so far. Although it sometimes took a bit too much of my time, my PhD would have been far less successful without you. You are my home and safety.

And my family: grandpa, grandma, my sister Reina, uncle Dirk, Quinten, Martin, Sylvia, Tjeerd and mom, thank you for raising me in a warm, loving and safe environment after which you gave me all the freedom to explore life. Sometimes for the better, sometimes for the worse but I know you were always there watching my back. Quinten, you are the coolest, smartest little guy I know :-). Mom, thank you for everything.

A

Steps towards quantifying transport limitation in biodegradation of MSW from emission measurements

A

A.1. Introduction

Many studies have investigated the rate limiting steps of biodegradation of Municipal Solid Waste (MSW) into biogas (CO_2 and CH_4). Insight in these steps such as hydrolysis is crucial for understanding the emission behavior from wastebodies. As was discussed in chapter 3, the rate of hydrolysis is much lower in landfills than in more 'ideally mixed' environments such as lysimeter or lab scale experiments. Characterization (and quantification) of the influence of these rate limiting steps can directly reduce uncertainty in models for prediction of emission potential.

The general consensus is that there are three common slow steps in biodegradation of MSW: 1) hydrolysis/fermentation, 2) methanogenesis and 3) mass transport of nutrients such as Volatile Fatty Acids (VFA) between regions of hydrolysis/fermentation and methanogenesis. These steps are schematically presented in figure A.1. The kinetics of the first two steps are related to fundamental characteristics of the bacteria/enzymes that perform these reactions. These have been intensively studied and therefore a lot of information is already available about their maximum rates and inhibitions as was also discussed in chapter 1 and 2.

Figure A.1: Sketch of the slow steps in biodegradation.

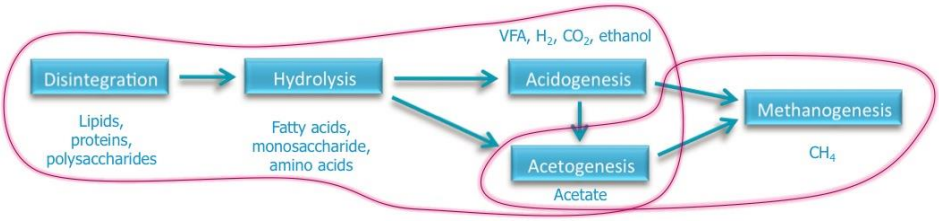

The impact of transport limitation, however, is very system dependent and should therefore be seen more as a system characteristic than a fundamental property. Slow mass transport between regions can cause pH inhibition of hydrolysis by building up of VFA concentration or substrate (VFA) limited methanogenesis. So far, it has been suggested that on a field scale mass transport is the main process limiting biodegradation but it has not yet been characterized or quantified from measured data.

Our aim is to demonstrate that mass transport limitation can be quantified from gas and leachate emission measurements. Given that both regions behave like 'ideally mixed' batch reactor following fundamental kinetics, inhibitions and stoichiometry, the delay in biodegradation and gas production should be directly correlated to the mass transport between both regions. We further hypothesize that this transport is diffusional and is therefore characterized by the length of the diffusional path (x_{diff}) since diffusion constants in water are relatively well known. Connecting both region together with a diffusional transport in a forward model therefore allows to infer the diffusion length from measured gas and leachate data. Insight in this system property reduces uncertainty in the forward prediction models such

as described in chapter 3.

As a first step, we demonstrate quantification of diffusion length in laboratory scale experiments with an idealized MSW: white cabbage and kale. First, rates of hydrolysis and methanogenesis are identified for a non-limiting environment to calibrate the reaction networks for both regions separately. Then, both regions are connected via diffusional transport with a known diffusion length. Finally, this diffusion length is inferred from the measured gas and water concentrations via modeling and compared to the actual diffusion length applied.

A.2. Theory

A.2.1. Experiments

Rates under a non-limiting environment

Four types of experimental setups were used to identify rates of hydrolysis and methanogenesis under a non-limiting environment. These four setups are schematically represented in figure A.2. The principle of all four setups is the same, only the initial conditions and the type of measurements of gas and water quality, quantity are different. The broth containing nutrients and bacteria are placed into either a 2 L (a,b) or 0.25 L (c,d) glass (Duran) bottle. The broth is stirred with a magnetic stirrer throughout the experiment and changes in solid, water and gas compositions are measured.

Gas production is measured by pressure increase with a manometer (i.a. Oxitop), collection in a gas bag, volume ticks in a gas clock or produced volume in a eudiometer. Figure A.3 presents a schematic representation of the eudiometer. Produced gas pushes the water in the left column upwards which results in transportation of some water from the left to the right column. The increase in mass in the right column is continuously measured with a scale. pH is either continuously measured with a sensor or by discrete sampling of the broth volume.

Additional measurements were performed on the samples of the water and gas phases: Gas chromatography (i.e. CO_2, CH_4, N_2 and O_2), fotospectroscopy (i.e. VFA and NH_4^+), HPLC (i.e. Succinate, Lactate, Formate, Glycerol, Acetate, Butyrate, Ethanol, Valerate), Dry weight (water content), LOI (organic carbon content) and ICP-MS (i.e. Ca^{+2}, Mg^{+2}, PO_4^{-3}, Na^+ and K^+).

The initial conditions for all type of experiments are listed in table A.1. Several experiments were performed. Hydrolysis of white cabbage and kale were investigated under relative non-limiting environments. Methanogenesis with a mix of VFA or Acetate as substrate were investigated. And also the overall rate of hydrolysis and methanogenesis of kale without an imposed mass transport limitation was investigated. Prior to the start of all experiments, the reactors were sparged with nitrogen gas to create an anaerobic environment.

Emission under the influence of mass transport limitation

Three types of experiments were performed to investigate the influence of mass transport limitation on the rate of biodegradation. In the first type, a region with hydrolytic products (VFAs) is separated from a region with methanogenic bacteria

A

Table A.1: Initial conditions of experiments under a non-limiting environment.

	Setup	Substrate	Nutrients	Trace elements	Buffer	Temperature	Bacteria	V_{broth}
Hydrolysis of white cabbage	a	White cabbage, 35 [g]	-	-	-	295 [K]	-	0.12 L
Hydrolysis of kale	c, d	Kale, 5, 10, 20 [g]	0.15 [L]	50 μL	H_2PO_4, 15 [mM]	295 [K]	-	0.15 L
Methanogenesis of VFA_{mix} [1)]	b	VFA_{mix}^{total}, 7.53 [mM] and 28.04 [mM]	-	-	-	295 [K]	0.08 L (Biothane)	0.5 L
Methanogenesis of NaAcetate	c	NaAcetate, 12.5 [mM]	x	x	-	295 [K]	50 g (Attero)	0.16 L
Hyd & meth of kale	c	Kale, 20 [g]	0.05 [L]	50 μL	H_2PO_4, 15 [mM]	295 [K]	50 [g] (Attero)	0.11 L

1) This experiment was performed with a low and high substrate concentration. For both, a mix of Succinate, Lactate, Formate, Acetate, Propionate and Butyrate was used with respectively the ratios: 0.013:0.0013:0.27:0.21:0.086:0.42 and 0.0039:0.0014:0.14:0.37:0.037:0.45. Both mixtures are obtained from the hydrolysis of white cabbage experiment after respectively 13 and 20 days.

Table A.2: Initial conditions of experiments with imposed mass transport limitation.

	Setup	Substrate	Nutrients	Trace elements	Buffer	Temperature	Bacteria	V_{broth}
VFA_{mix} & Meth	b	$VFA_{mix}^{total,1)}$, 0.7 [M]	-	-	H_2PO_4, 10 [mM]	295 [K]	High concentration (Attero)	-
1) NaAc & Meth [2)]	a	NaAc, 0.1 [M]	x	x	-	295 [K]	50 [g] (Attero)	0.10 L (both)
2) NaAc & Meth	a	NaAc, 0.1 [M]	x	x	-	295 [K]	50 [g] [3)] (Attero)	0.10, 0.17 L (left,right)
3) NaAc & Meth [4)]	a	NaAc, 0.1 [M]	x	x	H_2PO_4, 5 [mM]	295 [K]	50 [g] (Attero)	0.1 L (both)
Hyd & Meth	a	Kale, 20 g	x	x	H_2PO_4, 10 [mM]	295 [K]	50 [g] [5)] (Attero)	0.1 L (both)

1) The VFA_{mix} has the ratio 0.29 Acetate, 0.29 Propionate and 0.42 Butyrate. 2) Methanogenic region was pre-seeded with 0.12g NaAc, pump was started after 2 days. 3) The methanogenic reactor of previous experiments was used here which meant that the bacteria were activated but probably diluted compared to 50 g. 4) Methanogenic region was pre-seeded with 0.082g and nutrients, trace elements accordingly. 5) Sludge was washed with 6 L demi-water and sieved with a 0.125 mm filter.

by a diffusion barrier (agar gel) of a specified thickness as sketched in figure A.4 (bottom part). Several layer thicknesses were studied. In the second and third type, regions are separated in different bottles and the broth from the left region is pumped into the right region (figure A.4, top). The left region is diluted with the same pumping rate. Different pumping rates represent different 'diffusion distances'. In the second type, the left region is filled with NaAcetate and in the third type it is filled with kale, so therefore a real hydrolyzing region. The same type of measurements were performed on these types of experiments as during the non-limiting experiments.

The initial conditions for the three type of experiments are listed in table A.2. The column used in setup b is a cylinder with a length of 18 cm and a diameter of 6.8 cm. The layers are approximately for $\frac{2}{3}^{\text{th}}$ filled with solution or gel. The length of the methanogenic region was 4 cm for all diffusion barrier thicknesses. The investigated diffusion thicknesses were 0, 1.5, 3.5 and 6 cm. The length of the region filled with VFA was changed accordingly. The pumping rate applied in the second and third type of experiment was $0.01\ \frac{\text{ml}}{\text{min}}$.

Figure A.2: Sketch of the four experimental setups used for identification of rates under non-limiting environmental conditions.

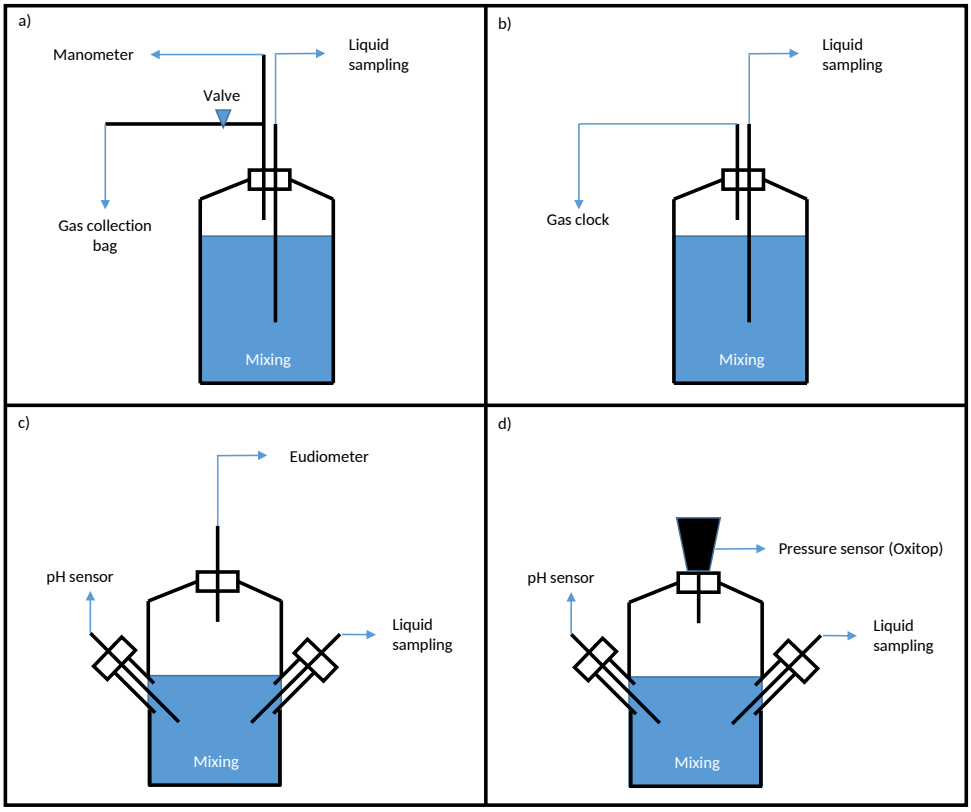

Figure A.3: Sketch of the automatized eudiometer measurement.

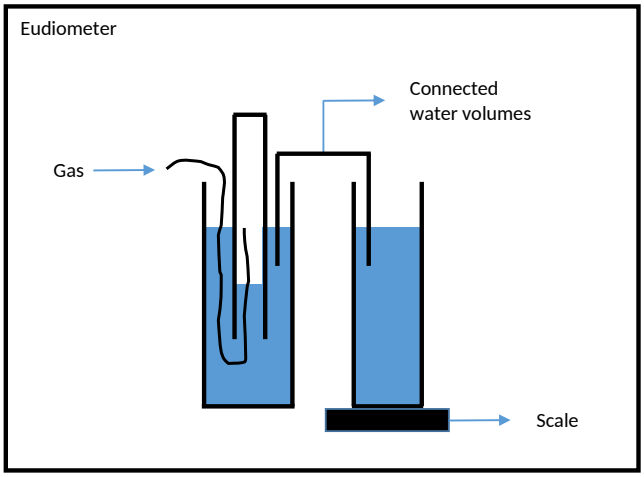

Figure A.4: Sketch of the experimental setups used to investigate biodegradation influenced by mass transport limitation.

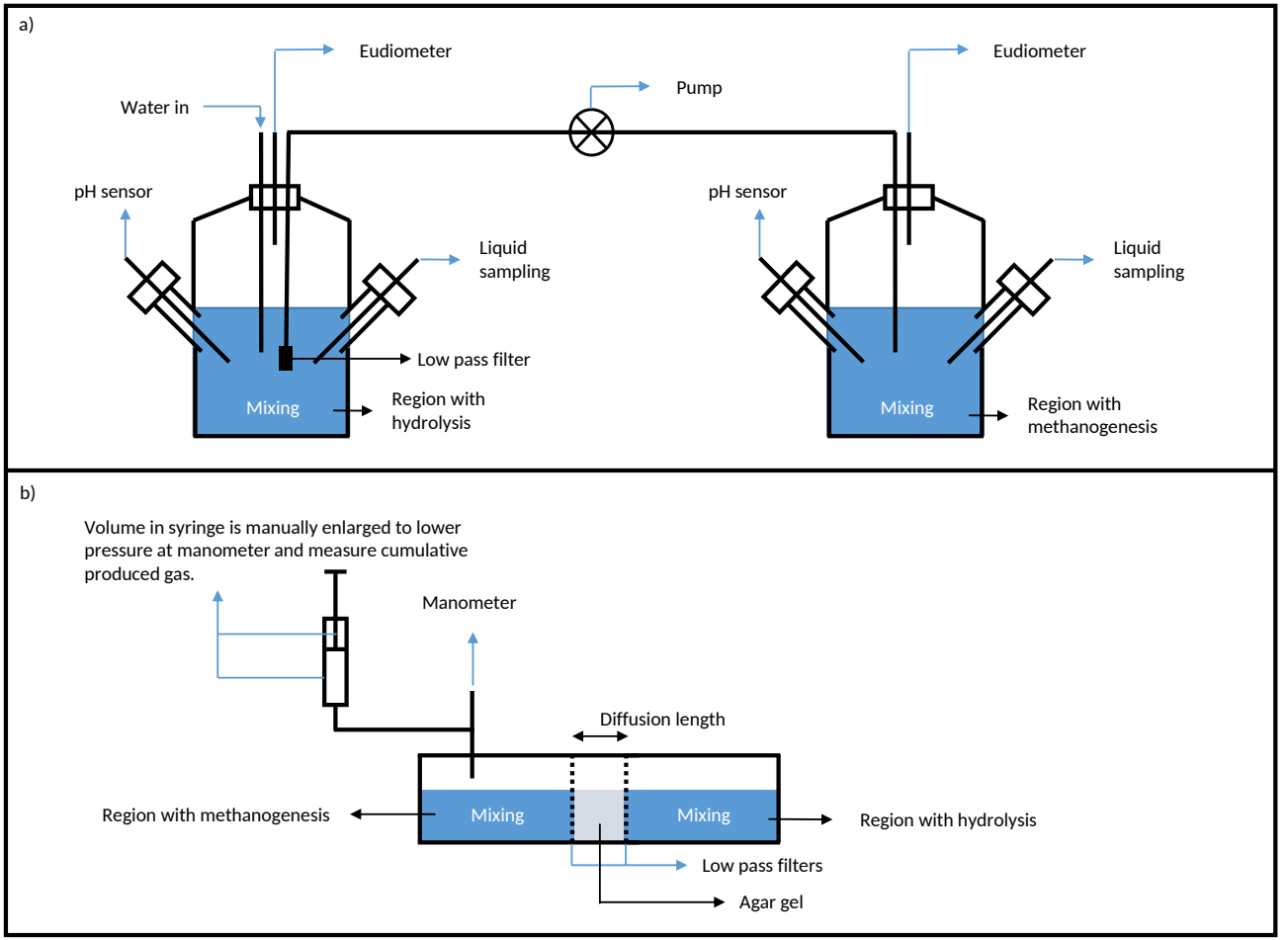

A.2.2. Forward models

The forward models to simulate the experiments are build with the toolbox described in detail in chapter 1. Per reactor in an experiment, a reaction network was build including all dominant processes such as kinetics, inhibitions and limitations influencing the experiment as described in chapter 1. We extended the toolbox such that it is possible to connect two reaction networks together via mass transport following a diffusion or a convection (pumping) type of mechanism.

A.3. Results & Discussion

A.3.1. Hydrolysis of white cabbage and kale under non-limiting environments

Figure A.5 shows the mixture of VFAs released during hydrolysis of white cabbage. It displays a typical hydrolysis with fermentation pattern. At the start of the experiment glucose is produced. Later on, it is converted into VFAs and CO_2. The main VFAs released are Lactate, Butyrate, and Acetate. The high concentration of Succinate is very likely a measurement error since it is not expected to be produced. Also, a significant amount of ethanol is produced during the final days of the experiment. This indicates that some oxygen was present in the reactor at the beginning of the experiment.

Figure A.5 also presents the cumulative released amount of carbon which is the sum of the carbon in Glucose, VFAs and CO_2. The trend in released carbon follows nicely the expected first order kinetics indicating that hydrolysis is the rate limiting step. The total amount of released carbon agrees with the estimation of the maximum amount of carbon in the solid phase to be released indicated with the dashed blue line). The maximum hydrolysis constant with the best fit is $0.24\,\mathrm{d}^{-1}$ which is a high but reasonable value given the relative ideal environmental conditions and the fact that the cabbage was shredded into small particles.

The co-release of nitrogen in the form of NH_4^+ is also presented in figure A.5. The ratio of released C:N measured at the end of the experiment is approximately 0.01. Interestingly, not all solid N is dissolved during the hydrolysis while all solid C was. It seems that N is retained into solid form by some other mechanism.

Also the hydrolysis of kale was investigated under relative non-limiting environmental conditions with two different setups. In one setup, produced gas was measured with the eudiometer and the other with a manometer (Oxitop). The production of gas and pH was measured for three kale concentrations (fig. A.6). All solutions were buffered with $15\,\mathrm{mM}$ phosphate buffer.

The results from both setups are mostly similar although the Oxitop setup produces slightly lower pHs and higher gas production peaks for all three substrate concentrations. Also in the Oxitop setups, it seems that there was a leak in the gas phase because gas pressures drop gradually at the end of the experiment. That this effect was caused by dissolution of gas seems unlikely because the pH is quite stable and the effect was also not observed in the experiments with the other setup.

Based on loss of ignition, we expect that a release of approximately $5.5\mathrm{mmol}$ carbon per $5\mathrm{g}$ of kale. The total amount of C measured in gas and solution (VFA) at

Figure A.5: Carbon and nitrogen produced during hydrolysis of white cabbage under a non-limiting environment.

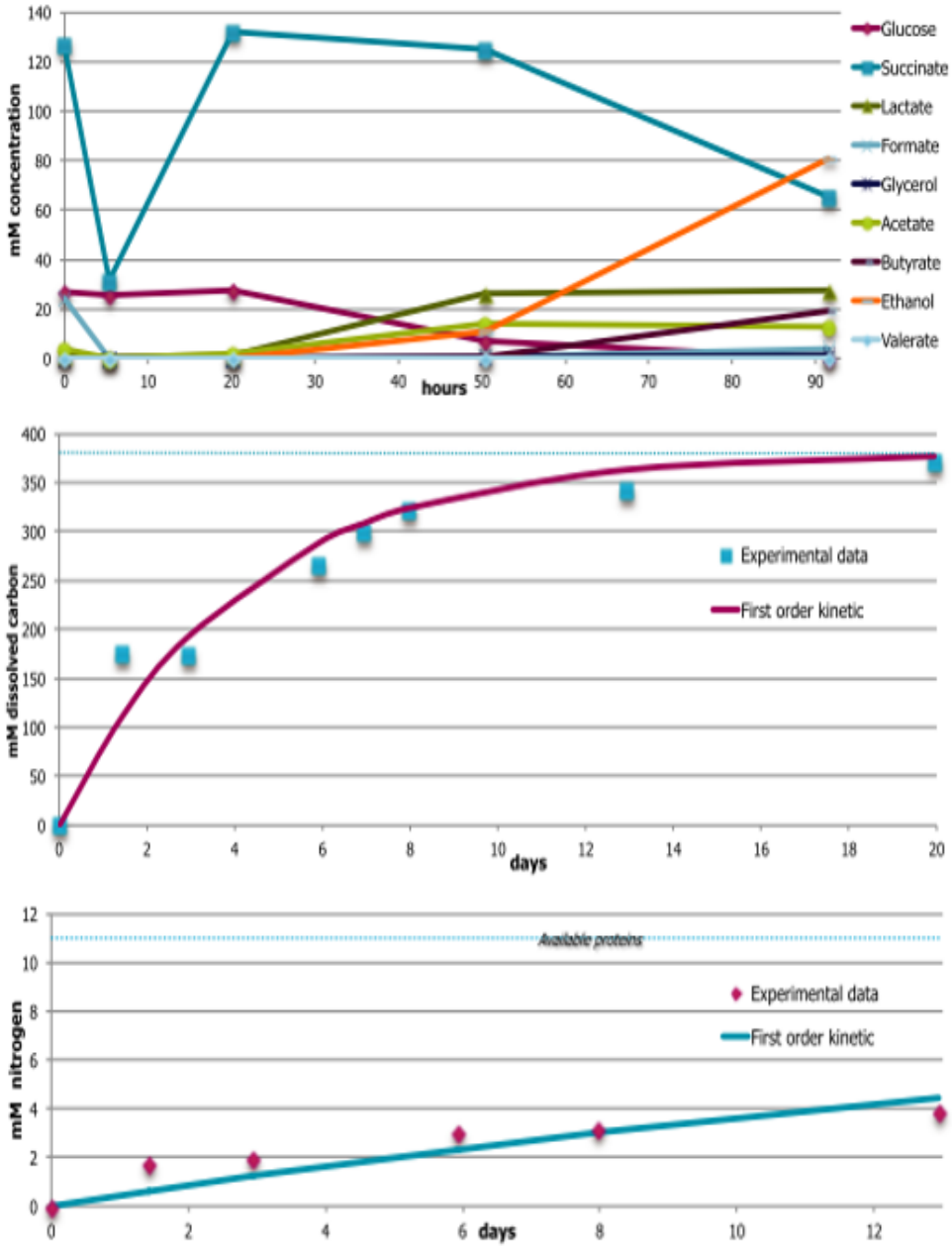

Figure A.6: Results hydrolysis of kale under non-limiting environment.

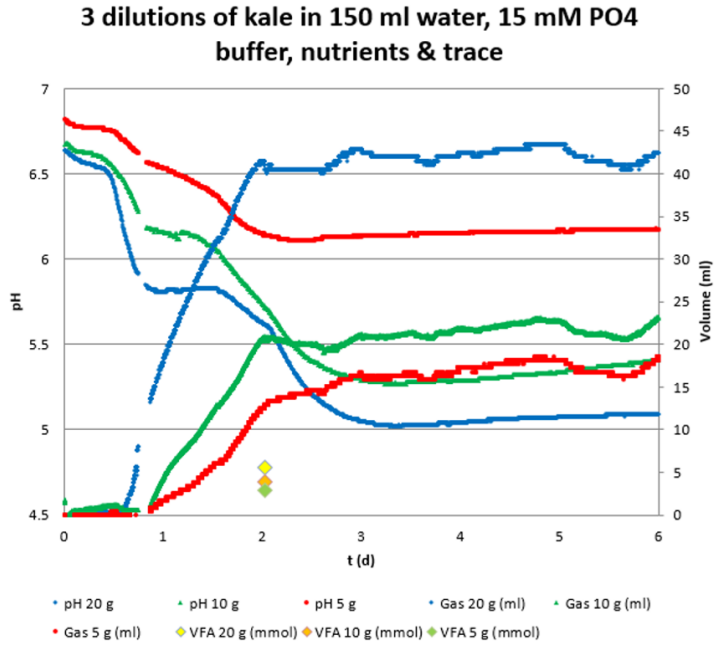

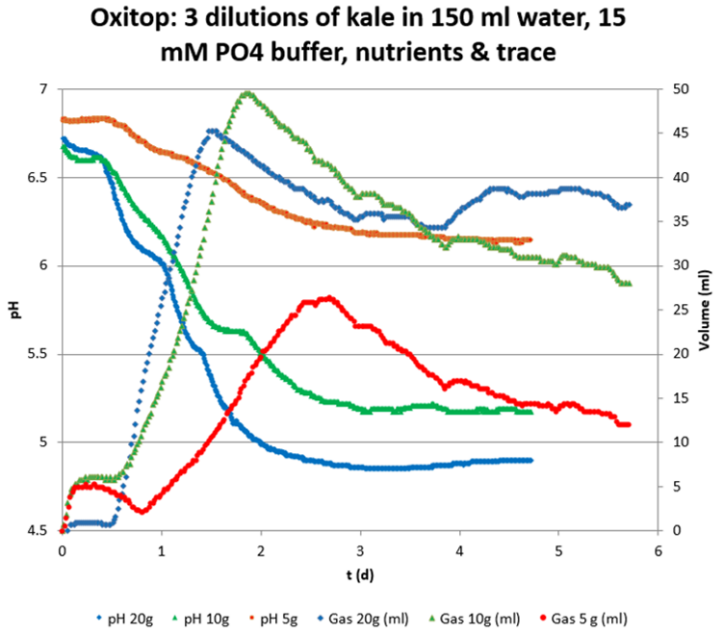

a substrate concentration of $5\mathrm{g}$ is $6.3\,\mathrm{mmol}$ which is in reasonable agreement given the accuracy of the measurements. In this case, the hydrolysis was not inhibited by the pH which did not drop below 6.2. The hydrolysis for the two higher substrate concentrations seems, however, inhibited by pH. For both cases, a much higher release of carbon was expected. Interestingly, hydrolysis suddenly stops at a pH of around 5.6 for $10\ \mathrm{g}$ and $20\ \mathrm{g}$ kale in both setups. Below this value hydrolysis is highly inhibited which is in agreement with previous observations in literature.

The non-inhibited hydrolysis rate constant for $5\mathrm{g}$ is approximately $1.5\mathrm{d}^{-1}$. This value is higher than the rate constant for white cabbage. The main reason is likely the higher liquid to solid ratio in the experiment with kale. Other reasons may be the lack of added nutrients in the experiments with white cabbage or that kale more easily disintegrates.

A.3.2. Acetogenesis/methanogenesis of VFA under non-limiting environments

The maximum rate of VFA degradation into biogas was investigated under a non-limiting environment for both types of anaerobic sludges (Biothane and Attero). The concentration of bacteria in the sludge was considered very high and therefore not limiting the degradation rate. The left, top graph in figure A.7 presents the cumulative produced volume of gas with substrate concentrations of $20.2\mathrm{mM}$ and $78.8\mathrm{mM}$ carbon. Both experiments produced a bit more biogas than expected on the basis of carbon in the substrate. Reasons may be endogenous biogas production of the sludge and release of $\mathrm{CO_2}$ from dissolving $\mathrm{CaCO_3}$ because of addition of acids to the broth, lowering pH. The maximum rates are 460 and $110\ \frac{\mathrm{ml}}{\mathrm{d}}$. Clearly, the maximum rate of biogas production is influenced by the substrate concentration. Nevertheless, at a VFA concentration of $7.53\mathrm{mM}$ still a degradation rate of $4.5\,\frac{\mathrm{mmol}}{\mathrm{d}}$ is achieved.

The activity of the sludge from Attero was also investigated. The results (figure A.7 top, right) show a maximum rate of $80\,\frac{\mathrm{ml}}{\mathrm{d}}$ at an acetate concentration of $12.5\mathrm{mM}$ ($=25\mathrm{mM}$ C). The actual biogas production rate is roughly two times higher, $160\,\frac{\mathrm{ml}}{\mathrm{d}}$, because NaAc is used as substrate and therefore most produced $\mathrm{CO_2}$ is retained in solution to serve as a counter ion for $\mathrm{Na^+}$. During methanogenesis, the ratio of produced $\mathrm{CO_2}$ and $\mathrm{CH_4}$ is roughly 1:1. Overall, the activity of both sludges appears to be similar.

Figure A.7: Results $\mathrm{VFA_{mix}}$ (left) and NaAc (right) degradation into biogas under a non-limiting environment.

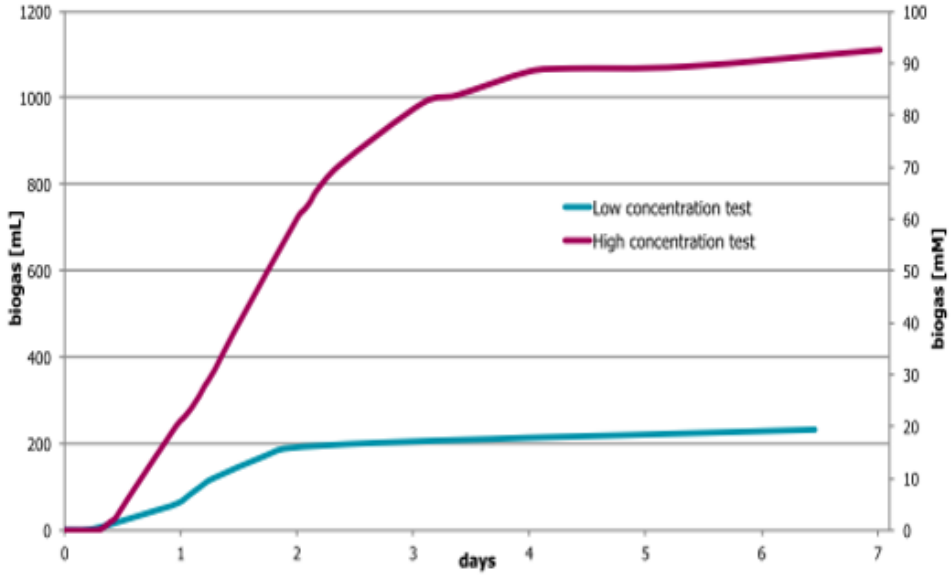

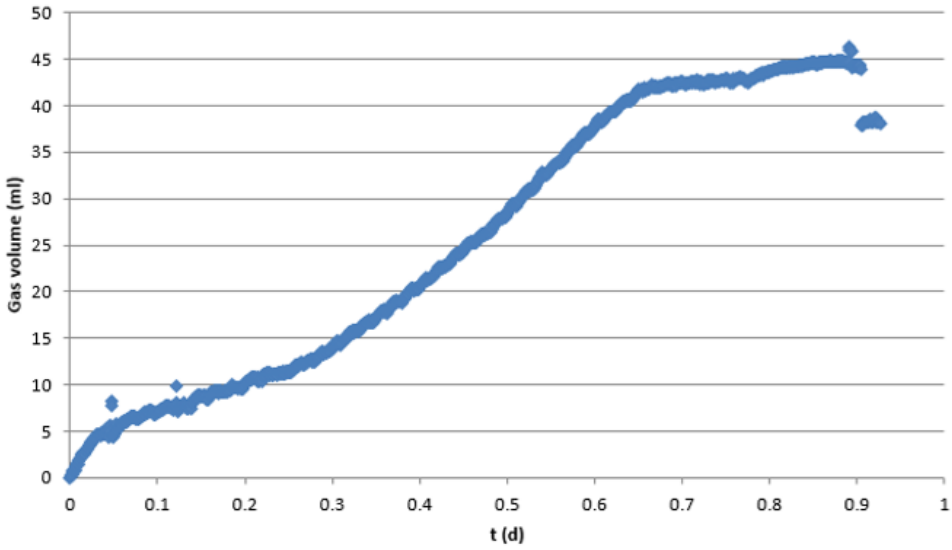

A

A.3.3. Combined hydrolysis/fermentation/methanogenesis of kale under a non-limiting environment

To investigate the overall rate of biodegradation with minimal mass transport limitation, kale ($20\mathrm{g}$) and anaerobic sludge was added together in a perfectly mixed broth. Measured gas production and pH are presented in figure A.8. The drop in pH at the beginning of the experiments indicates an almost immediate onset of hydrolysis while the delay in biogas production (~ 1 day) indicates a short lag phase of the methanogenic bacteria. After this lag phase, methanogenic activity is high enough to prevent the pH from decreasing to inhibiting levels for hydrolysis and methanogenesis. The pH continues to increase because of the removal of VFA by methanogenesis and the release of cat ions such as Na^+, K^+ and $\mathrm{NH_4}^+$ (measured with ICP-MS). The total amount of carbon in produced gas at day 15 is approximately $20.7\ \mathrm{mmol}$ which is in agreement with the expected release of carbon from $20\mathrm{g}$ kale (=$22\mathrm{mmol}$, measured with LOI). Most likely, some $\mathrm{CO_2}$ has also remained in solution to counter balance released cat ions.

The results show that the addition of sludge prevented the pH to decrease to inhibiting levels for hydrolysis and therefore all organic carbon in the kale could be degraded. This in contrast with the inhibited hydrolysis of kale without sludge which was presented in figure A.6. Also, the first order rate constant of the overall biodegradation is approximately $0.25\mathrm{d}^{-1}$. This is lower than the rate constant estimated for the hydrolysis of $5\mathrm{g}$ kale, however, is similar to the rate constant estimated for white cabbage experiment in which the liquid to solid ratio was similar as in this experiment. The value indicates that hydrolysis was the rate limiting step in the overall biodegradation and hydrolysis and overall biodegradation were not inhibited or limited by mass transport limitation as expected. The decrease in gas volume at the end of the experiment may have been the result of leakage or the release of additional cat ions which caused part of the $\mathrm{CO_2}$ to re-dissolve.

A.3.4. Hydrolysis and methanogenesis separated by mass transport

The influence of mass transport on the processes of hydrolysis and methanogenesis was investigated. First, the influence of mass transport on methanogenesis was investigated of which the results are presented in figure A.9. In three very similar experiments, NaAc was supplied to a reactor with anaerobic sludge. Solution was pumped from a reactor with $0.1\mathrm{M}$ NaAc at a pumping rate of $0.01\frac{\mathrm{ml}}{\mathrm{min}}$. The initial biogas production rate in the methanogenic reactor was therefore expected to be around $70\frac{\mathrm{ml}}{\mathrm{d}}$ when all $\mathrm{CO_2}$ goes to the gas phase. This agrees very well with the measured rates of biogas production during the first day. The variation in rates between the experiments are likely caused by slightly different actual pumping rate during the experiments.

The decrease in production rate observed in all three experiments over time nicely displays the impact of dilution of NaAc in the supplying reactor and dilution of substrate and bacteria in the reactor with sludge due to pumping. NaAc dilution in the supply reactor is caused by inflow of water at the same pumping rate. Methanogenic activity decreases with lower substrate concentrations as also

observed in the experiments under non-limiting environments (fig. A.7).

The early inactivity in experiment 2 is probably because the sludge used in this experiment was already washed and centrifuged multiple times which may have damaged and diluted the bacteria. The sudden jump in biogas production after day 1 in experiment 1 is caused by an short increase in the pumping rate. The additional supply of substrate was quickly converted indicating that the activity of the bacteria was mainly limited by substrate supply. The pH of all three experiments follows a slight decreasing trend caused by the increasing partial pressure of CO_2 and dilution of the broth. The value of the initial pH is mostly influenced by the time length of N_2 sparging prior to the experiment. Sparging time was longer for experiment 2 resulting in a higher initial pH because more CO_2 was stripped.

In a second type of experiment, the influence of supply of a mix of VFA to the methanogenic region through a diffusion barrier was investigated. Four diffusion distances were investigated: ~ 0, 1.5, 3.5 and 6 cm. The measured produced biogas for all four cases is presented in figure A.10 with markers. Surprisingly, the experiment with the largest diffusion distance had the highest biogas production rate and the experiment with the smallest distance showed the one to lowest production rate. Clearly, more than only diffusional transport was playing a role in the overall conversion rate of VFA such as inhibitions.

For comparison, also the results from modeling the experiment are included in figure A.10. In this model, the maximum rates were used as identified in the previous experiments and diffusional transport was included with parameters from literature. No inhibition mechanisms were however included yet. The comparison shows that the experiments with $x_{diff} \sim 0cm$ and $x_{diff} = 1.5cm$ have lower gas production rates than expected and those with larger distances have higher rates than expected. The higher observed rates may be explained by some leakage along the side walls of the diffusional barrier which resulted in partly convective transport of VFA, therefore a higher supply rate. The lower observed rates are likely caused by pH inhibition of the methanogens because of too fast supply of VFA, especially when leakage along the side walls occurred. The experiments with larger distances were probably protected from pH inhibition because the transport distances were still large enough.

In further studies, it would be interesting to repeat the experiments without leakage and compare the results with results from a model that includes pH inhibition of methanogenesis. If experimental and model results then agree, it strongly indicates that the delay in biogas production observed in waste-bodies for instance can be explained with well known mechanisms such as maximum rates, inhibitions and diffusion limitation. Characterizing the diffusion length through inverse modeling of field scale data, then strongly reduces uncertainty in field scale emission models by identifying the main rate limiting step.

A

Figure A.8: Results combined hydrolysis and methanogenesis of kale under non-limiting environment.

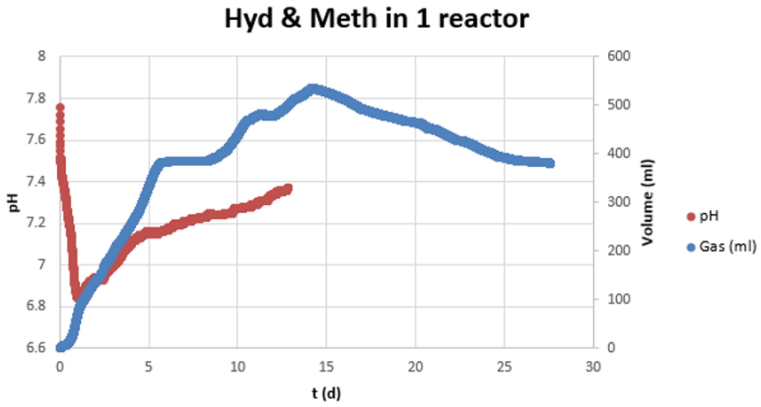

Figure A.9: Results pump limited methanogenesis of NaAc.

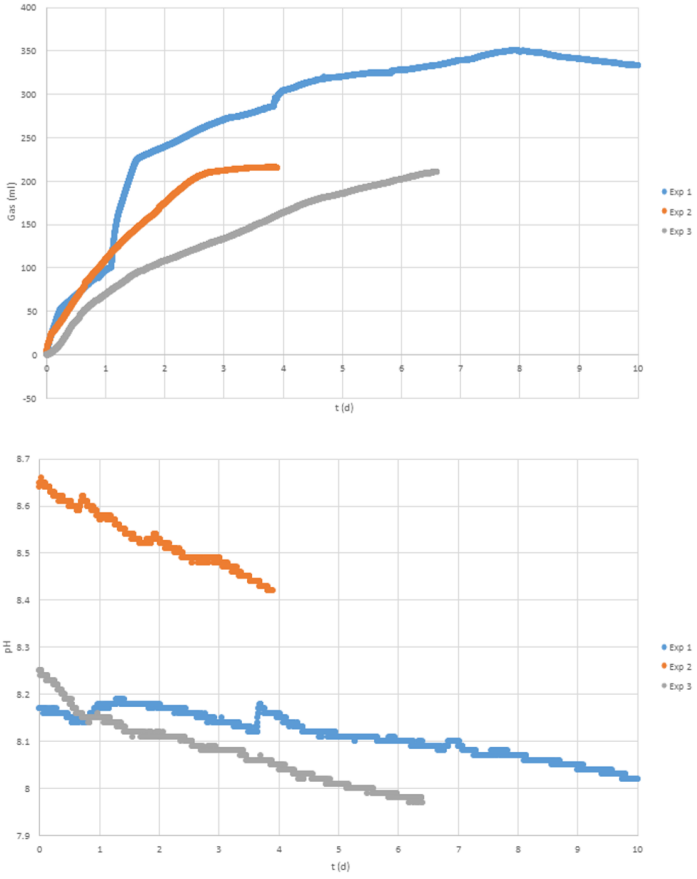

Figure A.10: Results diffusional barrier between hydrolytic products (VFAs) and methanogenesis.

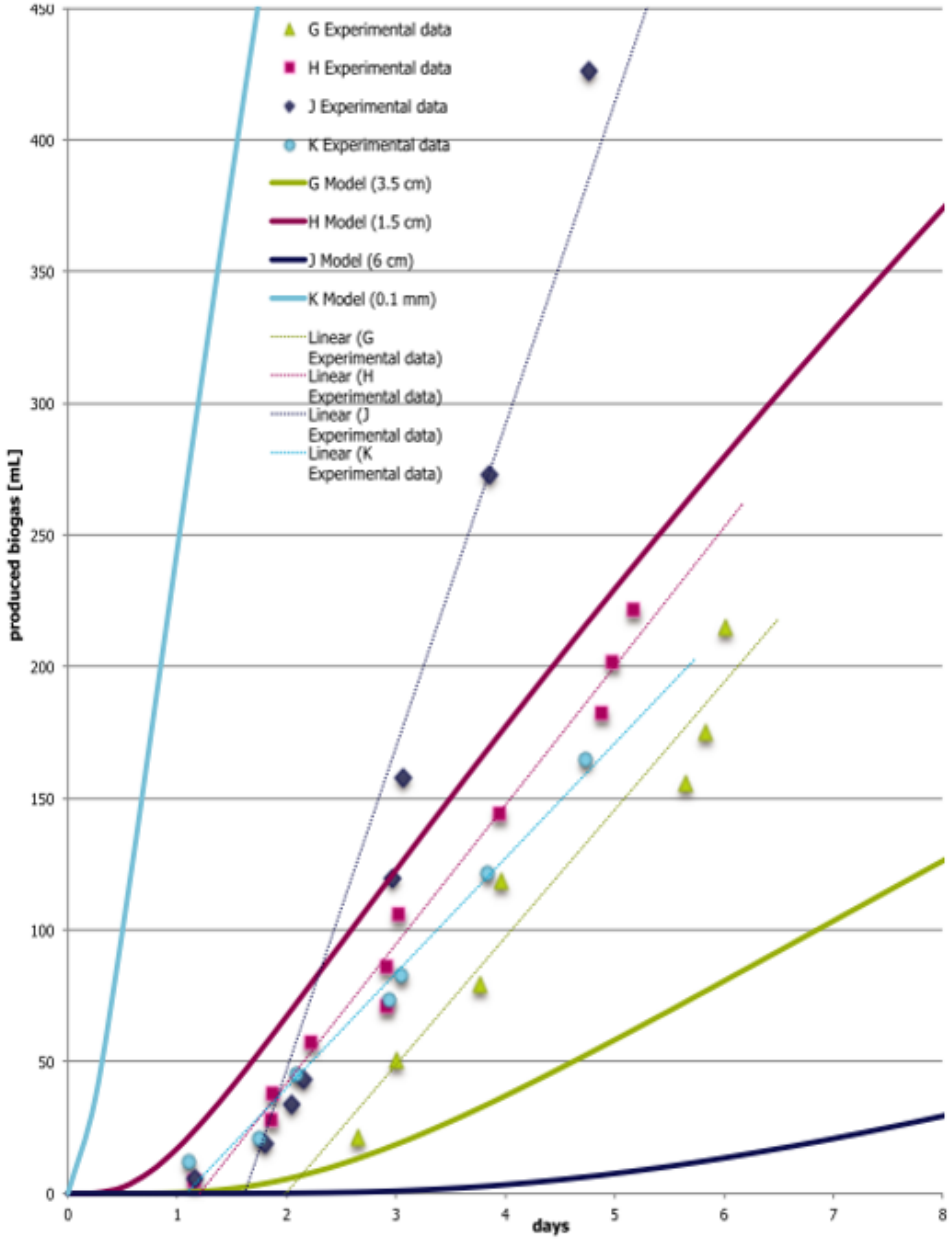

In a similar fashion, the impact of mass transport limitation on both hydrolysis and methanogenesis was investigated. Only this time transport limitation was imposed by pumping broth from the reactor with hydrolysis (R_{hyd}) to the reactor with sludge (R_{meth}) instead of placing a diffusion barrier. To still mimic diffusional transport, water is also added to the reactor with hydrolysis with the same pumping rate diluting the hydrolyzing broth. Measured biogas production, pH and reactor volume are presented in figure A.11.

In first instance, the hydrolyzing region behaves the same as in the experiment under a non-limiting environment. Within 2 days, pH decreases to around 5.5 and the biogas production rate is similar with also a delayed onset. However, because of transport and dilution of VFA concentration (as would occur with diffusional transport) the pH did not decrease further and slightly increased allowing the hydrolysis to continue. A balance between the hydrolysis rate and transport rate was established such that allowed the overall biodegradation to continue.

Unfortunately, the measurements of the methanogenic region are heavily influenced by problems faced during the experiment with the setup such as clogged filters. Replacement of this filters, temporarily stopped the transport of substrate to the methanogenic region but also required to open the gas phase to the atmosphere. Both explain the frequent jumps and irregularities observed in the measured pH and produced biogas. Nevertheless, the general trends observed tell a story.

The pH slowly decreases as the partial pressure of CO_2 increases in the reactor which was also observed in previous experiments (fig. A.7). Dilution of the broth may also have played a role in the decrease of pH. The gas production in the methanogenic region is low because the supply of VFAs to the methanogenic region is small because of the combination of a low pumping rate and a low concentration of VFAs in the hydrolyzing region. The gas production seems to display periods of biogas production alternated with periods without activity. An explanation is that the concentration in the methanogenic reactor first needs to sufficiently increase (via pumping) to a high enough concentration which (re-)activates the bacteria to produce biogas. After consuming most VFAs during such a biogas production phase, another build up phase starts.

The total amount of produced biogas so far is reasonable. A maximum of around 500ml is expected but only around 300ml has been produced. The increasing trend in biogas production in the hydrolyzing reactor suggest that biodegradation could have continued if the experiment did not had to be stopped because of clogged filters.

The results also show that the overall biodegradation and biogas production rate is significantly decreased compared to the ideal case (fig. A.8) because of the imposed mass transport limitation. This is a first indication that the mechanisms and dominant processes proposed are indeed those responsible for the limited rates observed in waste-bodies. In further studies, it would be very interesting to repeat this experiments with an improved setup (without filter clogging problems) and infer the imposed transport limitation back from the measured data with a model and compare both. This would indicate that the combination of dominant processes

can be responsible for the delay in biodegradation in waste-bodies and gives a method to characterize diffusion lengths/degree of transport limitation from field scale measurements.

Figure A.11: Results hydrolysis and methanogenesis separated by pump limited mass transport.

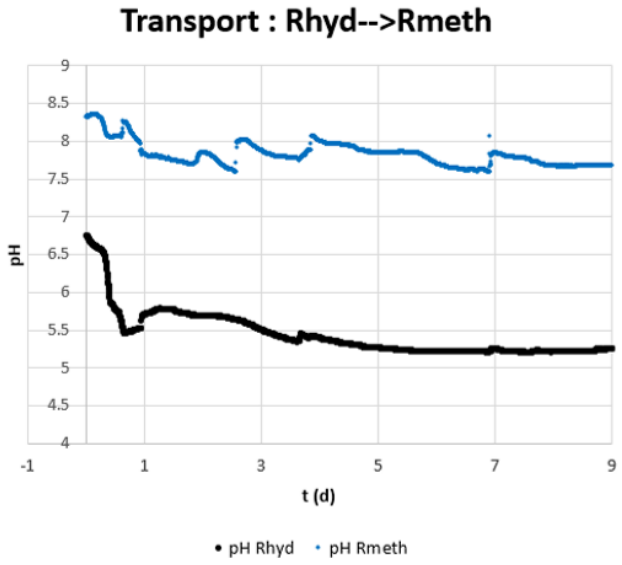

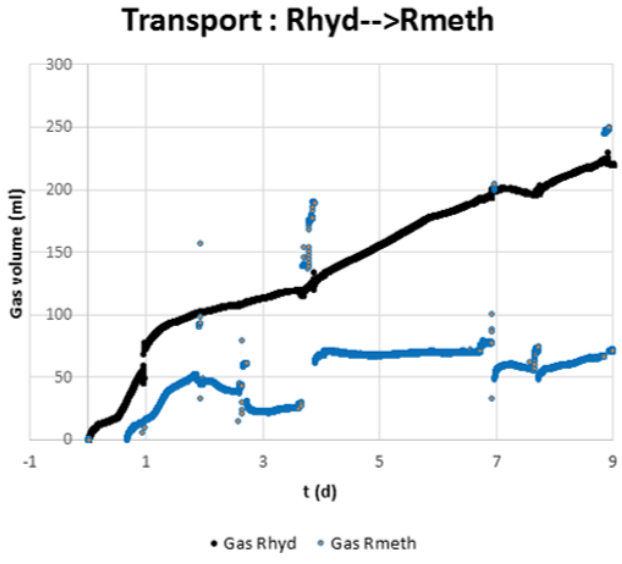

A

A.4. Experimental Instrumentation & Protocols

A.4.1. Instrumentation

1. VWR IKA Magnetic stirrers 442-0174 RH basic 2; Plate dimension: 125mm ∅ Speed range: 100-2000rpm; Heating power: 320 ^{o}C with setting accuracy of $\pm$10K.

2. Gas sampling collection bags; SKC Standard FlexFoil; Total capacity of 3L; Polypropylene septum fitting; Contained gas is stored at atmospheric pressure.

3. Vacuum vials; Vacuette (9ml) from Greiner Bio-one.

4. Consort Multimeter C3010; Two channel machine for measurements of pH - mV - Conductivity - Resistivity - Salinity - TDS - Temperature; pH and EC electrodes, both integrated with temperature probe, were used; Specifications: pH: -2...+16 pH; Conductivity: 0...2000 mS/cm; Temperature: -5...+105 ^{o}C; Resolution: 0.001 pH, 0.1 mV, 0.001 $\mu S/cm$, 0.1 ^{o}C.

5. Endress-Hauser, Deltabar S PMD 234; Differential Pressure Transmitter Specifications: Measuring rage: -100...+100 mbar; Resolution: 0.1 mbar.

6. Agilent 7697A Gas chromatography; Run time for samples 10 min.

7. High-Performance Liquid Chromatograph (HPLC); BioRad Aminex HPX-87H column and a UV/RI detector (Waters 2489); As a mobile phase 1.5 mM H3PO4 in Milli-Q water was used with a flow rate of 0.6 mL/min and a temperature of 60 ^{o}C; Before analysis samples were filtered at 0.45 μm; Injection volume was 100 μL. Each test was run for 30 min.

8. Hach-Lange DR 2800 VIS Spectrophotometer; Used with LCK303 cuvettes for ammonium test. Resolution 0.01 mg/L.

9. Hach-Lange LCK303 Ammonium cuvette test; Cuvette with pre-dosed reagents for photometric evaluation; Colorimetric method used: indophenol blue; Operating range: 2.0-47.0 mg/L NH 4 -N or 2.5-60 mg/L NH 4

10. Hach-Lange LCK365 Organic acid cuvette test; Cuvette with pre-dosed reagents for photometric evaluation; Operating range: 50-2500 mg/L Acetic acid or 75-3600 mg/L Butyric acid.

11. Milligas Counter Ritter; Display resolution 0.01mL; Full scale: 100 L; Resolution 19.3 mL.

12. Agilent 3000A micro GC; Columns: Molsieve 5A and PLOT U; Calibration executed with universal gas calibration standard.

13. Scale Sartorius Entris 6202I-1S; maximum 6200 g, d = 0.01 g.

14. Piston pump Gilson 305; type of piston is 25.SC.

15. OxiTop
16. Gelatine (agar) Dr. Oetker (standard)
17. Kale, Hollandse boerenkool (Albert Heijn); 450 g, frozen, sieved to size > 0.125 mm.
18. White cabbage, Jumbo, shredded with blender; sieved to size 0.6-1.2 mm.
19. Methanogenic sludge Biothane - VeoliaWaters, in Delft (NL).
20. Methanogenic sludge UASB inoculum, Attero Venlo.
21. Blender Tomado.
22. Syringe filter, $0.45\mu m$ nylon, Whatman.

A.4.2. Protocols

The agar for the diffusion layer is prepared by adding 1 sheet of gelatine per 40 ml of water. This solution is heated in a microwave for approximately 30 s and poured into the diffusion layer chamber.

The kale is prepared by defrosting it, sieving it with a grid > 0.125 mm and washing it with approximately 6 L water.

The nutrients used in the growth medium and the trace element solution are specified in table A.3.

Table A.3: Specification of growth medium and trace element solution.

Growth medium for 0.1 M NaAcetate

	$\frac{g}{L}$		$\frac{g}{L}$		$\frac{g}{L}$		$\frac{g}{L}$
KH_2PO_4	0.021	Na_2HPO_4	0.022	NH_4Cl	0.0975	NaCl	0.021
$MgCl_2$	0.0044	Na_2S-9H_2O	0.019				

Trace element solution for 100 M NaAcetate

	$\frac{g}{L}$		$\frac{g}{L}$		$\frac{g}{L}$		$\frac{g}{L}$
H_3BO_3	0.076	$ZnCl_2$	0.289	$CuCl_2$	0.072	$CoCl_2-6H_2O$	0.102
$NiCl_2-6H_2O$	0.153	$MnCl_2$	0.0148	$Na_2MoO_4-2H_2O$	0.037	$FeCl_3$	1.72
$CaCl_2-2H_2O$	0.045						

Curriculum Vitæ

André Gerard van Turnhout

20-03-1985 Born in s'Gravenhage, The Netherlands.

Education

1997–2003 Dalton Gymnasium, s'Gravenhage

2003–2011 Bachelor & Master in Life Science & Technology
+ minor in marketing, management & finances
Universiteit Leiden & Technische Universiteit Delft

2017 PhD. Geo-Engineering
Technische Universiteit Delft

Thesis:	Characterizing Dominant Processes in Landfills to Quantify the Emission Potential
Promotor:	Prof. dr. ir. T.J. Heimovaara
Co-promotor:	Dr. ir. R. Kleerebezem

List of Publications

Journal papers

8. **A.G. van Turnhout**, T.J. Heimovaara, *Coupled model of water flow, mass transport and biogeochemistry to predict emission behavior of landfills*, ready to submit.

7. **A.G. van Turnhout**, H. Oonk, H. Scharff, T.J. Heimovaara, *Optimizing landfill aeration strategy with a 3-D multiphase model*, ready to submit.

6. O. Ilie, **A.G. van Turnhout**, M.C.M. van Loosdrecht, C. Picioreanu, *Two-dimensional mathematical modelling of dental enamel subsurface lesion formation induced by dental plaque*, ready to submit.

5. **A.G. van Turnhout**, C. Brandstaeter, R. Kleerebezem, J. Fellner, T.J. Heimovaara, *Theoretical Analysis of Municipal Solid Waste Treatment by Leachate Recirculation under anaerobic and aerobic Conditions*, Waste Management (under review).

4. **A.G. van Turnhout**, R. Kleerebezem, T.J. Heimovaara, *A toolbox to find the best mechanistic model to predict the behavior of environmental systems*, Environmental Modelling & Software **83**, 344 (2016).

3. S.S. Salek, O.D. Bozkurt, **A.G. van Turnhout**, R. Kleerebezem, M.C.M. van Loosdrecht, *Kinetics of $CaCO_3$ precipitation in an anaerobic digestion process integrated with silicate minerals*, Ecological Engineering **86**, 105 (2016).

2. S.S. Salek, **A.G. van Turnhout**, R. Kleerebezem, M.C.M. van Loosdrecht, *pH Control in Biological Systems Using Calcium Carbonate*, Biotechnology and bioengineering **112**, 905 (2015).

1. O. Ilie, **A.G. van Turnhout**, M.C.M. van Loosdrecht, C. Picioreanu, *Numerical Modelling of Tooth Enamel Subsurface Lesion Formation Induced by Dental Plaque*, Caries Research **48**, 73 (2013).

Conference Proceedings (oral presentation)

11. **A.G. van Turnhout**, H. Oonk, H. Scharff, T.J. Heimovaara, *Optimizing landfill aeration strategy with a 3-D multiphase model*, Proceedings of the 16th international waste management and landfill symposium, (2017), Italy.

10. **A.G. van Turnhout**, T.J. Heimovaara, *Improving insight into the full scale emission potential of landfills with high resolution in-situ measurements*, Proceedings of the 16th international waste management and landfill symposium, (2017), Italy.

9. **A.G. van Turnhout**, T.J. Heimovaara, *Coupled modeling of water flow, mass transport and biogeochemical activity to predict emission behavior of landfills*, Proceedings of the 16th international waste management and landfill symposium, (2017), Italy.

8. **A.G. van Turnhout**, T. Carducci, T.J. Heimovaara, *Steps towards quantifying the slowest step in production of biogas in Municipal Solid Waste landfills*, Proceedings of the International Conference on Advances in Civil and Environmental Engineering, (2017), India.

7. **A.G. van Turnhout**, T.J. Heimovaara, *Quantification of the Emission Potential of a Waste Body*, Proceedings of the 9th intercontinental landfill research symposium, (2016), Japan.

6. **A.G. van Turnhout**, C. Brandstaeter, R. Kleerebezem, T.J. Heimovaara, *Investigating the impact of process parameters on aeration of MSW via a mechanistic biogeochemical reaction model*, Proceedings of the 6th International Workshop "Hydro-Physico-Mechanics of Landfill", (2015), The Netherlands.

5. **A.G. van Turnhout**, R. Kleerebezem, T.J. Heimovaara, *Building a mechanistic biogeochemical reaction network for upscaling: Characterization of mass transport limitation between regions of hydrolysis and methanogenesis*, Proceedings of the 6th International Workshop "Hydro-Physico-Mechanics of Landfill", (2015), The Netherlands.

4. **A.G. van Turnhout**, R. Kleerebezem, T.J. Heimovaara, *Can we extract transport limitation parameters from emission data to improve predictions on emission potential?*, Proceedings of the 8th intercontinental landfill research symposium, (2014), Florida.

3. **A.G. van Turnhout**, R. Kleerebezem, T.J. Heimovaara, *Grey box modelling of MSW degradation*, Proceedings of the 5th International Workshop "Hydro-Physico-Mechanics of Landfill", (2013), Scotland.

2. **A.G. van Turnhout**, R. Kleerebezem, T.J. Heimovaara, *Gray box modeling of MSW degradation: Revealing its dominant (bio)chemical mechanism*, Proceedings of the 14th international waste management and landfill symposium, (2013), Italy.

1. **A.G. van Turnhout**, R. Kleerebezem, T.J. Heimovaara, *Quantification of biogeochemical heterogeneous activity in full-scale landfills*, Proceedings of the NUPUS workshop on flow and deformation in porous media modeling, analysis, simulation, (2012), Germany.

Conference Proceedings

9. T.J. Heimovaara, **A.G. van Turnhout**, *A particle filter approach to quantify the mass balance of a MSW landfill*, Proceedings of the 16th international waste management and landfill symposium, (2017), Italy.

8. M. Afanasyev, J. Zhou, **A.G. van Turnhout**, L.A. van Paassen, T.J. Heimovaara, *A generic transport-reactive model for simulating microbially influenced mineral precipitation in porous medium*, Proceedings of the 9th International Conference on Porous Media, (2017), The Netherlands.

7. **A.G. van Turnhout**, T.J. Heimovaara, H. Oonk, H. Scharff, *Modeling Landfill Aeration: A parametric study in order to define the optimal aeration*, Proceedings of the 9th intercontinental landfill research symposium, (2016), Japan.

6. T.J. Heimovaara, A. Bun, **A.G. van Turnhout**, *Water balance modeling and estimation of emission potential using a data-assimilation approach*, Proceedings of the 15th international waste management and landfill symposium, (2015), Italy.

5. T.J. Heimovaara, A. Bun, **A.G. van Turnhout**, *Water balance modeling for estimation of residence time of water in a full scale landfill using a data-assimilation approach*, Proceedings of the 6th International Workshop "Hydro-Physico-Mechanics of Landfill", (2015), The Netherlands.

4. J. Zhou, **A.G. van Turnhout**, T.J. Heimovaara, M. Afanasyev, *A generic transport-reactive model for simulating microbially influence mineral precipitation in porous medium*, Proceedings of the 6th International Workshop "Hydro-Physico-Mechanics of Landfill", (2015), The Netherlands.

3. **A.G. van Turnhout**, R. Kleerebezem, T.J. Heimovaara, *Quantification of (bio)geochemical heterogeneous activity in full-scale landfills*, Proceedings of the 7th intercontinental landfill research symposium, 124 (2012), Sweden.

2. A. Bun, T.J. Heimovaara, S.M. Baviskar, **A.G. van Turnhout**, L.A. Konstantaki *Integrated modeling and up-scaling of landfill processes and heterogeneity using stochastic approach*, Proceedings of the 7th intercontinental landfill research symposium, 55 (2012), Sweden.

1. T.J. Heimovaara, A. Bun, **A.G. van Turnhout**, L.A. Konstantaki, S.M. Baviskar *Is it possible to quantify emission potential from high resolution monitoring of leachate dynamics?*, Proceedings of the 7th intercontinental landfill research symposium, 77 (2012), Sweden.